

44809

National Library
of CanadaBibliothèque nationale
du Canada

Canadian Theses Division / Division des thèses canadiennes

Ottawa, Canada
K1A 0N4**PERMISSION TO MICROFILM — AUTORISATION DE MICROFILMER**

- Please print or type — Écrire en lettres moulées ou dactylographier

Full Name of Author — Nom complet de l'auteur

RANDELL CHARLES RUDOLPH

Date of Birth — Date de naissance

SEPT 12 1953

Country of Birth — Lieu de naissance

CANADA

Permanent Address — Résidence fixe

120 BRIARWYND COURTS, EDMONTON TST OH4

Title of Thesis — Titre de la thèse

A NUMERICAL MODEL OF POLLUTANT
TRANSPORT IN A SMALL URBAN VALLEY

University — Université

UNIVERSITY OF ALBERTA

Degree for which thesis was presented — Grade pour lequel cette thèse fut présentée

MASTER OF SCIENCE

Year this degree conferred — Année d'obtention de ce grade

1980

Name of Supervisor — Nom du directeur de thèse

Dr. K. D. HAGE

Permission is hereby granted to the NATIONAL LIBRARY OF CANADA to microfilm this thesis and to lend or sell copies of the film.

L'autorisation est, par la présente, accordée à la BIBLIOTHÈQUE NATIONALE DU CANADA de microfilmer cette thèse et de prêter ou de vendre des exemplaires du film.

The author reserves other publication rights, and neither the thesis nor extensive extracts from it may be printed or otherwise reproduced without the author's written permission.

L'auteur se réserve les autres droits de publication; ni la thèse ni de longs extraits de celle-ci ne doivent être imprimés ou autrement reproduits sans l'autorisation écrite de l'auteur.

Date

APRIL 25 1980

Signature

Randy Rudolph



National Library of Canada
Collections Development Branch

Canadian Theses on
Microfiche Service

Bibliothèque nationale du Canada
Direction du développement des collections

Service des thèses canadiennes
sur microfiche

NOTICE

The quality of this microfiche is heavily dependent upon the quality of the original thesis submitted for microfilming. Every effort has been made to ensure the highest quality of reproduction possible.

If pages are missing, contact the university which granted the degree.

Some pages may have indistinct print especially if the original pages were typed with a poor typewriter ribbon or if the university sent us a poor photocopy.

Previously copyrighted materials (journal articles, published tests, etc.) are not filmed.

Reproduction in full or in part of this film is governed by the Canadian Copyright Act, R.S.C. 1970, c. C-30. Please read the authorization forms which accompany this thesis.

**THIS DISSERTATION
HAS BEEN MICROFILMED
EXACTLY AS RECEIVED**

AVIS

La qualité de cette microfiche dépend grandement de la qualité de la thèse soumise au microfilmage. Nous avons tout fait pour assurer une qualité supérieure de reproduction.

S'il manque des pages, veuillez communiquer avec l'université qui a conféré le grade.

La qualité d'impression de certaines pages peut laisser à désirer, surtout si les pages originales ont été dactylographiées à l'aide d'un ruban usé ou si l'université nous a fait parvenir une photocopie de mauvaise qualité.

Les documents qui font déjà l'objet d'un droit d'auteur (articles de revue, examens publiés, etc.) ne sont pas microfilmés.

La reproduction, même partielle, de ce microfilm est soumise à la Loi canadienne sur le droit d'auteur, SRC 1970, c. C-30. Veuillez prendre connaissance des formules d'autorisation qui accompagnent cette thèse.

**LA THÈSE A ÉTÉ
MICROFILMÉE TELLE QUE
NOUS L'AVONS REÇUE**

THE UNIVERSITY OF ALBERTA

A NUMERICAL MODEL OF POLLUTANT TRANSPORT

IN A SMALL URBAN VALLEY

by



RANDELL CHARLES RUDOLPH

A THESIS

SUBMITTED TO THE FACULTY OF GRADUATE STUDIES AND RESEARCH

IN PARTIAL FULFILMENT OF THE REQUIREMENTS FOR THE DEGREE OF

MASTER OF SCIENCE

IN

METEOROLOGY

DEPARTMENT OF GEOGRAPHY

EDMONTON, ALBERTA

SPRING, 1980

THE UNIVERSITY OF ALBERTA
FACULTY OF GRADUATE STUDIES AND RESEARCH

The undersigned certify that they have read, and recommend to the Faculty of Graduate Studies and Research, for acceptance, a thesis entitled " A Numerical Model of Pollutant Transport in a Small Urban Valley ", submitted by Randell Charles Rudolph in partial fulfilment of the requirements for the degree of Master of Science in Meteorology.

Kenneth R. Hays

Supervisor

Robert J. Blomfield

J. Dale

Date APRIL 22 1980

DEDICATION

To Stephanie and Daniel

ABSTRACT

The transport of pollutants in a cross-section of a small urban valley was numerically modelled using a particle-in-cell technique which solved the two-dimensional diffusion equation. The model was based on data gathered in the North Saskatchewan River valley in Edmonton, Alberta during clear-sky, light-wind, inversion conditions. Particles, representing specified amounts of carbon monoxide in a roadway plume, were created within a V-shaped valley. These particles were advected by a model wind field featuring double-vortex recirculation of pollutants and dispersed by a simulated turbulent diffusion process.

The model correctly predicted the trend to decreasing concentrations with increasing slope wind speed and decreasing source strength. Concentrations near the surface 100 m downslope from the source reached over 6 ppm while concentrations in the return flow 50 m upslope from the source reached nearly 5 ppm. Decreasing particle density increased concentration variability. Concentrations were sensitive to initial source diffusion but insensitive to the magnitude of eddy diffusivities away from the source.

ACKNOWLEDGEMENTS

Special thanks are due my supervisor, Dr. K.D. Hage. His direction and constructive criticism were invaluable to the completion of this thesis. I would also like to thank Drs. R.B. Charlton and J.D. Dale who, along with Dr. Hage, served on the examining committee. Useful discussions with Drs. G.C. Cree and R.F. Millar of the Mathematics Department are gratefully acknowledged.

Thanks are also due to the staff of Cartography and Photographic Services in the Department of Geography for their prompt and expert assistance.

Finally, I would like to thank the Research Secretariat, Alberta Environment, who provided financial support under contract 77-6 during part of this study.

TABLE OF CONTENTS

	PAGE
DEDICATION	IV
ABSTRACT	V
ACKNOWLEDGEMENTS	VI
TABLE OF CONTENTS	VII
LIST OF TABLES	X
LIST OF FIGURES	XI
LIST OF SYMBOLS	XVII

CHAPTER

I INTRODUCTION

1.1 Introduction	1
1.2 The Valley and its Micrometeorology..	2

II THE MODEL - THEORY

2.1 Introduction	8
2.2 General Description	10
2.3 Boundary Conditions	13
2.4 The Advection Velocity	14
2.5 The Diffusion Velocity	18
2.6 Sub-grid Scale Diffusion	24
2.7 The Source	27

III THE MODEL - PARAMETERIZATION

3.1 Introduction	28
3.2 The Valley	28
3.3 Cell Areas	30

CHAPTER		PAGE
	3.4 The Advection Velocity	32
	3.5 The Diffusion Velocity	35
	3.6 The Source	39
	3.7 The Timestep	43
	3.8 Particle Trajectories and Reflections	44
IV	RESULTS	
	4.1 General	48
	4.2 Gaussian and Concentration-Gradient Diffusion	53
	4.3 Sensitivity to Cell Size	55
	4.4 Sensitivity to Initial Source Size ..	64
	4.5 Sensitivity to Particle Density	68
	4.6 Sensitivity to Magnitude of Eddy Diffusivities	71
	4.6.1 No Diffusion	71
	4.6.2 A Range of Eddy Diffusivities ..	75
	4.7 Sensitivity to Advection Velocity ...	82
	4.8 Computer Requirements	86
V	SUMMARY AND CONCLUSIONS	
	5.1 Summary	88
	5.2 Conclusions	91
	5.3 Suggestions for Future Study	94
	REFERENCES	96

APPENDIX

A	An Illustration of a Particle Scatter	
	Graph Diagram Display	100
B	Computer Program	107

LIST OF TABLES

TABLE

PAGE

4.1:	Standard parameters of the computer model.....	50
4.2:	Eddy diffusivities and corresponding Figures for section 4.6.2.....	76

LIST OF FIGURES

FIGURE	PAGE
1.1: Cross-section of North Saskatchewan River valley in Edmonton and model approximation	4
2.1: Streamlines of the model advection velocity	19
3.1: Parameter N used in determining cell areas	34
3.2: Experimental and model wind profiles	34
3.3: Scheme for calculation of diffusion velocity U_D	40
3.4: Velocity interpolation scheme	40
3.5: Weekday mean traffic	46
3.6: Reflection of particles at groundline	46
4.1a: Gaussian dispersion of plume at $t=646s$	54
4.1b: Concentration-gradient dispersion of plume at $t=664s$	54
4.1c: Comparison of concentration-gradient and Gaussian diffusion	56
4.2a: Particle distribution produced by standard parameters (Table 4.1) at $t=3610s$	58
4.2b: Particle distribution produced by standard parameters (Table 4.1) at $t=7181s$	58
4.2c: Vertical profile of concentration 100 m	

downslope from source produced by parameters of Table 4.1	59
4.2d: Vertical profile of concentration 50 m upslope from source produced by parameters of Table 4.1	59
4.3a: Particle distribution at t=3608s produced by parameters of Table 4.1, except that INCX=40 m and INCZ=5 m	60
4.3b: Particle distribution at 7195s produced by parameters of Table 4.1, except that INCX=40 m and INCZ=5 m	60
4.3c: Vertical profile of concentration 100 m downslope from source produced by parameters of Table 4.1, except that INCX=40 m and INCZ=5 m	61
4.3d: Vertical profile of concentration 50 m upslope from source produced by parameters of Table 4.1, except that INCX=40 m and INCZ=5 m	61
4.4a: Particle distribution at t=3610s produced by parameters of Table 4.1, except that SDEVX=6 m and SDEVZ=4 m	65
4.4b: Particle distribution at t=7188s produced by parameters of Table 4.1, except that SDEVX=6 m and SDEVZ=4 m	65

4.4c: Vertical profile of concentration 100 m downslope from source produced by parameters of Table 4.1, except that SDEVX=5 m and SDEVZ=4 m	66
4.4d: Vertical profile of concentration 50 m upslope from source produced by parameters of Table 4.1, except that SDEVX=6 m and SDEVZ=4 m	66
4.5a: Particle distribution at t=3609s produced by parameters of Table 4.1, except that PWT=0.4g CO	69
4.5b: Particle distribution at t=7189s produced by parameters of Table 4.1, except that PWT=0.4g CO	69
4.5c: Vertical profile of concentration 100 m downslope from source produced by parameters of Table 4.1, except that PWT=0.4g CO	70
4.5d: Vertical profile of concentration 50 m upslope from source produced by parameters of Table 4.1, except that PWT=0.4g CO	70
4.6a: Particle distribution at t=3604s produced by parameters of Table 4.1, except that no diffusion is allowed - advection only	73
4.6b: Particle distribution at t=7181s produced by	

parameters of Table 4.1, except that no diffusion is allowed - advection only ...	73
4.6c: Vertical profile of concentration 100 m downslope from source produced by parameters of Table 4.1, except that no diffusion is allowed - advection only	74
4.6d: Vertical profile of concentration 50 m upslope from source produced by parameters of Table 4.1, except that no diffusion is allowed - advection only	74
4.7a: Particle distribution at $t=3617s$ produced by parameters of Table 4.1, except that $INCX=40$ m, $INCZ=5$ m, $DKMX=1.0 \times 10^{-3} m^2 s^{-1}$, and $DKMZ=5.0 \times 10^{-5} m^2 s^{-1}$	77
4.7b: Particle distribution at $t=7204s$ produced by parameters of Table 4.1, except that $INCX=40$ m, $INCZ=5$ m, $DKMX=1.0 \times 10^{-3} m^2 s^{-1}$, and $DKMZ=5.0 \times 10^{-5} m^2 s^{-1}$	77
4.7c: Vertical profile of concentration 100 m downslope from source produced by parameters of Table 4.1, except that $INCX=40$ m, $INCZ=5$ m, $DKMX=1.0 \times 10^{-3} m^2 s^{-1}$ and $DKMZ=5.0 \times 10^{-5} m^2 s^{-1}$	78

- 4.7d: Vertical profile of concentration 50 m upslope
 from source produced by parameters of Table
 4.1, except that INCX=40 m, INCZ=5 m,
 $DKMX=1.0 \times 10^{-3} \text{ m}^2 \text{ s}^{-1}$, and
 $DKMZ=5.0 \times 10^{-5} \text{ m}^2 \text{ s}^{-1}$ 78
- 4.8a: Particle distribution at t=3601s produced by
 parameters of Table 4.1, except that
 INCX=40 m, INCZ=5 m, $DKMX=1.0 \times 10^{-1} \text{ m}^2 \text{ s}^{-1}$,
 and $DKMZ=5.0 \times 10^{-3} \text{ m}^2 \text{ s}^{-1}$ 79
- 4.8b: Particle distribution at t=7218s produced by
 parameters of Table 4.1, except that
 INCX=40 m, INCZ=5 m, $DKMX=1.0 \times 10^{-1} \text{ m}^2 \text{ s}^{-1}$,
 and $DKMZ=5.0 \times 10^{-3} \text{ m}^2 \text{ s}^{-1}$ 79
- 4.8c: Vertical profile of concentration 100 m
 downslope from source produced by parameters
 of Table 4.1, except that INCX=40 m,
 INCZ=5 m, $DKMX=1.0 \times 10^{-1} \text{ m}^2 \text{ s}^{-1}$, and
 $DKMZ=5.0 \times 10^{-3} \text{ m}^2 \text{ s}^{-1}$ 80
- 4.8d: Vertical profile of concentration 50 m upslope
 from source produced by parameters of
 Table 4.1, except that INCX=40 m, INCZ=5 m,
 $DKMX=1.0 \times 10^{-1} \text{ m}^2 \text{ s}^{-1}$, and
 $DKMZ=5.0 \times 10^{-3} \text{ m}^2 \text{ s}^{-1}$ 80

4.9a:	Particle distribution at $t=3633s$ produced by parameters of Table 4.1, except that INCX=40 m, INCZ=5 m, and AVWF = 0.25 ms^{-1}	83
4.9b:	Particle distribution at $t=7225s$ produced by parameters of Table 4.1, except that INCX=40 m, INCZ=5 m, and AVWF = 0.25 ms^{-1}	83
4.9c:	Vertical profile of concentration 100 m downslope from source produced by parameters of Table 4.1, except that INCX=40 m, INCZ=5 m, and AVWF = 0.25 ms^{-1}	84
4.9d:	Vertical profile of concentration 50 m upslope from source produced by parameters of Table 4.1, except that INCX=40 m, INCZ=5 m, and AVWF = 0.25 ms^{-1}	84
A1:	Particle distribution at $t = 900 \text{ s}$	102
A2:	Particle distribution at $t = 1800 \text{ s}$	103
A3:	Particle distribution at $t = 2700 \text{ s}$	104
A4:	Particle distribution at $t = 3600 \text{ s}$	105
A5:	Particle distribution at $t = 7200 \text{ s}$	106

LIST OF SYMBOLS

SYMBOL

a	horizontal dimension of "membrane"
b	vertical dimension of "membrane"
D	length of segment of infinite line source
EF	vehicle emission factor
F	fraction representing diurnal traffic cycle
G	domain of rectangular "membrane"; source strength
h	hour(s)
k	von Karman's coefficient
K	eddy diffusivity tensor
K_{xx}	horizontal eddy diffusivity
K_{zz}	vertical eddy diffusivity
K_1	vertical eddy diffusivity at fixed reference height
\ln	natural logarithm
L	Monin-Obukov length
m	power law wind profile exponent
n	power law diffusivity profile exponent
N	indicator of cell shape
NV	total daily traffic count on line source
Q	source strength
t	time
T	model time
u	horizontal wind speed

SYMBOL

u_A	horizontal component of advection velocity
\bar{U}	average horizontal wind speed
\vec{U}_A	advection velocity
\vec{U}_D	diffusion velocity
U_{Dx}	one-dimensional diffusion velocity
\vec{U}_p	pseudo-transport velocity
\bar{U}_1	mean horizontal wind at fixed reference height
U_*	friction velocity
w	vertical wind speed
w_A	vertical component of advection velocity
x_D	distance from particle to plume center of mass
α	proportionality constant in Helmholtz equation; power law horizontal diffusivity profile exponent
ϵ	rate of eddy energy dissipation
ζ	atmospheric static stability
σ_{ox}	initial horizontal plume standard deviation
σ_x	horizontal plume standard deviation
σ_z	vertical plume standard deviation
ϕ_m	dimensionless shear of mean wind
χ	pollutant concentration
$\bar{\chi}$	average pollutant concentration
ψ	stream function
$\vec{\omega}$	two-dimensional vorticity

CHAPTER I

INTRODUCTION

1.1 Introduction

Many cities in the world are located near major river valleys. These cities were built at a time when waterways were often used for travel. As the cities grew the river valleys formed natural cores for settlements. Today, different parts of the valley are often reserved as sites for recreation, as areas of industry, or as corridors for transportation. Therefore, urban river valleys have the potential for bringing large numbers of people together. Because of their micrometeorology, urban valleys also have the potential for trapping large concentrations of pollutants. These two factors could produce a localized health problem. For this reason the study of the micrometeorology of urban river valleys is important.

There are few published studies concerned with small valley micrometeorology although some observational work does exist (for example, Klassen, 1962). More recently an experimental

program was undertaken at the University of Alberta in Edmonton. Some of the results derived from this project can be found in Paterson (1978), Hwang (1978) and Hage (1979). Although substantial progress has been made in understanding the micrometeorology of the small valley, few of the new hypotheses have been tested. It is evident that computer simulations must bridge the gap between the present knowledge of valley circulation and future progress.

This thesis is part of a three-way plan to model the unique micrometeorology of a small urban river valley. Part one is an attempt to model the evolution of a temperature field throughout the valley. This has been undertaken by di Cenzo (1979). In part two, Stovel (1979) attempts to show how a valley wind system evolves from the time-dependent thermal fields of part one. This thesis is part three of the plan. The author attempts to model the dispersal of pollutants in a small urban valley utilizing the valley wind system of part two.

1.2 The Valley and its Micrometeorology

Observations in the North Saskatchewan River valley (a small urban valley) in Edmonton provided data on which the present model is based. These data were not used in verification because of the model's simplicity, but rather as clues to model development. As a first step in modelling pollutant dispersion

within the valley a summary of the valley structure and known micrometeorology is presented. The North Saskatchewan River valley is typically about 1 km wide and 50 m deep. It meanders through the center of the city in a generally north-eastward direction. Typically, the meandering causes one wall of the valley to be rather sheer from the river's edge to the ridgeline. The other side of the valley contains a flood plain that serves variously as an area of recreation, industry, residence or transportation. It is likely that this valley asymmetry contributes to its unique micrometeorology. Figure 1.1 is a diagram of a representative cross-section of the valley, along with the model approximation of it.

Evidence that the microclimate of the valley is different than that of the city is found in Hage (1972). Minimum temperatures in the valley were observed to be comparable to those measured at rural stations under clear sky conditions. The effect of the valley was to cancel the heat island effect of the city in this instance.

Some understanding of the nature of circulation induced in small river valleys can be gained by investigating mountain and large valley winds. Observations showed that well-developed local circulations with marked diurnal variations are formed in valleys leading into mountain ranges. During the day the winds were upslope and upvalley; at night the winds were downslope and downvalley. The slope winds were always initiated first and the valley winds followed. Defant (1951) described an

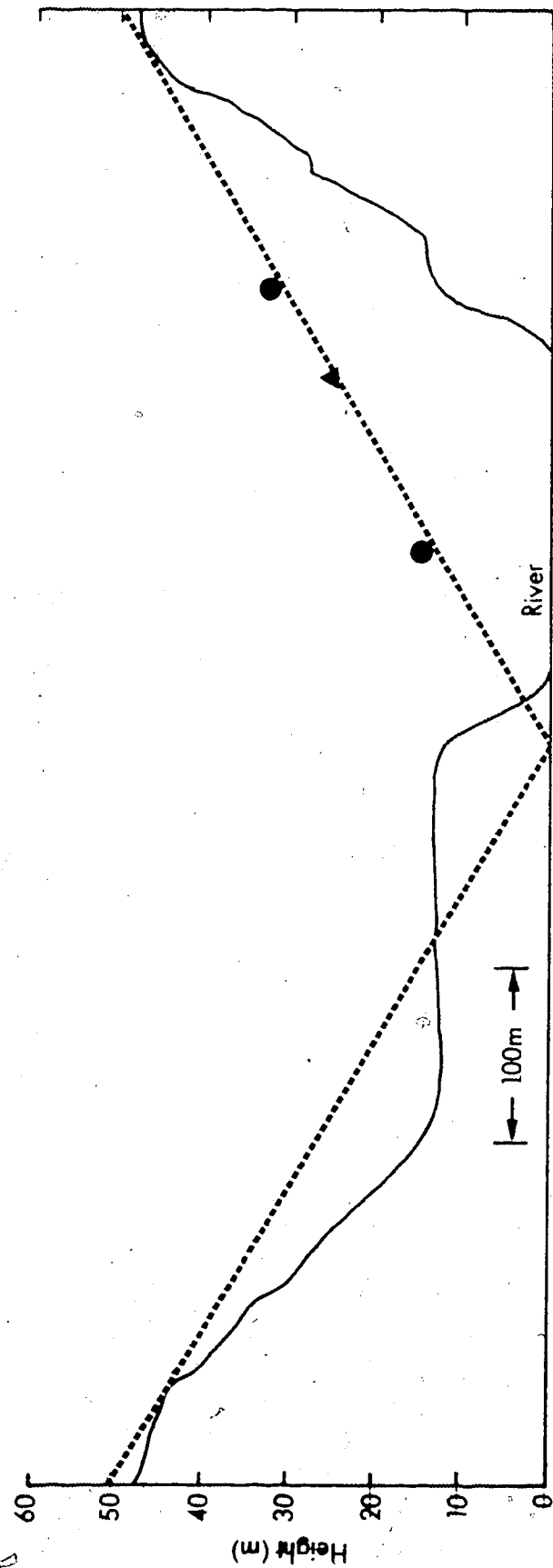


Figure 1.1: Cross-section of North Saskatchewan River valley in Edmonton (solid lines) and model approximation (dashed lines). Triangle denotes position of source. Circles denote positions of "monitoring stations".

idealized version of the diurnal change in valley winds.

Observations in the North Saskatchewan River valley by Klassen (1962) and Hage (1979) generally confirmed those made in mountain valleys. During periods of strong prevailing winds, or lighter winds and overcast skies, no valley wind regime developed. The vertical temperature structure was essentially isothermal; the air in the valley was well-mixed with that of the plains above. When the sky was clear and the prevailing wind was light, the slope (drainage) wind began at about sundown. Initially the speed of the slope wind was small and the depth of flow was shallow. Both increased to their maximum values within two hours and persisted at or near those values until sunrise. The fully developed slope wind was variable. It rarely exceeded 1.0 ms^{-1} and its average value was about 0.2 ms^{-1} . The depth of flow varied from about 5 m to 15 m or more.

Observations of the temperature profiles in the valley revealed distinct differences between the two valley slopes under calm, clear sky conditions. Both slopes developed inversions, but that slope first receiving shading developed an earlier and a more intense inversion. Inversions over both slopes were more intense than that which developed over the urban plains above the valley.

The vertical shear of the slope wind has also been investigated (Paterson, 1978; Hage, 1979). In well-mixed conditions the wind speed increased with height above the slope. As the stability increased, the wind speed tended to become

constant with height. Under the most favourable conditions, the speed of the slope wind decreased with height and the height of the maximum wind speed existed below 1.0 m. It was thought that this regime extended to the height of the ridgeline where once again the wind speed increased with height.

Klassen (1962) found evidence of a double-vortex circulation system within the valley. Fog which formed after rain or hail drained down the slope into the river valley. Above the river some of the fog rose vertically and flowed back toward the rim of the valley. The remainder of the fog subsided laterally and then flowed down the valley. Therefore, the trajectory of a particle caught in the circulation system appeared to be a helix with its axis oriented downvalley. Paterson and Hage (1979) estimated that the time required for a particle to complete one circuit of this valley vortex by advection alone is 40 minutes to 2.5 hours.

Measurements of carbon monoxide (CO) concentration showed evidence of a distinct valley circulation (Hage, 1979). On most days a typical CO trace had a peak in concentration near 1700 MST. This corresponds to the late afternoon rush hour traffic maximum. On some days a second peak in concentration existed near 2100 MST, well after the traffic maximum. At the downtown monitoring station the second peak was usually secondary in importance compared to the traffic peak; whereas, in the valley the second peak was dominant. The evening maximum tentatively can be attributed to the development of a surface-based inversion

formed by radiative cooling. If the transition from unstable to stable stratification occurs rapidly enough, the decrease in vertical spread of the CO plume may overcompensate for the increase in source strength after the late afternoon traffic peak. This can result in an evening concentration maximum. Because the inversion is more intense inside the valley the evening peak in concentration will be relatively larger there. Most of the time the magnitude of the peaks is greater at the downtown station because this station is in the midst of the large downtown area source. Occasionally the peak concentrations were larger at stations inside the valley than at the downtown station even though source strengths are much larger downtown (Hage, 1979). A tentative cause of this exceptional occurrence is the recirculation of pollutants made possible by the valley winds, in association with the intensification and deepening of the inversion. The magnitude of the evening concentration peak is indirect evidence for the existence of a double-helix circulation regime for the valley winds.

The object of this thesis is to investigate the effects of the proposed circulation system on the CO distribution within a small urban valley. The magnitude of the effect will be of prime importance in elucidating the proposed circulation regime in areas of the valley inaccessible to measurement.

CHAPTER II

THE MODEL - THEORY

2.1 Introduction

Traditionally two approaches have been used to solve fluid dynamics problems. In general these methods subdivide the region of interest into smaller cells and transform the differential equations involved into suitable finite-difference form (Gifford, 1975; Lamb et al., 1974).

In the Lagrangian approach the grid of cells is embedded in the fluid and moves with it. Masses and velocities are usually defined at the cell corners while other time dependent properties of the fluid are defined at the cell center. Each cell corner is always associated with the same part of the fluid. Therefore, the cells are distorted as the fluid undergoes distortion. This can occur when, for example, large velocities exist normal to a solid boundary (Amsden, 1966).

In the Eulerian method the mesh of cells remains fixed

relative to an observer while the fluid moves through the cells. In its strict application each cell is homogeneous with respect to all fluid properties (Hanna, 1975). Cells may vary in size but because the cells are fixed in space the method is unable to resolve fine-scale structures that move with the fluid without introducing a fine-scale grid throughout the entire region. The method also produces a fictitious diffusion. Fictitious diffusion arises when errors in mass or concentration within a cell are introduced by the assumption of homogeneity (Lange, 1978). Since, in gradient-transport theories, diffusion is related to concentration, errors in diffusion rates also arise. This diffusion is not real but rather a by-product of the Eulerian method.

In an attempt to utilize the desirable aspects of both methods, the present model is based on the Particle-in-Cell technique (PIC). The PIC method is a hybrid; it has elements of both the Lagrangian and Eulerian modes. The region through which the fluid moves is subdivided into a finite grid of Eulerian cells which are fixed in space and time. In general, velocities are defined at cell corners and concentrations are defined at cell centers. Masses (concentrations) and velocities are allowed to be time dependent. In addition the fluid itself is represented by Lagrangian particles or mass points which move through the Eulerian mesh. These particles act as markers for the fluid motion. Each particle is assigned a mass and the

total mass or concentration of a cell is determined by the number of particles inside the cell. For a complete description of the Particle-in-Cell technique, as well as its applicability to a wide variety of fluid dynamics problems, see the references Welch et al. (1965), Amsden (1966), and Lange and Sherman (1977). The PIC method has been applied specifically to the study of the dispersal of atmospheric pollutants by Lange (1973; 1978). A particular PIC model developed by Lange (ADPIC) has been assessed as a regional model in Alberta (Padro, 1979; Reid et al., 1979).

Following the example of Lange, the present model solves the two-dimensional nonlinear transport-diffusion equation in its flux conservative form, relying on a given advection field varying in time and space, complex terrain, and time- and space-varying diffusion coefficients with only minor modifications to the computer code.

2.2. General Description

The nonlinear transport-diffusion equation can be written in the following form

$$\frac{\partial X}{\partial t} + \vec{U}_A \cdot \vec{\nabla} X = \vec{\nabla} \cdot \{K \cdot \vec{\nabla} X\} \quad (2.1)$$

where χ is a scalar concentration, K is the eddy diffusivity and \vec{U}_A is the given advection velocity field. Equation (2.1) can be simplified if the flow can be assumed incompressible.

In the atmosphere, for small values of the Mach number, the only compressibility effect of importance is that related to the change of density with height. The domain of the model was the lower 50 m of the boundary layer. Therefore, the density can be assumed to be constant. For velocities of the order of 1 ms^{-1} that were observed in small valleys under inversion situations, the Mach number will be very small. Therefore, the assumption of incompressibility is a good one.

If the flow is incompressible, then

$$\vec{U}_A \cdot \vec{\nabla} \chi = \vec{\nabla} \cdot (\chi \vec{U}_A) \quad (2.2)$$

Combining the divergence terms the transport-diffusion equation (2.1) can be written as

$$\frac{\partial \chi}{\partial t} = \vec{\nabla} \cdot (\chi \vec{U}_p) = 0 \quad (2.3)$$

where \vec{U}_p is the pseudo-transport velocity and is defined as follows


$$\vec{U}_p = \vec{U}_A + \vec{U}_D = \vec{U}_A - \frac{K \vec{\nabla} \chi}{\chi} \quad (2.4)$$

where \vec{U}_D is a diffusion velocity.

Each timestep of the model was divided into an Eulerian and a Lagrangian part. The Eulerian part consisted of summing the particles in each cell, determining the particle

concentration and calculating the diffusion velocity. The diffusion velocity was then added to the advection velocity to yield the pseudo-velocity. In the Lagrangian step each marker particle was transported along a pseudo-velocity streamline. Particles transported outside the grid system were counted as destroyed. Particles transported into the ground of the valley were reflected back into the fluid proper. Based on the new particle positions, new Eulerian concentrations were calculated and the cycle was repeated.

Cell particle concentrations were defined at cell centers and the velocities \vec{U}_p , \vec{U}_A and \vec{U}_D were defined at cell corners. These velocities were then interpolated to each particle position. The cells in the present application were rectangles of uniform size. The locations of the particles representing fluid motion were defined by their coordinates within the fixed grid. The specific mass of the marker particles was assumed to be equal to the specific mass of air. Therefore, deposition was non-existent; the marker particles delineated a plume of pollutants.



2.3 Boundary Conditions

Because of the hybrid nature of the PIC method, the boundary conditions were broken into two sets, one imposed on the Eulerian velocity field and the other on the Lagrangian particles. Both sets must be consistent with each other. For example, if there is outflow at the boundaries, then the particle flux must accurately represent the mass flux of the pseudo-velocity field. The concentration field must be smooth enough when it reaches the boundary so that boundary velocities can be specified by assuming a constant flux of particles through the boundary.

The particle boundary conditions were simple. When a particle passed through the upper or side boundary, it was counted as annihilated. When a particle passed through the lower (valley surface) boundary it was reflected.

Two basic boundary conditions were imposed on the pseudo-velocity field. They were the mass flux $\chi \vec{U}_p = 0$, corresponding to reflection of the particles at a boundary, and $\chi \vec{U}_p = \text{constant}$, corresponding to inflow and outflow of particles through the boundary. To be consistent with the particle boundary conditions, the mass flux was zero at the valley surface. The flux of mass was always outward at other boundaries.

2.4 The Advection Velocity

It was mentioned earlier that observations made in the North Saskatchewan River valley in Edmonton and in mountain valleys in the United States and Europe indicated the likely existence of a double-vortex circulation system in the valley during inversion situations and that this circulation was largely separated from the large-scale flow. The model attempted to duplicate these observations by assuming that the advection term in the pseudo-velocity forms a double-vortex circulation.

A typical nighttime inversion situation was modelled. The inversion was fully developed, that is, it filled the entire valley. Therefore, the double-vortex circulation also filled the entire valley and was assumed to be independent of the large-scale flow. The flow was downslope along the valley sides, upward (by continuity) near the valley center and then outward toward the valley ridge. Since the model was two-dimensional, the downvalley component of the observed winds was ignored.

Several methods exist for generating valley winds. See, for example, Tang and Peng (1974), Tang (1976), and Stovel (1979). Most solve a set of differential equations including the momentum equations and the heat equation in some suitable fashion. Considerable complexity is introduced if account is taken of the nonlinear coupling of the horizontal and vertical equations of motion and the heat equation. This complexity was thought

to be beyond the scope of the present model.

Instead, a simple two-dimensional mass-conserving flow was sought. This can be satisfied by writing the velocity components in terms of the stream function ψ . Then the magnitude of the vorticity vector $\vec{\omega}$ which is everywhere normal to the flow is given by

$$\vec{\omega} = - \left[\frac{\partial^2 \psi}{\partial x^2} + \frac{\partial^2 \psi}{\partial z^2} \right] . \quad (2.5)$$

For two-dimensional flow the vorticity associated with a fluid element is constant; in steady flow the paths of the elements are streamlines. Therefore, $\vec{\omega} = \vec{\omega}(\psi)$. Provided the distribution of vorticity is known, solutions to (2.5) exist. This distribution is arbitrary for inviscid fluids (Batchelor, 1974) so one may choose specific forms of $\vec{\omega}(\psi)$ for which solutions to (2.5) are known. One convenient choice is $\vec{\omega} \propto \psi$, which yields the linear Helmholtz equation

$$\frac{\partial^2 \psi}{\partial x^2} + \frac{\partial^2 \psi}{\partial z^2} = -\alpha^2 \psi . \quad (2.6)$$

Equation 2.6 is similar to that for transverse vibrations of an elastic membrane. Solutions are known for a number of shapes of membrane on which ψ is constant. Of particular interest is the rectangular membrane which covers the domain $G(0 \leq x \leq a, 0 \leq z \leq b)$. Proceeding in the normal way, assume a variables-separable solution, $\psi = f(x) g(z)$. For the boundary condition $\psi = 0$, with $\alpha = 1$, the eigenfunctions can be shown to be products of $\sin \frac{n\pi x}{a}$ $\sin \frac{m\pi z}{b}$. The complete solution is,

therefore,

$$\psi = c \sum_{n=1}^{\infty} \sum_{m=1}^{\infty} \sin \frac{n\pi x}{a} \sin \frac{m\pi z}{b}, \quad (2.7)$$

where c is an arbitrary constant and a and b are the horizontal and vertical dimensions of the membrane. The eigenfunction products form a complete orthogonal system of functions in G .

The solution appropriate for valley winds was found in the following way. Assume the valley shape to be formed by one half of the rectangular membrane - a triangular valley. If an additional boundary condition is imposed, namely $\psi = 0$ on the diagonal, the new solution to (2.6) is included in (2.7). In other words the stream functions for a triangular valley will be a specific set of the complete solution. Courant and Hilbert (1953) show the appropriate solution to be

$$\psi = \psi_{12} + \psi_{21}, \quad (2.8)$$

that is,

$$\psi = c \left(\sin \frac{\pi x}{a} \sin \frac{2\pi z}{b} + \sin \frac{2\pi x}{a} \sin \frac{\pi z}{b} \right). \quad (2.9)$$

In this case b is the depth of the valley and a is one-half the width. The two-dimensional non-divergent velocity field in cartesian components is then given by

$$\begin{aligned} u_A &= - \frac{\partial \psi}{\partial z} \\ w_A &= \frac{\partial \psi}{\partial x} \end{aligned} \quad (2.10)$$

It was a simple matter to reflect the values of the stream functions resulting from (2.9) about the valley axis so that the desired valley winds were produced.

A comment about the realism of the velocity field as generated by (2.9) and (2.10) is in order. The field was experimentally reproduced on a finely spaced grid and the maximum values of u_A and w_A were found. The ratio of the maximums (u_A/w_A) was found to be approximately 6.5. For synoptic-scale flow, this ratio is the order of 1000 (Polten, 1972). As it is in synoptic-scale flow, the ratio of horizontal to vertical wind speed in a valley is governed by the dimensions of the boundary. For example, the ratio in synoptic-scale flows depends on the height of the tropopause and the horizontal size of synoptic disturbances. A similar relationship was assumed to exist for the flow in a river valley. The North Saskatchewan River valley is approximately 800 m wide and 50 m deep. The expected ratio in the valley is, therefore, nearer to 16. The ratio in the generated velocity field can be shown analytically to be a/b , twice the ratio of the valley dimensions. Thus (2.9) yields values of vertical velocity that are larger by a factor of two over those expected. The finite-difference forms of (2.10) further enhance the vertical velocity relative to the horizontal. The vertical dimension of a pollutant plume trapped in such a velocity field should, therefore, be increased.

A more serious departure of the model winds from inferred small valley winds was the relatively large maximum in the horizontal velocity that occurred near the upper boundary. Model horizontal velocities here were comparable to or larger than those on the valley slope; whereas, actual velocities here are believed to be smaller. Thus, a plume traversing a circuit of the model double-vortex circulation system should undergo relatively less vertical diffusion. Streamlines of arbitrary magnitude are shown in Figure 2.1.

2.5 The Diffusion Velocity

All ramifications of gradient-transport theory depend ultimately on the notion that the flux of a quantity is proportional to its gradient. That there seems to be no precise physical basis for this assumption is emphasized in Slade (1968). The theory does, however, provide useful results and will be used to define the diffusion velocity as that velocity (of a pollutant particle) resulting from a concentration gradient. The diffusion velocity is given by

$$\vec{U}_D = - \frac{K \vec{\nabla} \chi}{\chi} \quad (2.11)$$

where K is the eddy diffusivity and χ the scalar pollutant concentration. This definition follows directly from (2.4).

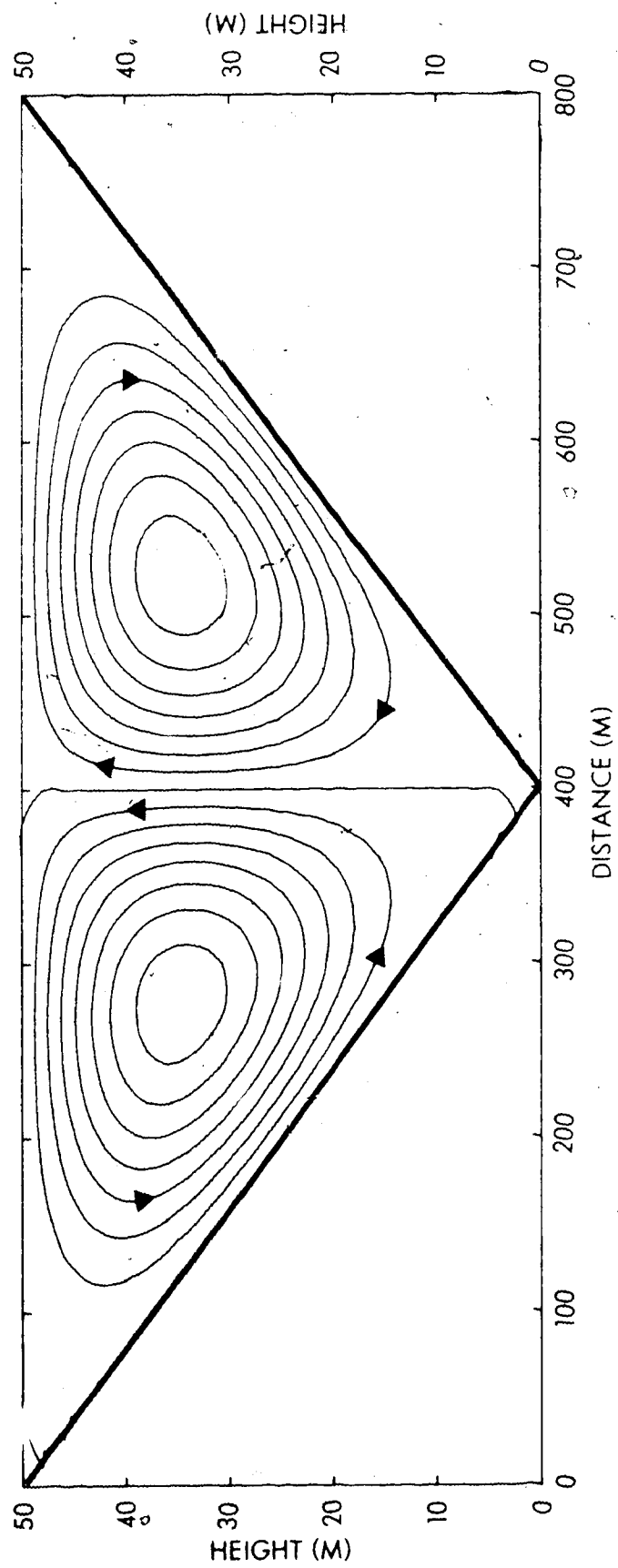


Figure 2.1: Streamlines of the model advection velocity.

The concentration χ is simply the total number of Lagrangian marker particles in a unit volume. (The length of the downstream component is arbitrary.) The finite-difference form of (2.11) will be discussed in Section 3.5. The remainder of this section will be used to discuss particular diffusion parameters.

In principle the model can accommodate the full two-dimensional cartesian eddy diffusivity tensor K_{ij} . In practice, however, the turbulence was assumed to be isotropic so that only the diagonal elements, K_{xx} and K_{zz} , survived. It then remained to determine forms of the vector eddy diffusivities that were both realistic and tractable. To do this, it is necessary to review some of the wind-profile observations made in the North Saskatchewan River valley.

The time of interest was nighttime, after approximately 2200 MST. The inversion was entrenched throughout the entire depth of the valley, as were the valley winds. The maximum downslope wind was found to exist below a height of 0.8 m (Hage, 1979). Therefore, the downslope wind decreased with height and, except perhaps for the lowest few centimeters, a constant momentum flux layer did not exist in the valley. Indeed, because of the intense inversion, the valley air may be more accurately characterized as a zero vertical turbulent flux layer. Vertical velocities at this time were found to be below the resolution of sensitive propeller anemometers; they were

essentially zero. Horizontal velocities were thought to be much larger because of the large horizontal temperature gradient. These observations served to put severe limitations on the functional forms of the eddy diffusivities.

In an attempt to put bounds on the eddy diffusivities, a range of values were used (see Section 3.5). The vertical coefficient ranged from near molecular to near that predicted for a stably-stratified atmosphere assuming constant flux. The horizontal coefficient ranged from several orders of magnitude larger than molecular to a value consistent with stable stratification. For all cases except those assuming a constant flux, directional variations of the eddy diffusivities are not known. Therefore, constant values were used.

Functional forms of the eddy diffusivities have been postulated assuming the flux in the lower 50 m to 100 m to be constant. Even though this assumption is inferred to be incorrect for small valleys, the model retains the capability of computing eddy diffusivities from it. In the determination of a form for the vertical diffusivity, turbulent diffusion induced both by drag on the earth's surface by the atmosphere, and by thermal convection within the atmosphere must be taken into account. Assuming the inertial subrange hypothesis to be valid for the region of the boundary layer of this application, similarity theory can be used to determine the vertical diffusivity. A tacit assumption is that the flat plain forms of the eddy

diffusivities are approximately valid for a shallow to moderately sloped valley. With this approach K_{zz} can be shown to be

$$K_{zz} = \frac{U_* k z}{\phi_m} \quad (2.12)$$

where U_* is the friction velocity and k is the von Kármán coefficient. The dimensionless wind shear ϕ_m is given by

$$\phi_m = \frac{kz}{U_*} \frac{\partial \bar{U}}{\partial z} \quad (2.13)$$

where \bar{U} is the average horizontal wind speed. Semi-empirical relations have been used to determine values for ϕ_m . Businger (1973) gives the following relations based on the AFCRL Kansas experiments:

$$\phi_m = (1 - 15\zeta)^{-1/4}, \quad \zeta < 0 \quad (2.14)$$

$$\phi_m = 1 + 4.7\zeta, \quad \zeta > 0$$

where ζ is a measure of atmospheric static stability and is defined by the relation

$$\zeta = z/L \quad (2.15)$$

where z is the vertical height and L the Monin-Obukov length.

In order to be internally consistent one should calculate both U_* and ζ for use in determining K_{zz} . However, the calculation of ζ was thought to be beyond the scope of the model. In practice a value of static stability was specified as model input and U_* was calculated (and used as model input) from gathered

data.

Functional forms of the eddy diffusivity can be found by making assumptions about the shape of the wind profile and the vertical variation of the vertical eddy diffusivity (Pasquill, 1974). For a power-law profile, that is,

$$U(z) = \bar{U}_1 \left[\frac{z}{z_1} \right]^m \quad (2.16)$$

$$K_{zz}(z) = K_1 \left[\frac{z}{z_1} \right]^n$$

where K_1 and \bar{U}_1 are values at a fixed reference height z_1 , Davies (1950) gives the relationship

$$K_{xx} \propto z^m. \quad (2.17)$$

It has been observed in an atmosphere of neutral stability with a power-law wind profile, the value of the exponent m is approximately $1/7$. With $n = 1-m$ (the conjugate power-law condition), (2.17) results in a ground-level axial concentration varying as $x^{-1.40}$, whereas, the observed dependence is $x^{-1.75}$ for a continuous point source at ground level (Pasquill, 1974). To obtain this observed dependence, K_{xx} must vary as z^α , where

$$\alpha = 1 + m(1-3m)/(1+m). \quad (2.18)$$

For $m = 1/10$, indicative of a slightly stable atmosphere, α is approximately 1.07.

As a first approximation to the eddy diffusivities in a stably-stratified atmosphere, it might be assumed that K_{xx} and K_{zz} are of the same order of magnitude. If, as was supposed earlier, U_* and ϕ_m are constants, then $K_{zz} \propto z^{1.0}$. With this vertical dependency, K_{xx} and K_{zz} can be of the same order of magnitude for all z within the range of the model.

Equations (2.12) and (2.17) have an advantage in that neither is directly dependent upon the plume parameters σ_x and σ_z . This is valuable when marker particles from different sources (and in general different plume dimensions) intermingle. To treat them as separate plumes would be unrealistic in this situation.

2.6 Sub-grid Scale Diffusion

It can be shown (Lange, 1973) that when the particle distribution cannot be resolved by the grid mesh, errors in diffusion rates occur. This happens when continuous sources much smaller than the grid spacing are modelled. The problem is compounded in the presence of advection because the errors of inadequate resolution are carried downstream.

This problem was treated in the following way. The initial shape of the plume was assumed to be Gaussian. The particles were dispersed, the plume retaining its initial shape, until the plume could be resolved by the grid mesh. At this point

the locally-Gaussian assumption was discarded and diffusion was determined by the grid point concentration gradient method.

The Gaussian diffusion velocity can be found in the following way. Assume the concentration field in one dimension to be given by

$$X = \frac{Q}{\sqrt{2\pi}\sigma_x} \exp\left[-\frac{X_D^2}{2\sigma_x^2}\right] \quad (2.19)$$

where Q is the source strength, σ_x the plume standard deviation and X_D the distance from the particle to the plume center of mass. From the definition of the diffusion velocity

$$\vec{U}_D = -K_{xx} \frac{\partial \ln X}{\partial x} \quad (2.20)$$

Substituting from (2.19),

$$\vec{U}_D = \frac{K_{xx} \cdot X_D}{\sigma_x^2} \quad (2.20)$$

The diffusion velocity can also be written

$$\vec{U}_D = \frac{\partial X_D}{\partial t} \quad (2.21)$$

Equations (2.20) and (2.21) can be combined and integrated over the length of the timestep to yield a diffusion distance ΔX_D . However, assumptions must be made about the time- and space-dependence of K_{xx} and σ_x . For a constant diffusivity, $K_{xx} = \text{constant}$,

$$\sigma_x^2 = \sigma_{ox}^2 + 2K_{xx}t \quad (2.22)$$

where σ_{ox} is the initial standard deviation in the x-direction.

For this case the diffusion distance can be shown to be

$$\Delta X_D = X_D \left[\left(1 + \frac{\Delta t}{(\sigma_{ox}^2 / 2K_{xx}) + t} \right)^{1/2} - 1 \right]. \quad (2.23)$$

For three-dimensional, scale-dependent diffusion, Walton (1973) gives the following relations

$$K_{xx} = c\varepsilon^{1/3} \sigma_x^{4/3} \quad (2.24)$$

$$\sigma_x^2 = (\sigma_{ox}^{2/3} + 2/3 c\varepsilon^{1/3} t)^3 \quad (2.25)$$

where ε is the rate of eddy energy dissipation and c is a constant of the order of 1. Because the vertical turbulence is to a large extent suppressed, a case can be made for using Lin's (1972) two-dimensional forms of (2.24) and (2.25).

However, they were not used here. With $c = 1$, the diffusion distance can be shown to be

$$\Delta X_D = X_D \left[\left(1 + \frac{\Delta t}{1.5 \left(\frac{\sigma_{ox}}{\varepsilon} \right)^{1/3} + t} \right)^{3/2} - 1 \right]. \quad (2.26)$$

Similar relations hold for the vertical direction. The total distance travelled by the particle is then

$$\Delta X = \Delta X_D + u_A \Delta t. \quad (2.27)$$

It should be noted that the sub-grid scale diffusion scheme was used only to produce a realistic source configuration on a

scale that can be resolved by the grid mesh. The grid was assumed to resolve the plume when the standard deviation of the plume becomes greater than one cell length (i.e. $\sigma_x \geq \Delta x$).

2.7 The Source

The source under consideration in this model was a plume resulting from automobile exhausts. Although hydrocarbons, particulates, carbon dioxide, water vapor, and oxides of sulphur and nitrogen are also exhaust components, only carbon monoxide was considered. In addition it was assumed that CO is a chemically inert species, although this is not precisely true (Sandhu, 1975).

In general the diffusion of pollutants from motor vehicles depends on the following factors (Fanaki and Kovalick, 1974):

- 1) number, type and age of the vehicle used,
- 2) geometry and configuration of roadways,
- 3) emission rate (a function of vehicle speed),
- 4) vehicle aerodynamics and vehicle spacing on the road, and
- 5) atmospheric variables.

Included in 5) above are factors such as wind speed and direction and atmospheric stability. Factors 1) and 3) can be approximated by using an appropriate value of the emission factor, as in

Taylor (1973). By restricting the model to two dimensions, the complexity of factor 2) is reduced. See Section 3.6 for details of the roadway configuration.

The last two factors contribute to the shape of the exhaust plume in two ways. Exhaust buoyancy is created by a high exhaust temperature (a typical value is 227 C). The height of rise, and so the vertical dispersion of the plume, are dependent on stability. One means of dealing with this is by determining an effective source height, where the effective height is defined to be that height where buoyant rise can be neglected. In addition, mechanical mixing is important in the wake of the moving vehicle. Because horizontal dispersion is augmented by mechanical mixing, Fanaki and Kovalick (1974) assume a virtual point source to exist upwind of the roadway under the effect of an across-road wind. Danard (1972) uses a value of $20 \text{ m}^2 \text{ s}^{-1}$ for K_{zz} in the lowest 3 m as a means of dealing with increased vertical dispersion.

In practice the present model treated factors 4) and 5) in a common fashion. Buoyancy was ignored and the source was assumed to be at ground level. The effects of mechanical mixing were dealt with by assuming constant values for the initial horizontal and vertical standard deviation of the plume. See Section 3.7 for the particular values used.

CHAPTER III

THE MODEL - PARAMETERIZATION

3.1 Introduction

Chapter II contains the theory that forms the basis of the model. In this chapter, model parameters are introduced, finite-difference forms for the equations are inspected and the calculations used in the computer code are reviewed.

3.2 The Valley

Although the model can, with minor modifications to the computer code, accomodate a valley of any well-behaved shape, the valley shape chosen was a simple V. This simplified the production of an advection velocity featuring return flow and was thought to be a reasonable starting point in determining the suitability of the Particle-in-Cell approach for modelling

valley winds on this scale. The model used a valley depth of 50 m and a width of 800 m although they were input variables and could be changed to suit the application. These dimensions are approximately those of the North Saskatchewan River valley in Edmonton. Experiments at this site provided both input data and verification data. Summaries of the experimental results can be found in Paterson (1978) and Hage (1979).

Because the valley wind system was assumed to fill the valley, the model assumed no large scale flow; in this application the model was independent of the overlying flow. Thus, the valley may be oriented in any direction. The domain of the model extended from the valley bottom to the ridge in the vertical and from ridge to ridge in the horizontal. Again, the model has the capability of an extended range in the vertical by altering the appropriate input parameter. This will necessitate the specification of an overlying flow.

The choice of grid size depends on the scale of the flow to be modelled and on the scale of the turbulence to be resolved. The grid size (along with the length of the timestep) was also chosen so as to minimize efficiently the truncation errors inherent in the finite-difference schemes that were used. The cells were chosen to be of uniform size throughout the grid. They were rectangles and varied in height from 2 to 5 m and in length from 20 to 40 m, although the size was constant during each run. Again, grid size was an input variable.

3.3 Cell Areas

Subroutine SRAREA of the program (Appendix B) computes the sizes of all cells in the grid. This allows the model to use a valley of arbitrary shape. Associated with an arbitrarily shaped valley are cells of arbitrary shape. The code assumes, however, that the valley surface is linear between grid points. Since the valley was chosen to be V-shaped, minor modifications must be made to the computer code to allow for an arbitrary valley shape. In particular, the slope which in this application is constant must be allowed to vary.

The cell mesh was set up throughout the entire domain of the model. The cell number was chosen to be a two-dimensional array with origin at the bottom left cell coordinate. In this way cell number was linked directly to cell position. The cell area was defined to be that area within the valley "atmosphere", excluding any part below the valley groundline. The four corners of each cell were checked to see whether they were above or below the valley surface. The parameter N was introduced to facilitate this. Beginning at the lower left corner, N was increased appropriately if the corner in question was above the valley surface. See Figure 3.1. For example, if the upper right corner was in the free atmosphere, $N = N + 100$. For a cell totally above ground, $N = 1111$. Based on the value of N, an appropriate scheme was used to calculate the cell area. The area of a "complete" cell was simply the product of horizontal

and vertical grid spacing. The area of a cell totally below groundline was set to -1. The area of "incomplete" cells was found by finding the intersection of the cell walls and the valley groundline. Since the valley was linear between grid-points, the area was found by the appropriate summing of the areas of smaller rectangles and triangles.

3.4 The Advection Velocity

According to the experimental results in Paterson (1978), an average value for the magnitude of the downslope wind in the time period from 2200 to 2400 MST was approximately 0.2 ms^{-1} although the real wind is quite variable. By varying the constant in (2.9), it was possible to produce advection velocities of this magnitude. The difference between downslope and horizontal was neglected because of the shallow slope in this application. Setting the constant $C = 4.0$, the maximum value of $|u_A|$ approached 0.5 ms^{-1} ; $|w_A|$ approached 0.07 ms^{-1} . This ensured a reasonable value for u_A . Note that although the wind field in the present application was steady state, considerable complexity could be introduced by choosing the "constant" C to be time-dependent. In fact, Defant's (1951) diurnal variation of an idealized valley wind could be approximated in two dimensions. If the height of the inversion and the eddy diffusivities are also allowed to be time varying, then the

valley wind system can be made quite realistic.

The vertical shear of the horizontal advection velocity was also investigated for comparison with that observed in the North Saskatchewan River valley. Figure 3.2 shows the results for a position near the middle of the valley slope. The advection velocity assumed by the model had a vertical shear that was similar to the observed shear for the time period in question. A similar shear existed at the upper boundary even though this may not be realistic. The model wind had its maximum velocity at the valley surface; whereas, the real wind has its maximum below 0.8 m but above a height of several centimeters above the surface (the viscous sub-layer). In this respect, too, the model wind was not entirely realistic.

As mentioned in Section 2.2, the advection and diffusion velocities were defined at cell corners. The advection velocities were derived from the stream function field using central difference approximations

$$u_A(x, z) = \frac{\psi(x, z - \Delta z) - \psi(x, z + \Delta z)}{2\Delta z} \quad (3.1)$$

$$w_A(x, z) = \frac{\psi(x + \Delta x, z) - \psi(x - \Delta x, z)}{2\Delta x} \quad (3.2)$$

where Δx and Δz are the cell dimensions in the horizontal and vertical. The truncation error of u_A (w_A), that is, the magnitude of the remaining terms in a power series expansion of $\psi(x, z)$, is of the order of Δx^2 (Δz^2) (Haltiner, 1971). In

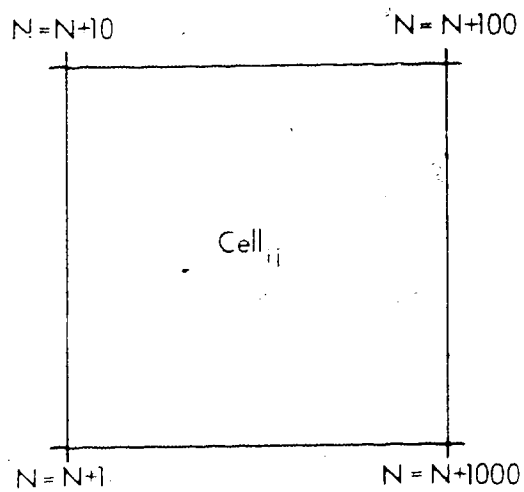


Fig. 3.1: Parameter N used in determining cell areas.

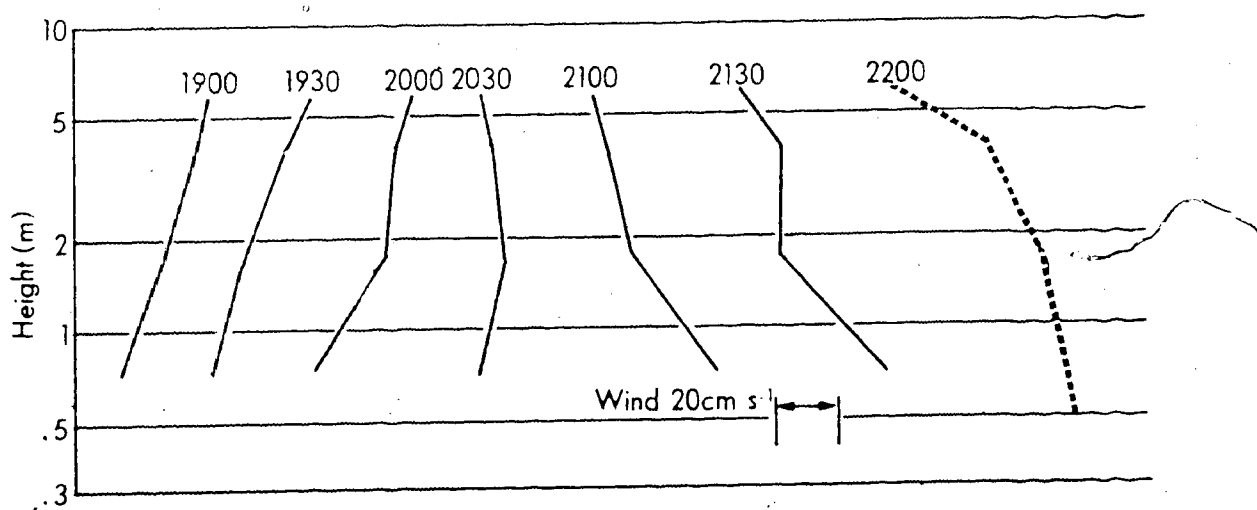


Figure 3.2: Experimental and model wind profiles. Solid lines are typical experimental profiles (from Hage, 1979). Dashed line is model wind profile. Local time.

general, the higher the order of the truncation error, the more accurate is the finite-difference approximation.

The program is capable of producing any desired wind speed by the choice of a value for the constant C . The user may also specify the advection velocities to be everywhere zero; that is, dispersion will take place by turbulent diffusion only.

3.5 The Diffusion Velocity

The diffusion velocity was defined in Section 2.4 as

$$\vec{U}_D = -K \frac{\vec{\nabla} \chi}{\chi} \quad (2.11)$$

A range of values for K are considered. Determine first an upper bound for the eddy diffusivities. On a flat plain in a stably stratified atmosphere (2.12) and (2.17) are valid. However, the presence of the valley adds complications. Two factors tend to limit diffusion. Firstly, the dimensions of the plume are controlled ultimately by the size of the valley. Secondly, the rates of horizontal and vertical diffusion are decreased by increased stability (Tennekes and Lumley, 1972). Since the inversion is more intense in the valley, diffusion there should be retarded relative to the flat plains. The relative magnitudes of these two factors in a small valley are uncertain. However, for simplicity it was assumed that they

cancel approximately any increase in dispersion which may be due to complex terrain in the valley. Therefore, as an upper bound consider the case of a slightly stable atmosphere in a constant-flux layer. Then (2.12) and (2.17) are approximately valid. As a first approximation, it is desired that K_{xx} and K_{zz} be of the same order of magnitude. Therefore, assume

$$K_{xx} = K_{zz} \cdot \frac{z^{1.07}}{z^{1.0}} = \frac{U_* k z^{0.07}}{\phi_m} \quad (3.3)$$

The value of the von Kármán coefficient k was set to 0.35. This procedure (3.3) is valid only for a time period near 1800 MST (see Figure 3.2), and was used only to find an approximate upper bound. A value of 0.1 ms^{-1} was suggested for U_* although it is an input variable. Because the non-dimensional shear ϕ_m is a function of stability ζ , the computer program also retains ζ as an input variable. A value of $\zeta = 1.05$ was used in this application. Use of these particular numbers resulted in values of K_{xx} and K_{zz} of the order of $0.1 \text{ m}^2 \text{ s}^{-1}$. However, in the time period under consideration the valley cannot be realistically thought of as having a constant-flux layer, as these equations imply. Without this simplifying assumption, formulations for K_{xx} and K_{zz} are probably more complex and are at present unknown. It has been shown, however, that an upper bound for the diffusivities should be of the order of $0.1 \text{ m}^2 \text{ s}^{-1}$. A further clue to their magnitude is that a large horizontal temperature gradient exists near the slope. With this in mind, an upper

bound for the diffusivities is suggested to be $K_{xx} = 0.1 \text{ m}^2 \text{ s}^{-1}$ and $K_{zz} = 5.0 \times 10^{-3} \text{ m}^2 \text{ s}^{-1}$. These were assumed to be constant throughout the valley. It should be stressed that, although the code was capable of calculating K_{xx} and K_{zz} directly from (2.12) and (2.17), this technique is valid only on a flat plain. Because forms of the diffusivities are unknown for small urban valleys, the present model experimented with a range of constant values.

Because the observed vertical velocity was very small, a reasonable lower bound for K_{zz} may be the kinematic viscosity ν . At a temperature of 10 C and a pressure of one atmosphere ν is approximately $1.8 \times 10^{-5} \text{ m}^2 \text{ s}^{-1}$.

A lower bound for K_{xx} was difficult to establish because guidelines do not exist as they did in the case of the upper bound. However, a much higher value than that for K_{zz} was expected because of the large horizontal temperature gradient near the slope. Using this fact as a guide, the model assumed a lower bound of $K_{xx} = 1.0 \times 10^{-3} \text{ m}^2 \text{ s}^{-1}$.

As stated earlier diffusion velocities were defined at cell corners and concentrations at cell centers. Therefore, \bar{x} was defined as the average concentration of the four cells adjacent to each corner. In the notation of Figure 3.3

$$\bar{x} = 1/4(x_1 + x_2 + x_3 + x_4) . \quad (3.4)$$

Consider the one-dimensional gradient $\nabla_x x$. In finite-difference form the gradient is written as

$$\nabla_x x = \frac{(x_1 - x_2 + x_4 - x_3)}{2\Delta x} \quad (3.5)$$

Therefore, the one-dimensional diffusion velocity U_{Dx} is written as

$$U_{Dx} = \frac{2K_{xx}}{\Delta x} \frac{(x_2 + x_3 - x_1 - x_4)}{(x_1 + x_2 + x_3 + x_4)} \quad (3.6)$$

Similar expressions are valid for $\nabla_x x$ and U_{Dz} . Equation 3.5 is accurate to second order in Δx .

The maximum diffusion velocity occurs when a single particle is surrounded by empty cells. The maximum velocity allowed by the computer code was

$$|U_D| = \frac{2 K_{xx}}{\Delta x} \quad (3.7)$$

A feel for the magnitude of the diffusion velocity can be found with the following example. For a horizontal eddy diffusivity of magnitude $0.01 \text{ m}^2 \text{ s}^{-1}$ and a horizontal grid spacing of 20 m, the maximum diffusion velocity was approximately 1 mm s^{-1} .

The diffusion velocity for cell corners below the valley groundline was set to zero. This acted to decelerate artificially particles diffusing toward the ground.

The advection velocities and diffusion velocities (when the particle was not considered part of a sub-grid scale plume) were interpolated to the particle positions from neighbouring grid points using a two-dimensional linear interpolation scheme. The forms for the horizontal u and vertical v velocities are given below in the notation of Figure 3.4:

$$u = \frac{x_2(U_2z_1 + U_1z_2) + x_1(U_4z_1 + U_3z_2)}{\Delta x \Delta z} \quad (3.8)$$

$$w = \frac{z_2(W_1x_2 + W_4x_1) + z_1(W_2x_2 + W_3x_1)}{\Delta x \Delta z} \quad (3.9)$$

3.6 The Source

It was stated in Section 2.7 that mechanical mixing due to vehicle motion is treated by assuming an initial source standard deviation. Zimmerman and Thompson (1975) assumed the standard deviation of the plume in the horizontal to be approximately equal to one-half of a car length and that the vertical standard deviation was somewhat less. The same logic was followed in this application. The initial horizontal standard deviation of the automobile plume was set to 3 m and the vertical to 2 m. Again, both parameters were input variables. The code used a Gaussian random number generator to produce

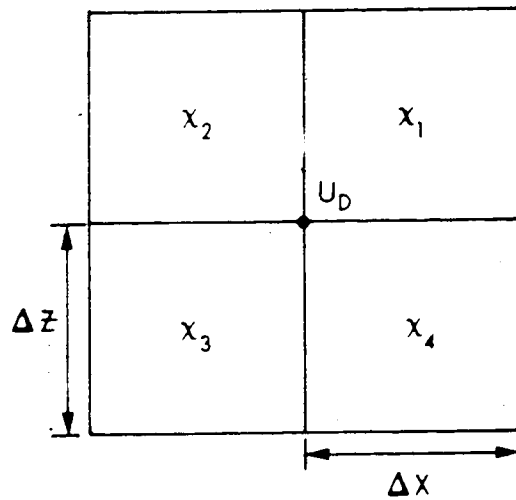


Figure 3.3: Scheme for calculation of diffusion velocity U_D .

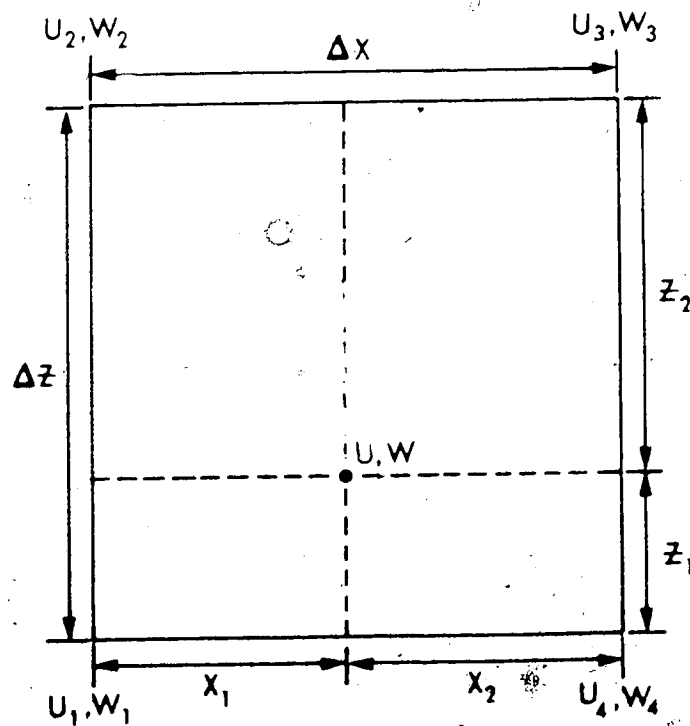


Figure 3.4: Velocity interpolation scheme.

particles of this configuration. These plume dimensions were valid only for the initial particle placement at each timestep. The variance of the plume at later times was calculated as the average of the sum of squared particle distances from the center of mass of the plume.

The number of particles produced at each timestep depended upon the traffic count at each source location. Ultimately the number depended upon the storage capacity of the computer and the expense of running the program. In its present form the code produced, on average, about 1 particle each second of model time. This was about 7000 particles for a two hour run. Naturally, the more particles produced at each timestep the better the resolution. Concentration and particle position fields were smoothed with increasing particle numbers. However, the time and cost of running the model with large numbers of particles can become prohibitive.

Each source in the model was essentially a point source (actually an area source because the plume had a finite initial dimension). Source coordinates were input to the program as variables. All sources at present were assumed to be on the surface of the slope. Since the model was two-dimensional, each point source represented an infinite line source running the length of the valley.

The mass per unit time of CO produced at each point source is given by

$$G = NV \cdot F \cdot EF \cdot D \quad (3.10)$$

where EF is the vehicle emission factor and D is the length of a segment of an infinite line source over which the emission factor is valid, NV is the total daily traffic count along the roadway, F is a fraction accounting for the diurnal traffic cycle and G is the mass of CO produced per unit time in km. Paterson (1978) used a value of 23 g km^{-1} per vehicle for the emission factor in approximating the traffic mix in the North Saskatchewan River valley. The same value was used here. The distance D was arbitrary but necessary when converting from model concentrations (particles per cell) to commonly used concentration units (ppm or gm^{-3}). A value of 50 m was assumed by the model.

The product $NV \cdot F$ yields the total number of vehicles passing through the distance D in one second. In this application the plume of only one source was modelled although the code set to ten the limit on the number of point sources that may be input. The point source modelled a line source such as River Road which runs parallel to and inside of the valley for a distance of several kilometers. The City of Edmonton (1978) provided traffic count data for River Road. These data were used to determine values for NV and F. The specific value used for NV was 16400 vehicles/day, a typical weekday total. A linear variation of traffic count with time was assumed for the hours 2200 to 2400 MST. With reference to Figure 3.5, the fraction F is of form

$$F = \frac{0.04 - 0.0075T/3600}{3600} \quad (3.11)$$

where T is model time in seconds. Hour zero model time is 2200 MST. The units of F are s^{-1} .

If one Lagrangian marker particle is equivalent to 0.20 grams of CO, then for a distance D of 50 m and cell dimensions as previously specified, the number of Lagrangian particles produced at each timestep is given by

$$N = 26.19 \Delta t (0.04 - 0.0075T/3600) \quad (3.12)$$

where Δt is the length of the timestep.

3.7 The Timestep

The choice of a timestep length is dependent upon several factors. Minimizing the timestep will minimize the truncation error inherent in the finite-difference schemes and will provide for smooth fields of concentration and particle position. Increasing the timestep will decrease computer costs. A third factor is also involved. Often one wishes to resolve "waves" or disturbances of a certain size in the concentration field. In this case, the length of the timestep should depend upon the "wavelength" to be resolved and on the particle velocity.

The model used an approach of this sort. The timestep was a function of the grid spacing and the maximum velocity components (Lange, 1973)

$$\Delta t = \text{MIN} \left[\frac{\Delta x}{2 u_{\text{max}}}, \frac{\Delta z}{2 w_{\text{max}}} \right] \quad (3.13)$$

This ensured that the maximum distance travelled by any particle was one-half of a grid spacing in any direction. Since the concentration field was found by summing the particles in a cell, the maximum resolution in the concentration field was the Nyquist wavelength - 2 grid lengths. The velocities u_{\max} and w_{\max} are the maximum velocities experienced by a particle. They are not velocities at grid points. The code allowed the timestep to be decreased as necessary from step to step but allowed an increase in the timestep of only 30%. This was to aid in stabilizing the model (Lange, 1973) although as a precaution only. The problem was not encountered here. It should be noted that the length of the first timestep must be input; the length of all later steps is calculated as in (3.13).

Once the length of the timestep had been calculated, the particle was advected along a pseudo-velocity streamline. The scheme used to do this was a forward timestep of the form

$$XP(t + \Delta t) = XP(t) + U_p \Delta t \quad (3.14)$$

where XP is the x-coordinate of the particle. The scheme is first order with respect to Δt . The calculation of a new vertical coordinate was identical.

3.8 Particle Trajectories and Reflections

Where a particle was transported below the groundline, the code reflected the particle back into the valley atmosphere.

In order to accomplish this the intersection of the particle trajectory and the groundline must be calculated. This was done in the following way. The slope of the trajectory could be calculated since the coordinates of the beginning and end points of travel were known. The slope of the groundline was given. Using an arbitrary point on each of these lines, the z-intercepts were determined and so the equation of each line. The calculation of the coordinates of intersection was then straightforward.

For a valley shape other than a simple V, the local slope must be estimated. In this case it was assumed that the distance travelled by the particle was small. Then the groundline between beginning and end points of travel could be assumed linear.

Once the intersection was known, the final, above-ground particle position could be determined. Refer to Figure 3.6. The distance AB could be found from the beginning and end points of the particle motion. The coordinates of the trajectory-groundline intersection were known. Therefore, the lengths OA and OB could be calculated. The slopes of the particle trajectory and groundline were known so that the angle of incidence i could be found. The point C was then determined, assuming the angles of incidence and reflection to be equal. The distances OB and OC were assumed equal; the "collision" of the particle with the slope was assumed elastic.

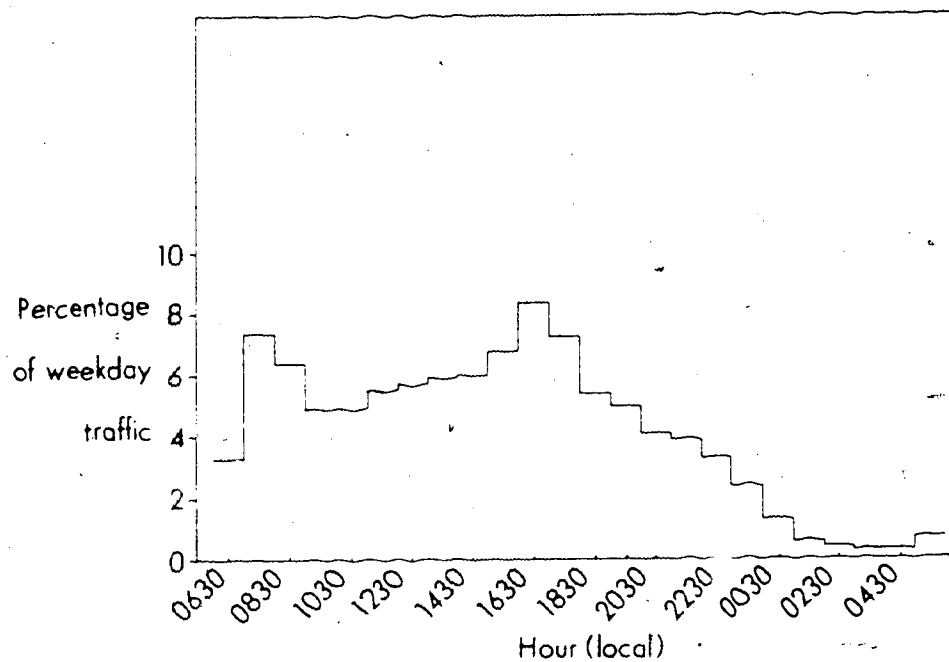


Figure 3.5: Weekday mean traffic. City of Edmonton: 1977.

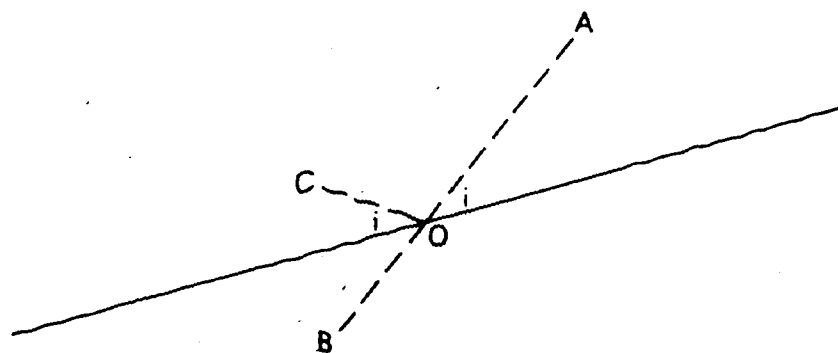


Figure 3.6: Reflection of particles at groundline (solid line). A denotes initial particle position. C denotes final position.

The above calculations necessarily involved the determination of the position of a particle relative to the valley surface. Either a particle was below the groundline or it was not. This entailed comparison of two numbers to the limits of their accuracy where errors due to computer round-off were important. Experience showed that those calculations compromised the accuracy of the last significant figure. The code, therefore, set an arbitrary accuracy limit. In cases where the position of a particle relative to the groundline was determined incorrectly beyond this limit, the particle involved was simply destroyed. Incorrect determination of particle position within the accuracy limit resulted in immediate termination of the computer run.

CHAPTER IV

RESULTS

4.1 General

In this chapter, the sensitivity of the model is appraised with regard to changes in grid spacing, magnitudes of the vertical and horizontal eddy diffusivities, initial sizes of the automobile exhaust plume, magnitudes of the advection velocity, and particle density.

Two methods were chosen to display predicted changes in CO concentration that result from variations of the above parameters. The first is a strikingly vivid scheme of plume visualization. Since the model represents pollutants as quantized particles, the locations of all particles within the grid can be displayed on a scatter diagram. Appendix A contains a series of these plume snapshots. Although they are very useful for displaying plume motion and relative density, they are of limited use in quantitative display. To this end a second form of display was used. Two points on the valley slope were chosen,

one 100 m downslope from the CO source and the other 50 m upslope from the source. At each of these positions, the CO concentration in parts per million of the three grid cells immediately above the valley surface was extracted at each timestep of the model. In practice, the length of the timestep ranged approximately from 12 s to 65 s depending on the particular parameters used, but was nearly constant during each simulation. For this reason, and to smooth the graphical output, the concentration in each of the chosen cells was averaged over approximately a three minute period. The result is a vertical profile of pollutant concentration as a function of model time at each location.

At this point it might be asked why the entire concentration field is not displayed and contoured, since this field was calculated and utilized as part of the computer code. The answer is that, in general, the boundaries of the cells and the valley surface were not aligned, nor was the valley surface coincident with the cell diagonals. Since the concentration of all cells totally below the valley surface was defined to be zero, computer contouring of the concentration field resulted in an unrepresentative display.

Table 4.1 contains a list of standard model input parameters. While some remained unchanged from run to run, others were allowed to vary as part of sensitivity analyses. The particular values appearing in Table 4.1 are those used by the computer

Table 4.1: Standard parameters of the computer model.
Parameters marked * are allowed to vary as part
of sensitivity analyses.

Parameter Symbol	Description	Value
L	valley width	800 m
HPRIME	valley depth	50 m
INCX*	horizontal grid size	20 m
INCZ*	vertical grid size	2 m
SDEVX*	initial horizontal standard deviation of exhaust plume	3 m
SDEVZ*	initial vertical standard deviation of exhaust plume	2 m
DKMX*	horizontal eddy diffusivity	$1 \times 10^{-2} \text{ m}^2 \text{ s}^{-1}$
DKMZ*	vertical eddy diffusivity	$5 \times 10^{-4} \text{ m}^2 \text{ s}^{-1}$
AVWF*	maximum advection velocity	0.5 m s^{-1}
TMAX	maximum length of simulation	7200 s
NS	number of sources	1
XS	horizontal coordinate of source	600 m
PWT*	representative weight of each particle	0.2 g CO

program in its standard simulation. Most sensitivity analyses were compared against this standard. It should be emphasized again that, although the computer code permits other alternatives, eddy diffusivities were held constant during each run. For the time period involved diffusivities were assumed to be independent of time and space. In all cases, source strength decreased linearly with time as in (3.11). Appendix B contains the complete computer program.

The remainder of this section contains a discussion of two important model assumptions. The first is conservation of mass. Although the advection field conserved mass, the presence of diffusion added complications. Were the two processes handled separately throughout the entire code, all particles diffusing through the upper boundary could have been annihilated. This mode would have increased the cost and decreased the accuracy of the computations. Instead, the model handled the two processes, as much as possible, as one and created the problem of determining whether an annihilated particle was diffused or advected through the upper boundary. The code dealt with this as follows. The ratio of maximum diffusion velocity to maximum advection velocity was computed. For the parameter of Table 4.1, this ratio was typically of the order of 10^{-3} to 10^{-5} or smaller. Thus, for example, every thousandth particle that was transported through the upper boundary was assumed to have been diffused there and was annihilated. Other

particles transported through the upper boundary were assumed to have done so because of the finite-difference representation of the advection velocity. For a two hour simulation, the number of particles annihilated as a result of this method ranged from zero to three. The total number of incidents of passage through the upper boundary was typically two to five thousand. Thus, the conservation of particle mass approximated the conservation of pseudo-velocity mass flux.

The second assumption concerns fictitious diffusion. Lange (1973) stated that the PIC technique on which the present model is based eliminates fictitious diffusion which is inherent in any Eulerian method. However, the term "fictitious diffusion" was not precisely defined and this caused some confusion. In its basic form, fictitious diffusion is caused by computer round-off. Multiple calculations increase the magnitude of the error. This type of error is impossible to eliminate in a numerical model. Fictitious diffusion is also created when concentrations and diffusion velocities are defined in terms of a grid. Theoretically, by choosing the grid and the timestep to be very small, these errors can be reduced to near the magnitude of the round-off error. In this application, predicted concentrations were sensitive to changes in cell size (see Section 4.3). Other processes contributing to fictitious diffusion were thought to be dominated by the effects of changes in cell size.

4.2 Gaussian and Concentration-Gradient Diffusion

As discussed in Section 2.4, the model relied on a concentration-gradient technique to simulate diffusion. For sub-grid size particle distributions, a Gaussian technique was used. This section briefly compares the dispersion produced by these two schemes.

For purposes of this comparison only, the source was positioned at the center of the valley (400 m, 25 m). The duration of the simulation was 20 minutes. Diagnostics indicated that, approximately 11 minutes after start-up, particles were reflected from the upper boundary. Since the source was at the valley center, reflection from the valley surface was expected at about the same time. Therefore, boundary effects will be minimized by examining dispersion within the first 11 minutes.

Figures 4.1a and 4.1b show dispersion estimated respectively by Gaussian and concentration-gradient diffusion at approximately 11 minutes after start-up. In both cases, vertical and horizontal diffusivities were set to a constant value of $0.1 \text{ m}^2 \text{ s}^{-1}$. Therefore, distortion of the plume from circular was produced by scaling. Horizontal grid spacing was 8 m; vertical grid spacing was 5 m. Initial size of the plume was large enough so that, for the case of concentration-gradient diffusion, the initially-Gaussian specification was unnecessary.

Some differences are evident between Figures 4.1a and 4.1b. The plume of Figure 4.1b appears smoother and more disperse.

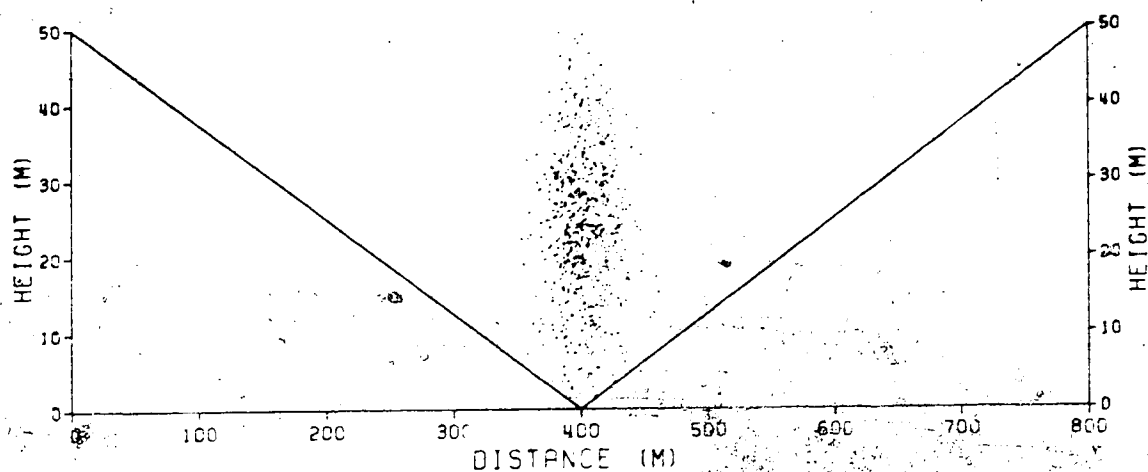


Figure 4.1a: Gaussian dispersion of plume at $t=646s$.

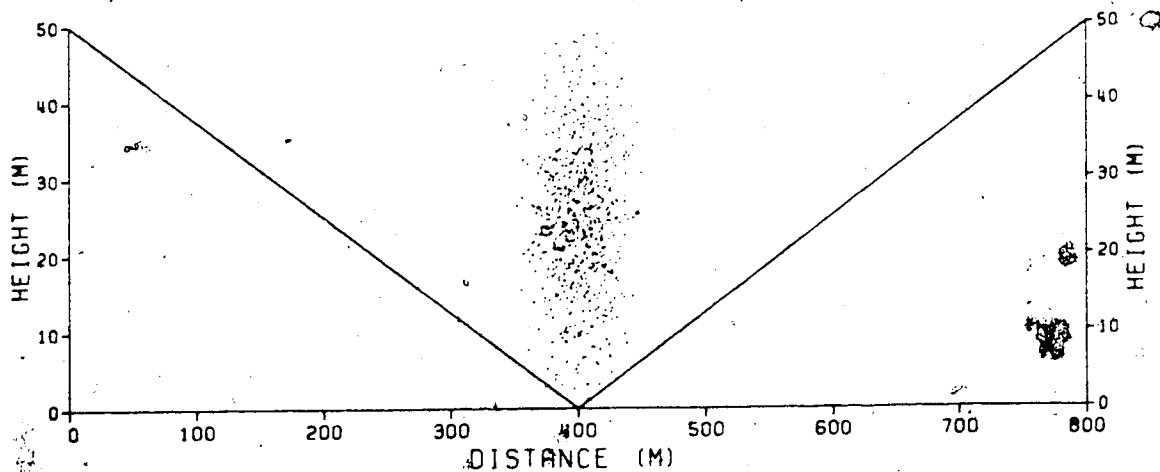


Figure 4.1b: Concentration-gradient dispersion of plume at $t=664s$.

In both cases approximately 650 particles were produced (about 1 particle each model second). However, due to the differences in method, the length of the timestep (and the number of particles produced each timestep) was larger by approximately 20% in the case of concentration-gradient diffusion. This is opposite to what might be expected by examining Figures 4.1a and 4.1b. The method with the larger timestep might be expected to produce a larger particle density near the center of the plume. Figure 4.1c is a plot of concentration vs. time of one model run for a cell with center at (428 m, 27 m). Plotted is the unsmoothed concentration at every fourth timestep. The concentration quantum was $0.025 \text{ particles/m}^2$. Figure 4.1c illustrates qualitatively that the rates of diffusion produced by the two methods are approximately equal on the large scale. This suggests that when the calculation of distance diffused by particles transfers from Gaussian to concentration-gradient technique, the change will not result in a discontinuity in the rate of diffusion. Differences in the appearance of Figures 4.1a and 4.1b may also be attributed to small variations in the rate of diffusion evident in Figure 4.1c.

4.3 Sensitivity to Cell Size

In this section the sensitivity of the computer model to changes in cell size (grid spacing) is investigated. The results

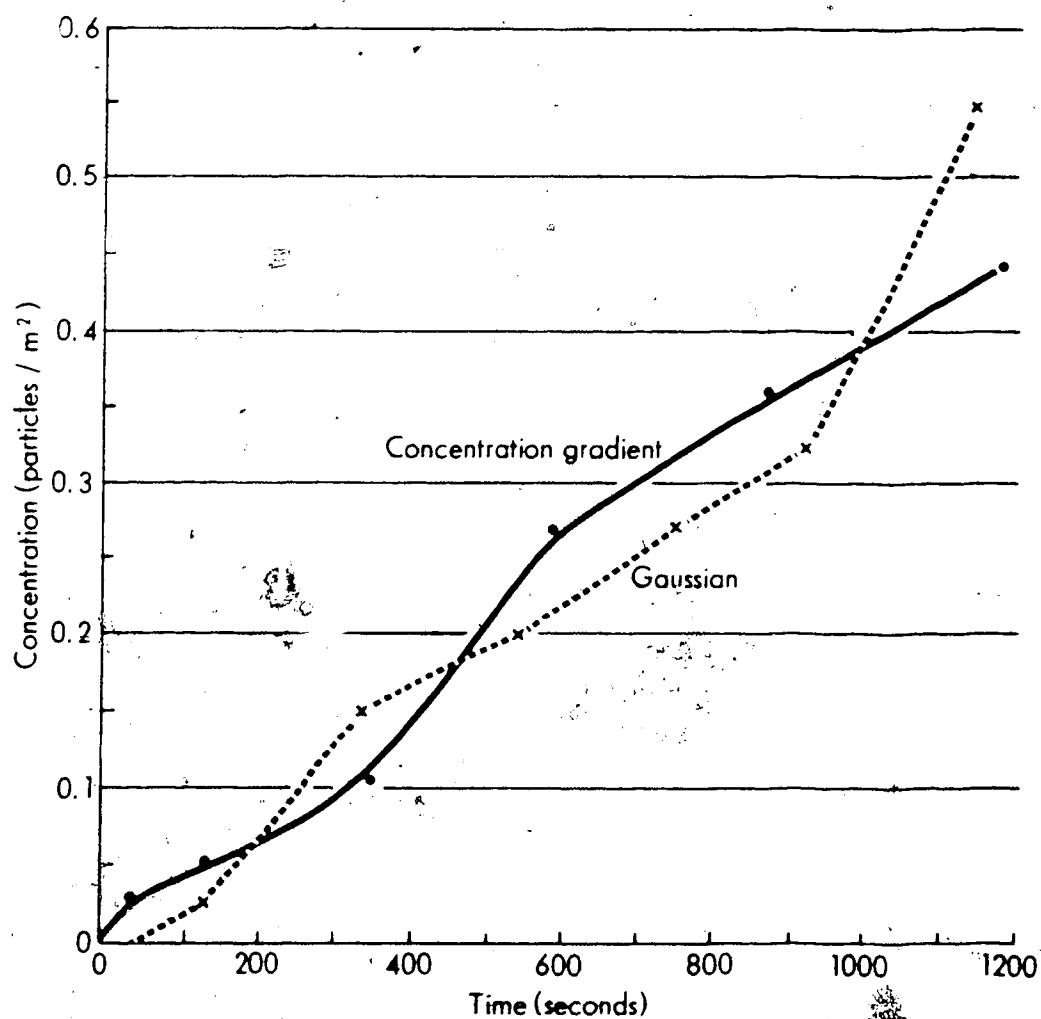


Figure 4.1c: Comparison of concentration-gradient and Gaussian diffusion. Concentrations at times greater than 600 s may be influenced by the boundary.

of a simulation using values of the parameters as listed in Table 4.1 are shown in Figures 4.2a to 4.2d. Figures 4.3a to 4.3d are the results using parameters as in Table 4.1 except that $INCX = 40$ m and $INCZ = 5$ m, i.e., the area of each cell was increased fivefold.

Immediately obvious from a comparison of Figures 4.2a and 4.3a with 4.2b and 4.3b is the fact that the smaller grid produced a smoother particle distribution. Both cell sizes showed a tendency for accumulation of particles in the lowest portion of the valley in the region of reduced wind speed. Also, both showed tendencies for particle accumulation in a preferred ring near the axis of the plume. This appears to be the path taken by the majority of particles around the valley vortex and may be due in part to convergence which may be produced by the interaction of the advection and diffusion velocities but more likely to the fact that most particles are emitted at this height and not diffused substantially from it (see Appendix A). Also of interest are the observations that the particle distribution did not reach steady state after 2 h model time (as expected) and that, at 2 h, a number of particles had diffused to the opposite side of the valley. These Figures show another interesting effect of changes in cell size. In a purely Eulerian mode, increased cell size generally "smears out" the concentration field, that is, distributes the pollutant over a wider area. However, the effect of increased cell size

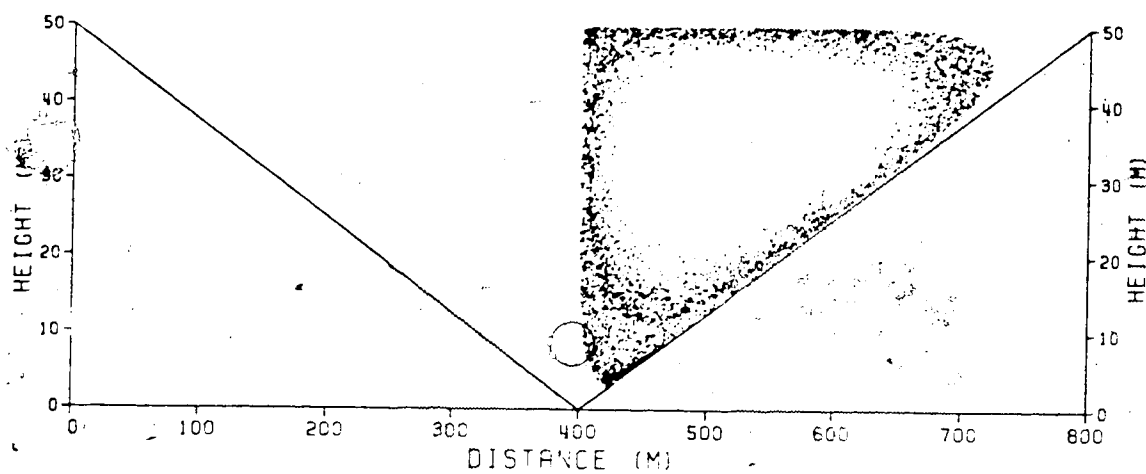


Figure 4.2a: Particle distribution produced by standard parameters (Table 4.1) at $t=3610s$.

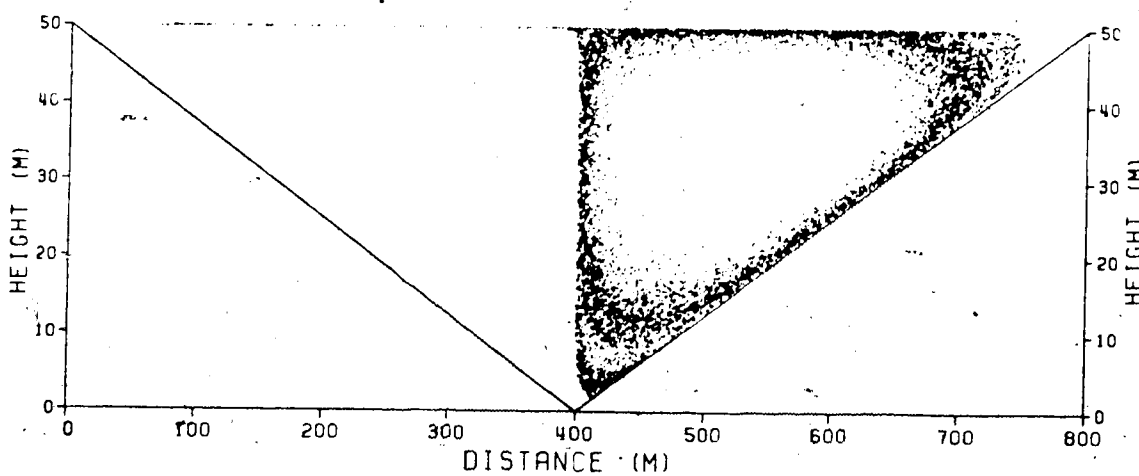


Figure 4.2b: Particle distribution produced by standard parameters (Table 4.1) at $t=7181s$.

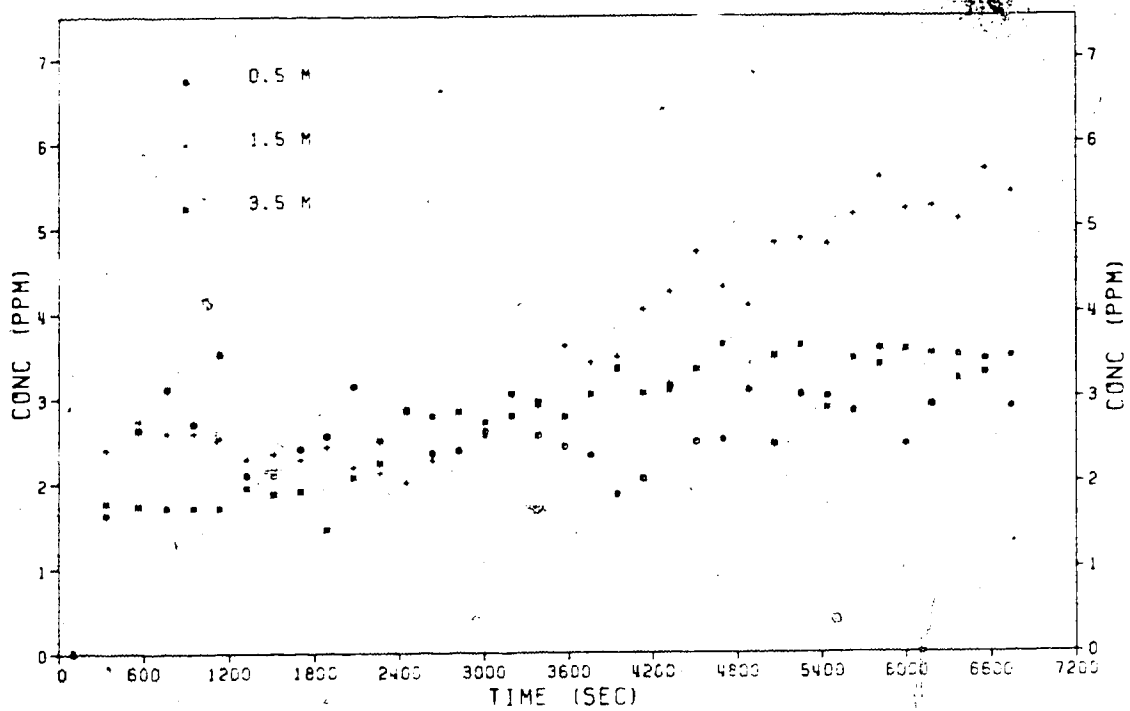


Figure 4.2c: Vertical profile of concentration 100m downslope from source produced by parameters of Table 4.1.

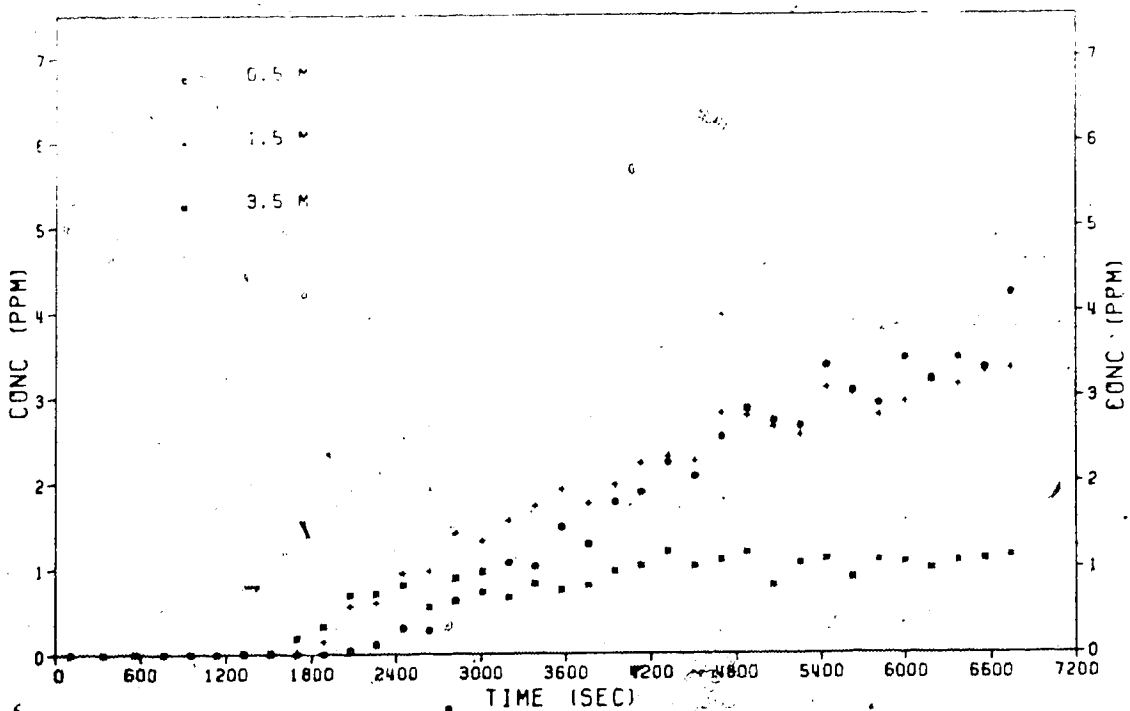


Figure 4.2d: Vertical profile of concentration 50m upslope from source produced by parameters of Table 4.1.

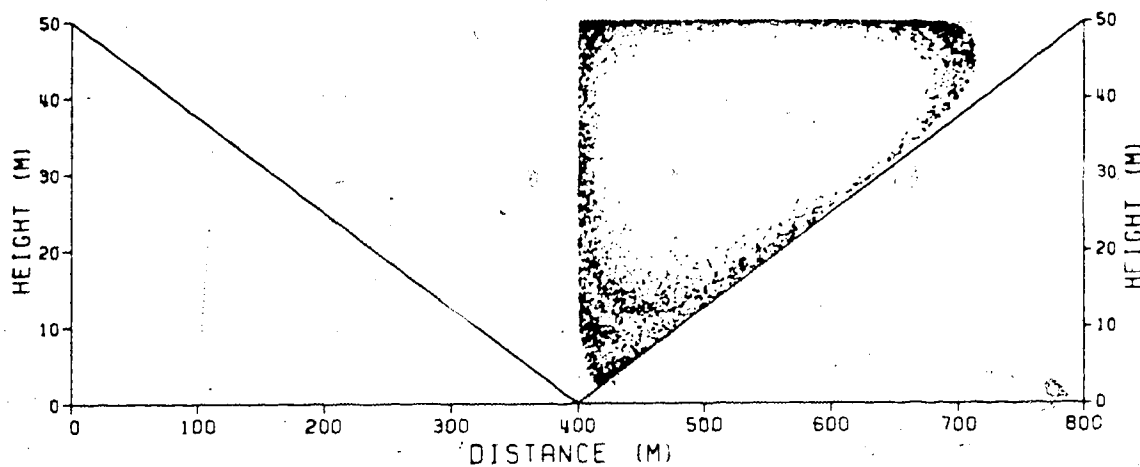


Figure 4.3a: Particle distribution at $t=3608s$ produced by parameters of Table 4.1, except that $INCX=40m$ and $INCZ=5m$.

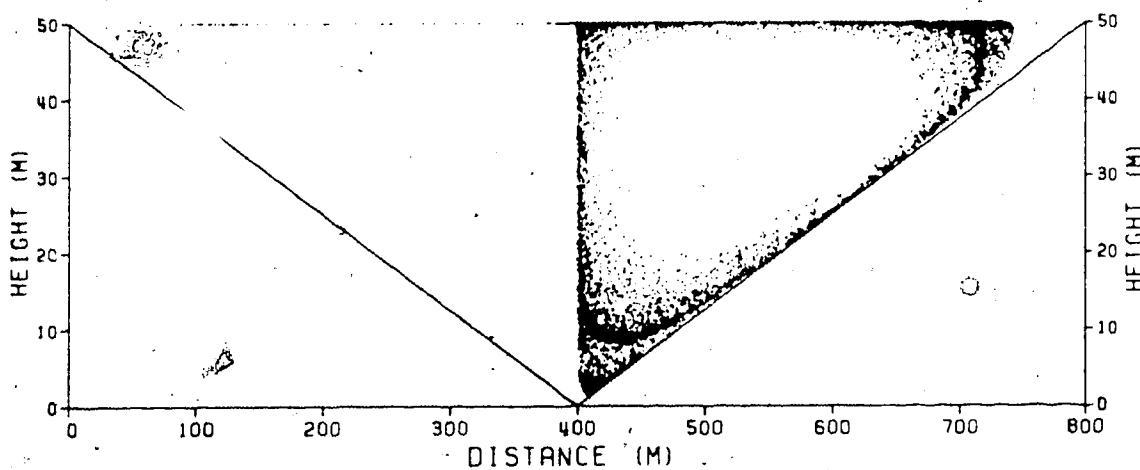


Figure 4.3b: Particle distribution at $t=7195s$ produced by parameters of Table 4.1, except that $INCX=40m$ and $INCZ=5m$.

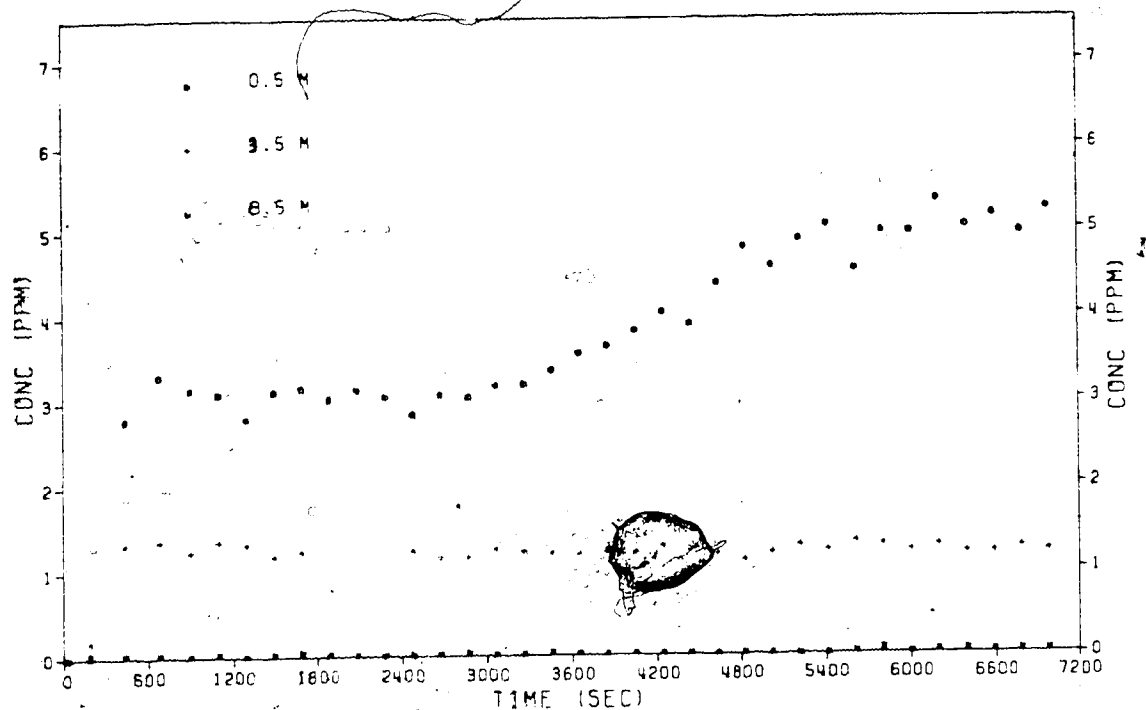


Figure 4.3c: Vertical profile of concentration 100m downslope from source produced by parameters of Table 4.1, except that INCX=40m and INCZ=5m.

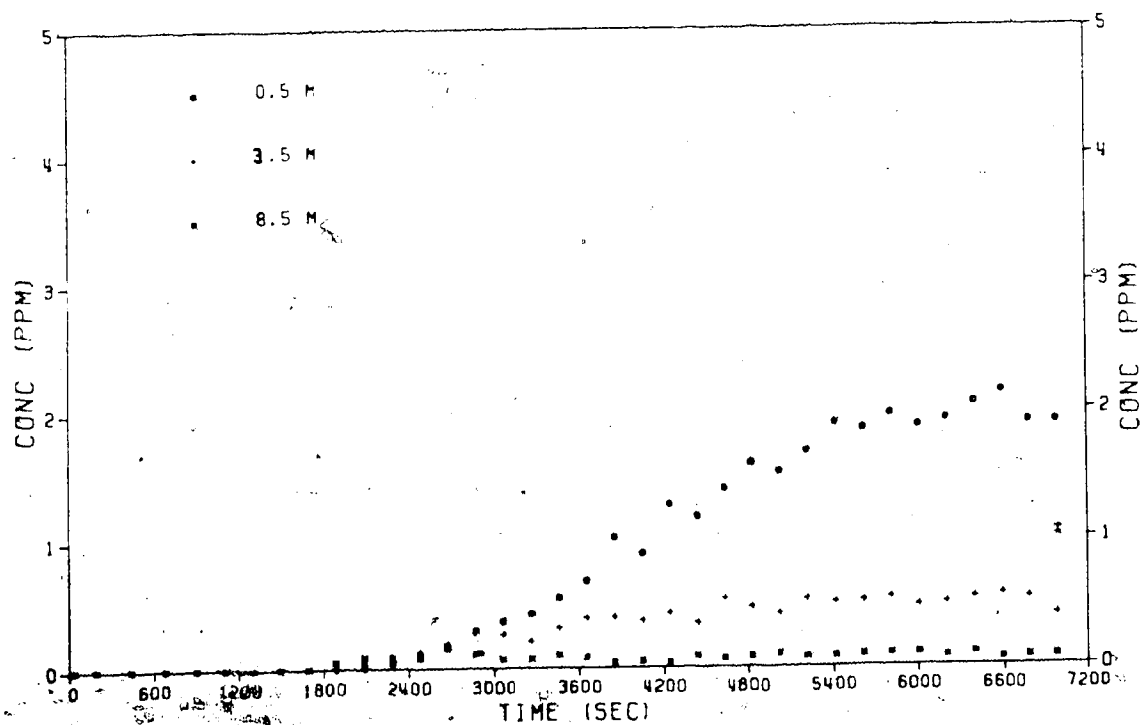


Figure 4.3d: Vertical profile of concentration 50m upslope from source produced by parameters of Table 4.1, except that INCX=40m and INCZ=5m.

on the present model appeared to be opposite. Particles accumulated near the upper boundary (and to a lesser extent near the valley center) rather than dispersed. The reason for this is unknown but indicated that the model was sensitive to changes in grid size.

The vertical profiles of concentration at the downslope "station" (100 m down the slope from the source), Figures 4.2c and 4.3c show interesting differences. While maximum concentrations in both cases were between 5 and 6 ppm, in the case of the larger grid the maximum occurred in the lowest cell, as might be expected. For the smaller grid the maximum occurred near 1.5 m. Again, this may be a result of the preferred track produced by the advection field, since movement by advection dominated movement by diffusion. Concentration curves were smoother for the larger grid because gain or loss of particles resulted in a smaller fractional change in concentration. Figure 4.2c illustrates that, for the smaller grid, concentrations in the lowest two cells were similar and variable for approximately the first hour. At that time the return flow had accumulated a sufficient number of particles in the cell centered at 1.5 m so that differentiation was possible. Concentrations in the highest and lowest cells remained equal and constant near 3 ppm. The concentration of the cell centered at 3.5 m in Figure 4.3c was much less than that of Figure 4.2c. Presumably this was due to its larger sampling interval in the vertical. The concentration of the 8.5 m cell

in Figure 4.3c was not influenced by the return flow.

Figures 4.2d and 4.3d show the vertical profile of concentration 50 m up slope from the source. All effects here were due to return flow; diffusion from the (downwind) source did not occur. The maximum concentrations observed at the 0.5 m and 3.5 m levels of the small grid case (Figure 4.2d) were approximately twice those of the large grid. The presumption that this is due to a smaller sampling extent in the vertical appears to be valid for the 3.5 m cell but not for the 0.5 m cell. Referring to Figure 4.2d, both the 0.5 m and 1.5 m cell reached concentrations of approximately 3.5 ppm. The 0.5 m cell of Figure 4.3d covers about the same vertical extent as the combined 0.5 m and 1.5 m cells of Figure 4.2d and yet the concentration was much less. The reason for this is not clear.

Comparison of Figures 4.2d and 4.3d also shows that the onset of fumigation occurred slightly earlier in the small grid case. An explanation for this may be found in the influence of the grid size that appears in the calculation of the timestep by (3.13). A larger timestep, combined with poorer resolution of the velocity field, may account for the delay in the case of the larger grid.

Another observation common to Figures 4.2d and 4.3d and reinforced by the results in Appendix A is that particles in the return flow arrived first in the upper-most of the lowest

three cells. This is consistent with the decreased path length and small vertical velocity gradient for elevated particles in the advection field.

Near the valley slope the plume was typically 5 m or less thick. The vertical dimension of the cells chosen ranged from 2 to 5 m. Because of this, changes in grid size resulted in large changes in cell concentration. This implies that smaller vertical grid sizes are needed in this application.

4.4 Sensitivity to Initial Source Size

Recall from section 3.6 that the initial size and shape of the automobile exhaust plume was produced by a normal random number generator with given horizontal and vertical standard deviations. In this section sensitivity of the model to changes in the initial size of the exhaust plume is investigated. The basis of comparison is Figure 4.2, produced using the parameters of Table 4.1. Figure 4.4 was produced using the parameters of Table 4.1 except that $SDEVX = 6$ m and $SDEVZ = 4$ m. The initial size of the plume was doubled. The most important consequence appears to be the doubling of the initial vertical extent of the plume.

Figures 4.2a, 4.2b, 4.4a, and 4.4b illustrate that, as expected, the plume produced with the larger initial size retained this size advantage throughout the 2 h simulation.

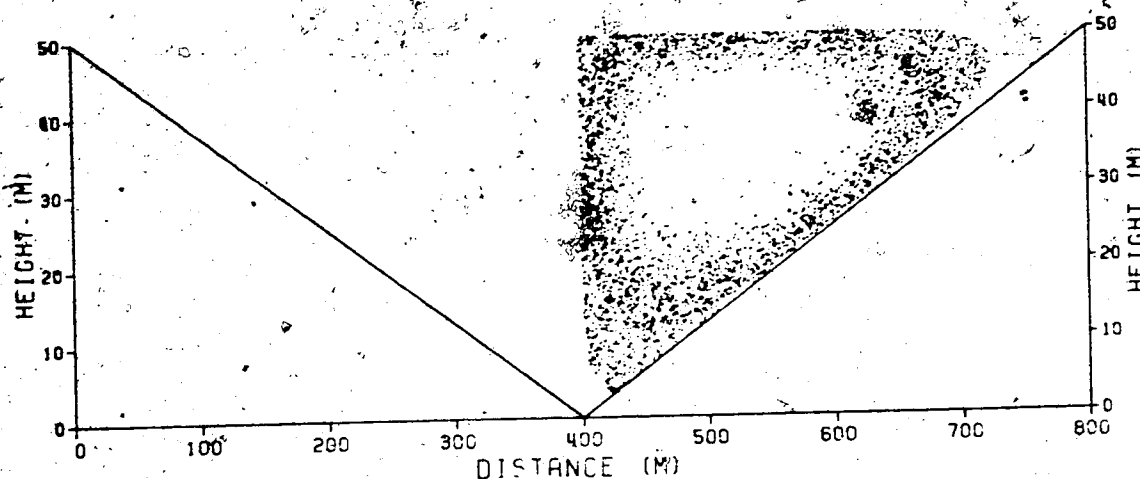


Figure 4.4a: Particle distribution at $t=3610s$ produced by parameters of Table 4.1, except that $SDEVX=6m$ and $SDEVZ=4m$.

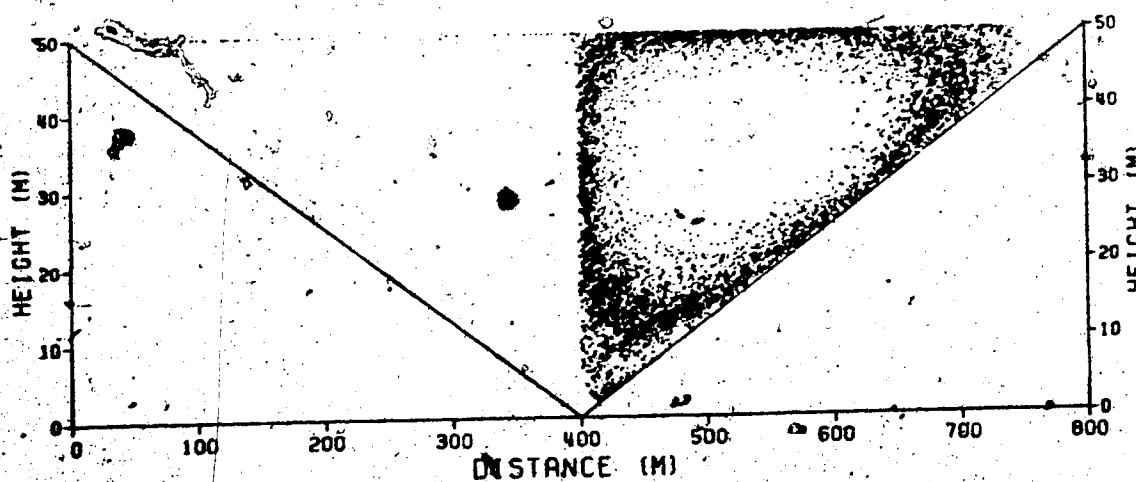


Figure 4.4b: Particle distribution at $t=7188s$ produced by parameters of Table 4.1, except that $SDEVX=6m$ and $SDEVZ=4m$.

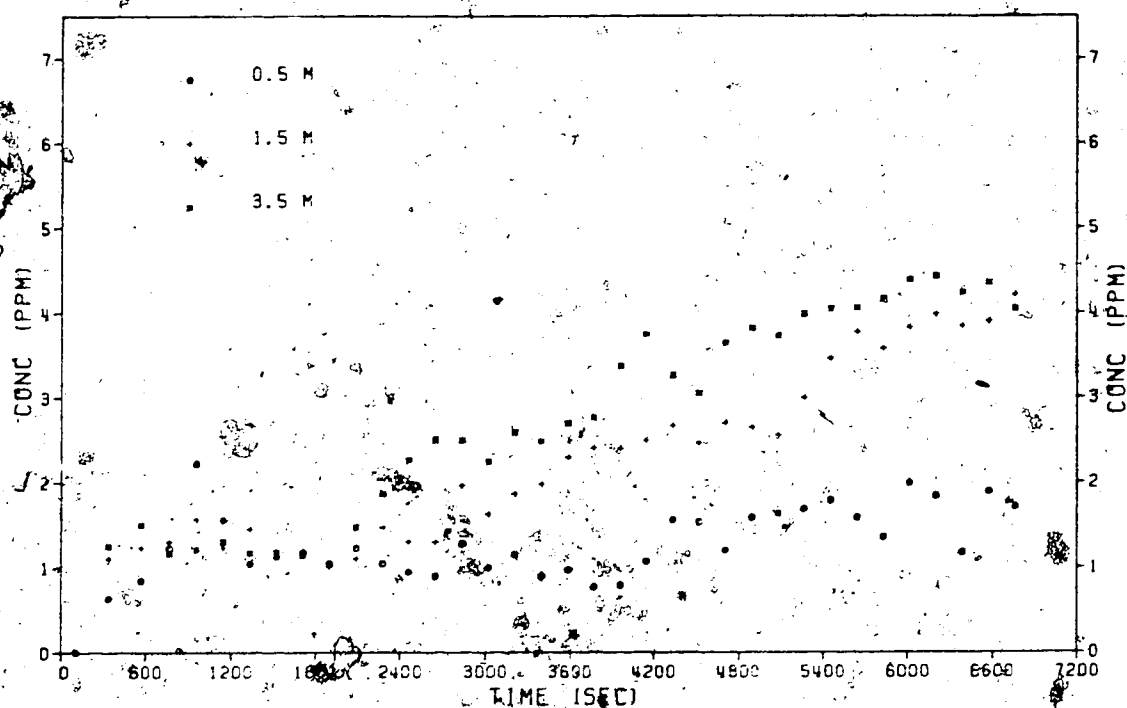


Figure 4.4c: Vertical profile of concentration 100m downslope from source produced by parameters of Table 4.1, except that SDEVX=6m and SDEVZ=4m.

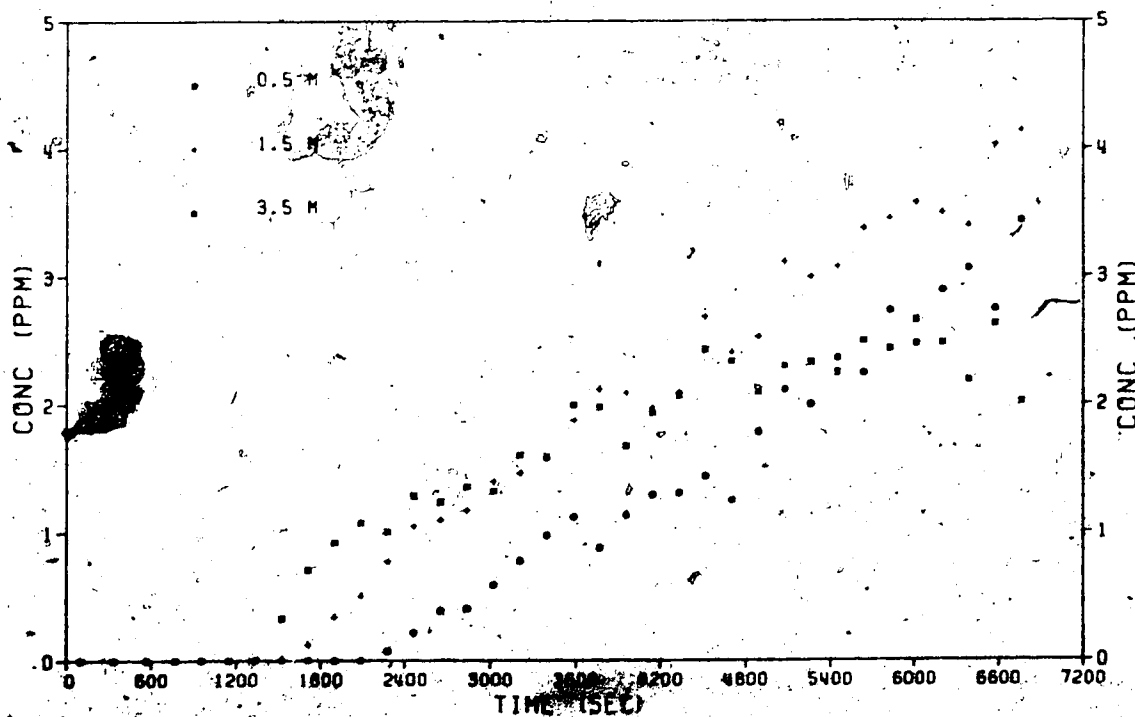


Figure 4.4d: Vertical profile of concentration 50m upslope from source produced by parameters of Table 4.1, except that SDEVX=6m and SDEVZ=4m.

Although the plume had a greater vertical extent in the large source case, the heights of the preferred path in both cases were similar. This again suggests that the preferred path was a result of the height at which the majority of particles were emitted.

Figures 4.2d and 4.4d reveal that, as expected, the 3.5 m cell received a larger share of the particles in the case of the large source size. These Figures show that the concentration in the 3.5 m upslope, large-source station reached more than 2 ppm, double that of the small source case. There was a general shift to larger concentrations in the upper cells. In both cases maximum concentrations at the upslope position were near 4 ppm at the end of the 2 h simulation.

Similarly, a comparison of Figures 4.4c and 4.4b shows an increase in the concentration of the upper cell in the large-source case. The concentration increased from about 3.5 ppm to 4.5 ppm. The lower two cells both experienced decreases in concentration. In the 0.5 m cell, it dropped from approximately 3 to less than 2 ppm. At the 1.5 m level, the concentration decreased to 4 ppm from about 5.5 ppm. Although the maximum concentrations were lower in the large-source case, the particles were distributed more evenly in the upper cells. This is evident in Figure 4.4b.

One indication that the pollutant was more evenly distributed in the large-source case is shown by the uniformity of the 1.5 m concentration. Figures 4.4c and 4.4d illustrate that, at

this height, concentrations at the upslope and downslope positions were approximately equal at most times. With increased source size, concentrations apparently became less dependent on position of measurement on the slope.

4.5 Sensitivity to Particle Density

This section examines the sensitivity of the model to a reduction in the particle density necessary for adequate resolution. Simulations were made using the parameters of Table 4.1, except that $PWT = 0.4 \text{ g CO}_2$, i.e., compared to Figure 4.2, approximately one-half the number of particles were created at each timestep, each representing twice the mass of CO_2 . Figure 4.5 is the result of this simulation; Figure 4.2 is the basis for comparison.

The particle position plots, Figures 4.5a and 4.5b, yield no new insights. There are no significant differences between these Figures and Figures 4.2a and 4.2b, except for the expected density difference.

Comparison of Figures 4.2c and 4.5c reveals no change in average concentration in any of the cells. However, there is more variability in the curves representing the less dense particle distribution, Figure 4.5c. Similar comments are valid concerning comparisons of Figures 4.2d and 4.5d.

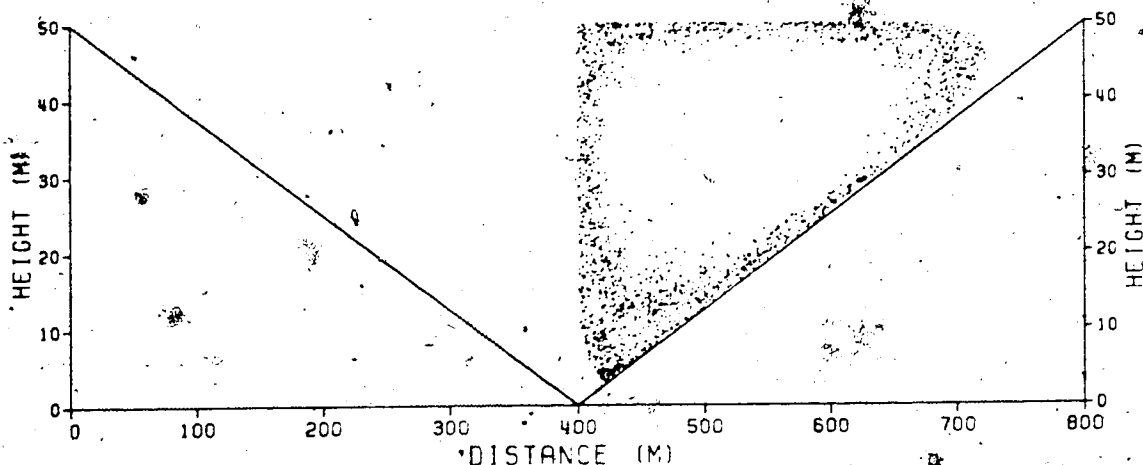


Figure 4.5a: Particle distribution at $t=3609s$ produced by parameters of Table 4.1, except that $PWT=0.4g\ CO$.

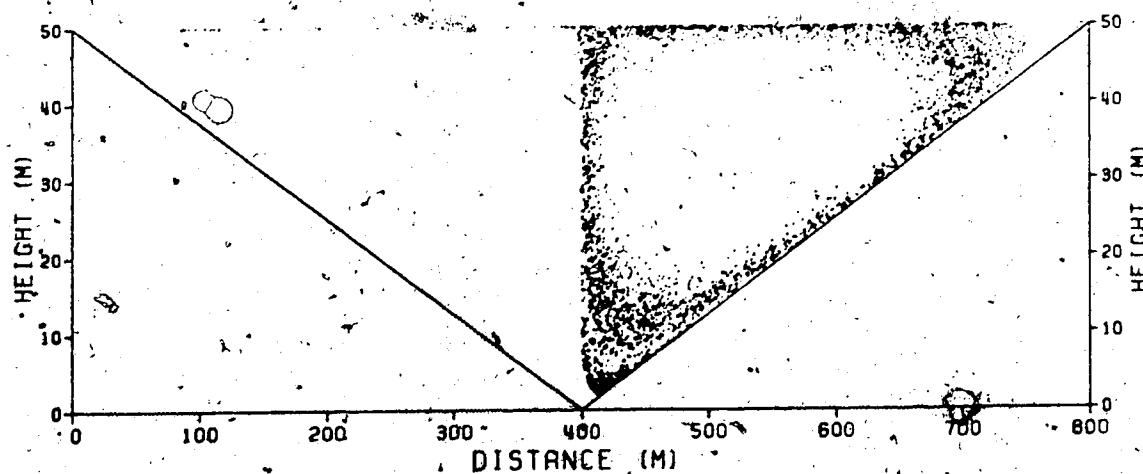


Figure 4.5b: Particle distribution at $t=7189s$ produced by parameters of Table 4.1, except that $PWT=0.4g\ CO$.

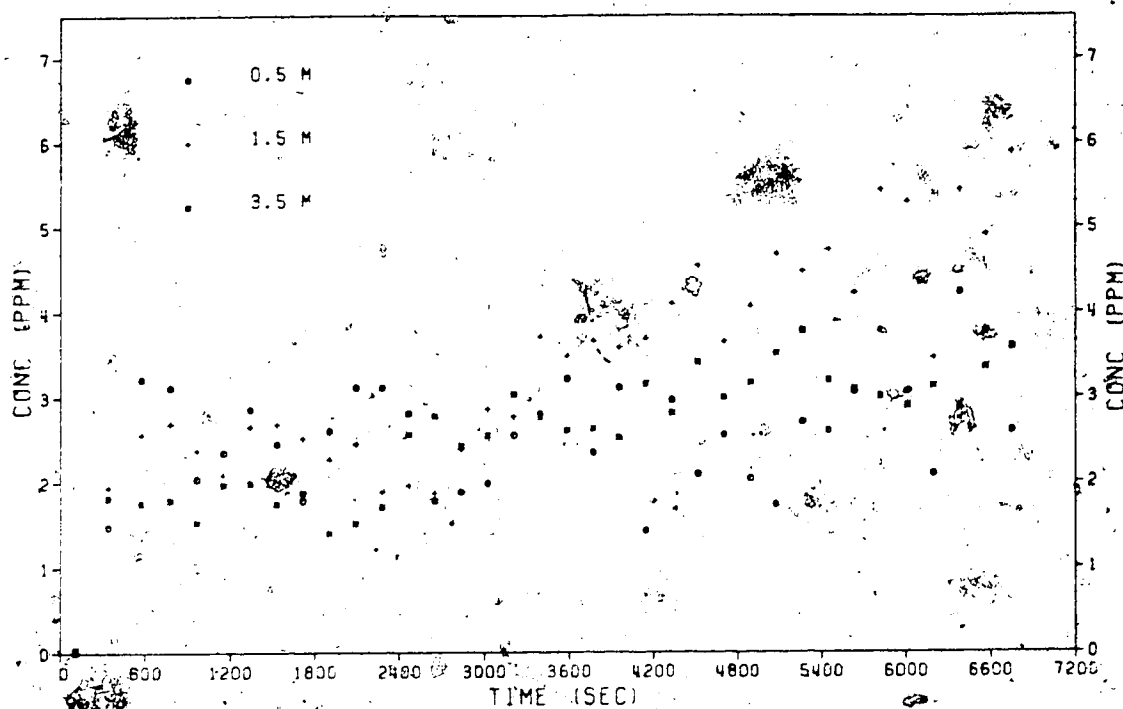


Figure 4.5c: Vertical profile of concentration 100m downslope from source produced by parameters of Table 4.1, except that PWT=0.4g CO.

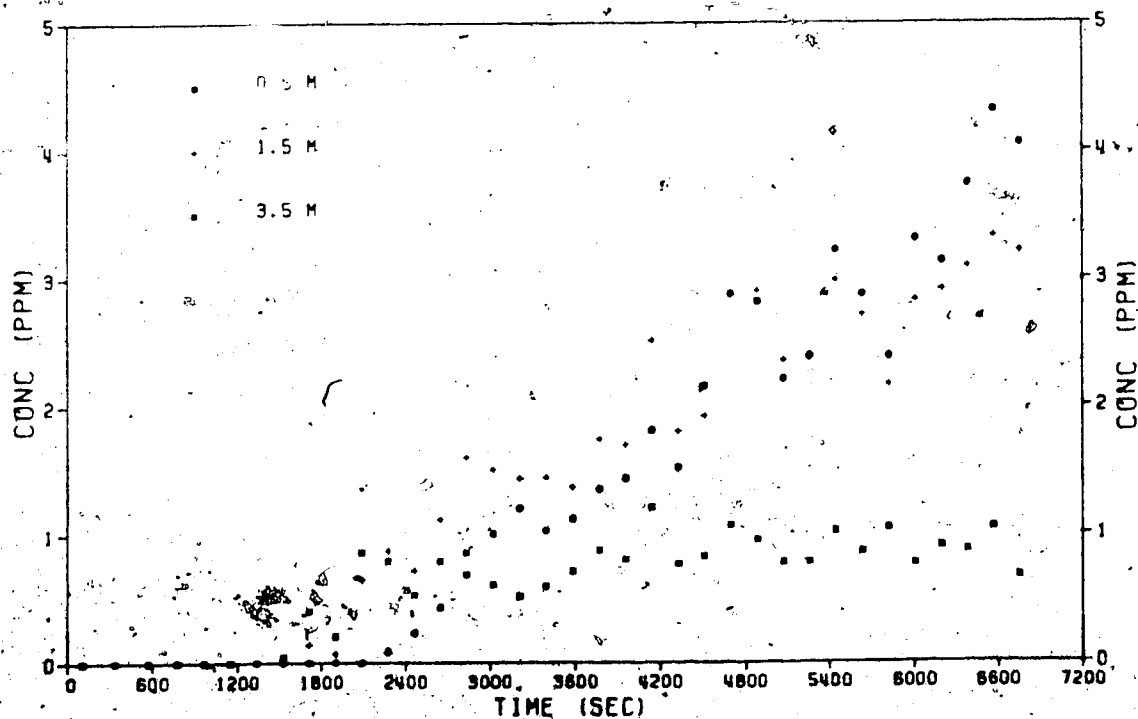


Figure 4.5d: Vertical profile of concentration 50m upslope from source produced by parameters of Table 4.1, except that PWT=0.4g CO.

71

It can be shown that, for the parameters of Table 4.1 at standard temperature and pressure, each part per million of concentration corresponded to approximately 12 particles in a complete (not dissected by the slope) cell. Therefore, each cell with a concentration of 3 ppm contained about 35 particles. In the case of the less dense distribution, 3 ppm resulted from about 17 particles. Thus, an increase in the variability of the concentration in the latter case might be expected but that adequate particles should exist to provide relatively smooth concentration curves.

Although more smoothing can be applied to the curves output by the computer program, little can be done efficiently at intermediate timesteps. Because of the technique's hybrid quality, both the concentration field and particle distribution would need to be smoothed. Adjusting the latter is difficult and may rival a simple increase in density in terms of cost effectiveness.

4.6 Sensitivity to Magnitude of Eddy Diffusivities

4.6.1 No Diffusion

This section compares the standard case (Figure 4.2) which used the parameters of Table 4.1 to the case for which no diffusion is permitted (advection only). The parameters for

this case are those of Table 4.1, except that $DKMX = 0$ and $DKMZ = 0$. Results are shown in Figure 4.6.

Comparison of Figures 4.2a, 4.2b, 4.6a, and 4.6b reveals nothing startling. No particles appeared in the left-hand vortex of the valley in Figure 4.6b. Thus, this aspect of Figure 4.2b may be attributed correctly to diffusion. Particles in the diffusion case tended to greater accumulation near the bottom of the valley. The reason for this is not entirely clear.

In the case of no diffusion, particles were advected parallel to the slope; very few particles were reflected by the slope.

was discovered during model development. When the diffusion process was included particles gained a velocity component normal to the slope. This could result in the following action. First, particles will tend to positions nearer the slope. Thus, they will be bound by pseudo-velocity streamlines which will carry them nearer the bottom of the valley (recall Figure 2.1). Advection velocities near the bottom of the valley are small. Therefore, interaction of advection and diffusion may allow particles to accumulate.

Concentration profiles, Figures 4.2c, 4.2d, and 4.6c, and 4.6d, at upslope and downslope positions, reveal little of interest. Concentrations in the uppermost cell were generally slightly lower in the case of no diffusion - fewer particles reached that level without the aid of diffusion. At the downslope station the lack of diffusion appeared to result in a slightly higher concentration in the 1.5 m cell. This is

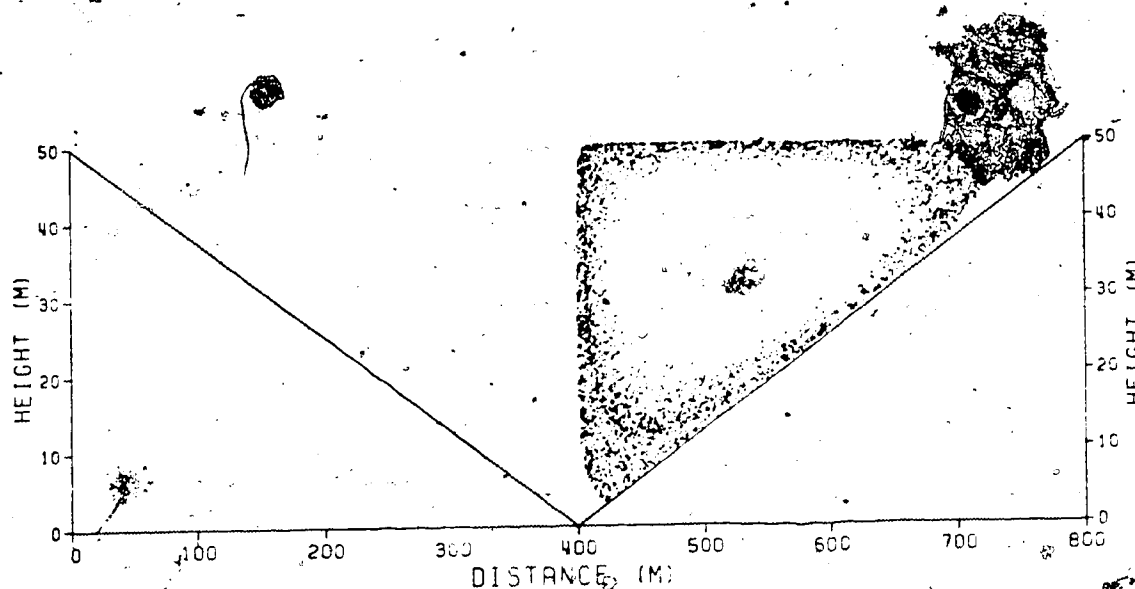


Figure 4.6a: Particle distribution at $t=3604s$ produced by parameters of Table 4.1, except that no diffusion is allowed - advection only.

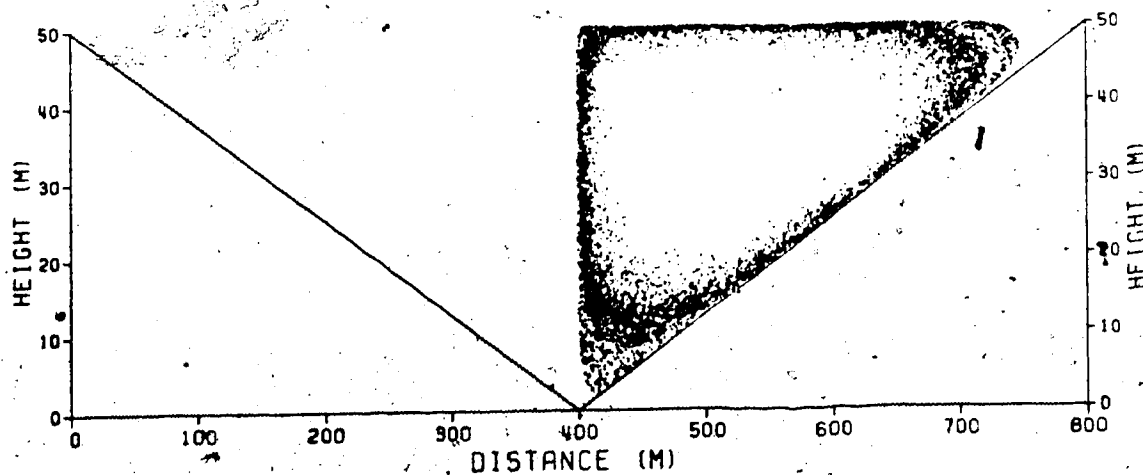


Figure 4.6b: Particle distribution at $t=7181s$ produced by parameters of Table 4.1, except that no diffusion is allowed - advection only.

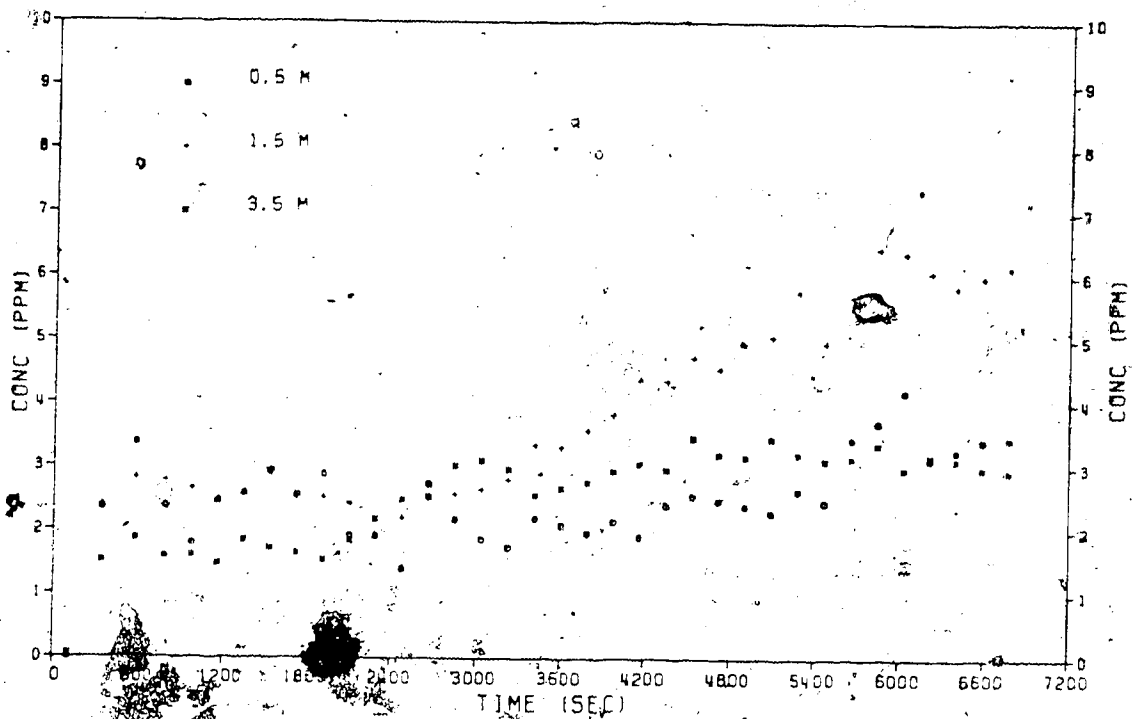


Figure 4.6b: Vertical profile of concentration 100m downslope from source produced by parameters of Table 4.1, except that no diffusion is allowed - advection only.

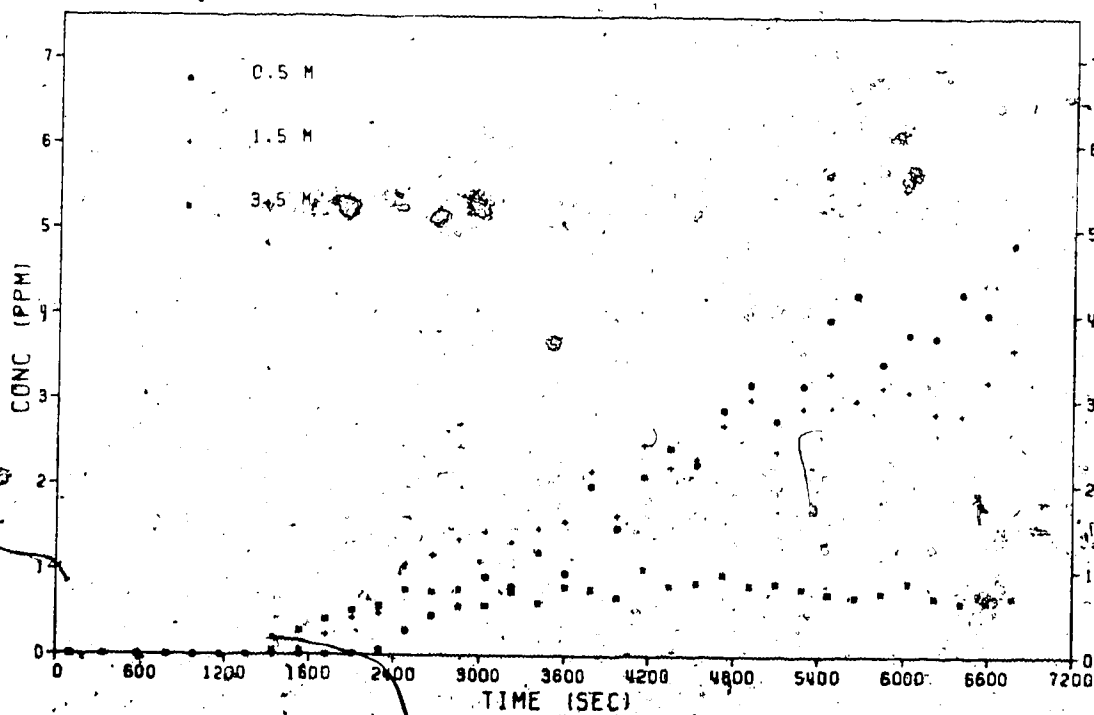


Figure 4.6d: Vertical profile of concentration 50m upslope from source produced by parameters of Table 4.1, except that no diffusion is allowed - advection only.

reasonable because, at the downslope station, the middle of the three cells is on the preferred route for particles circumnavigating the valley vortex (Figure 4.6b). Based on observations of concentration variability before averaging, the increase is probably not significant. Concentrations in the uppermost and lowest cell of Figure 4.6c appeared to be relatively uninfluenced by lack of diffusion.

At the upslope position (Figure 4.6d), concentration in the lowest cell increased slightly in the absence of diffusion. Presumably, this is because the preferred route of the particles is nearer the slope at the upslope station. The differences in concentration with and without diffusion were small. The differences in height of maximum concentration between the upslope and downslope positions was probably an artificiality of the model advection field. The exclusion of diffusion from particle transport had little effect on concentrations within the parameter range investigated.

4.6.2 A Range of Eddy Diffusivities

In this section the sensitivity of the results to the magnitudes of the horizontal and vertical diffusivities is examined. No comparisons are made to Figure 4.2. Parameters are those of Table 4.1, except for cell size and variable diffusivities. In these comparisons $INCX = 40$ m and $INCZ = 5$ m.

In all cases horizontal diffusivity and vertical diffusivity were varied concurrently. Table 4.2 contains Figure numbers and corresponding values of eddy diffusivities for this section.

Table 4.2: Eddy diffusivities and corresponding Figures for section 4.6.2. DKMX and DKMZ are, respectively, horizontal and vertical eddy diffusivity.

Figure	DKMX ($\text{m}^2 \text{s}^{-1}$)	DKMZ ($\text{m}^2 \text{s}^{-1}$)
4.7	1.0×10^{-3}	5.0×10^{-5}
4.3	1.0×10^{-2}	5.0×10^{-4}
4.8	1.0×10^{-1}	5.0×10^{-3}

As expected, Figures 4.3, 4.7 and 4.8 (a and b) show a general dilution in concentration throughout the valley vortex as diffusivities increase. In addition, as diffusivities increased more and more particles were diffused into the adjacent vortex. This accounts for part of the dilution. By inspection only, it is difficult to see any increase in plume spread caused by increasing diffusivities. Again, the diffusion process was nearly masked by advection with diffusivities of the magnitudes used here.

Figures 4.3c, 4.7c and 4.8c compare the results at the downslope station. Concentrations in the 8.5 m and 3.5 m

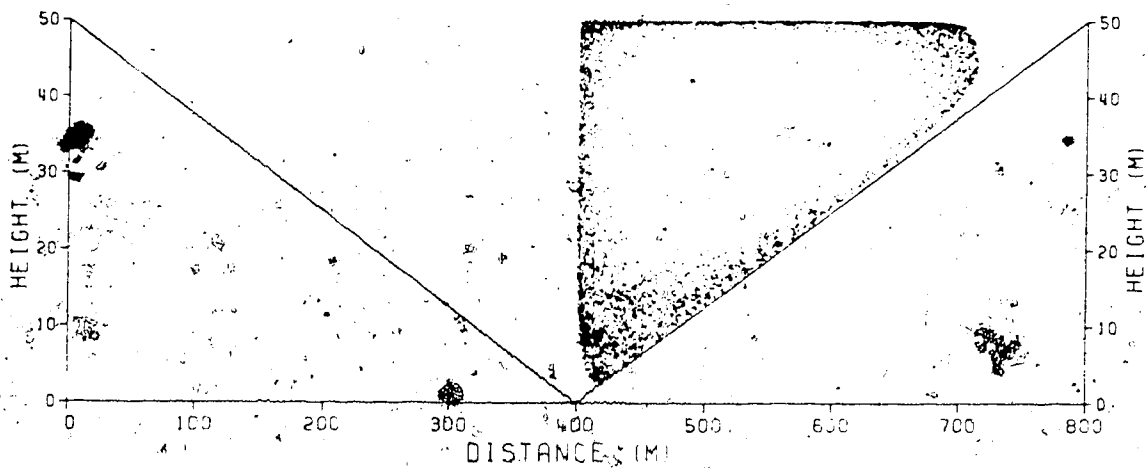


Figure 4.7a: Particle distribution at $t=3617s$ produced by parameters of Table 4.1, except that $INCX=40m$, $INCZ=5m$, $DKMX=1.0 \times 10^{-3} m^2 s^{-1}$, and $DKMZ=5.0 \times 10^{-5} m^2 s^{-1}$.

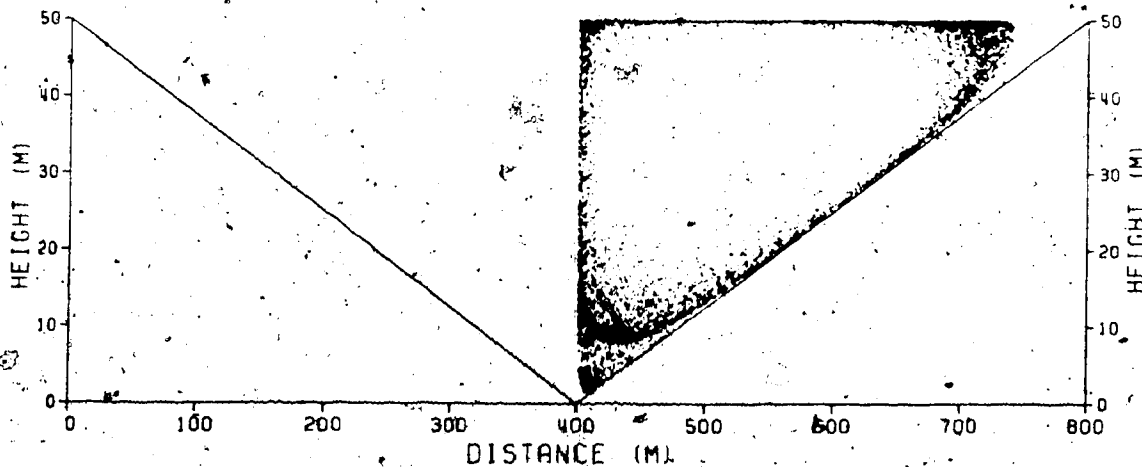


Figure 4.7b: Particle distribution at $t=7204s$ produced by parameters of Table 4.1, except that $INCX=40m$, $INCZ=5m$, $DKMX=1.0 \times 10^{-3} m^2 s^{-1}$, and $DKMZ=5.0 \times 10^{-5} m^2 s^{-1}$.

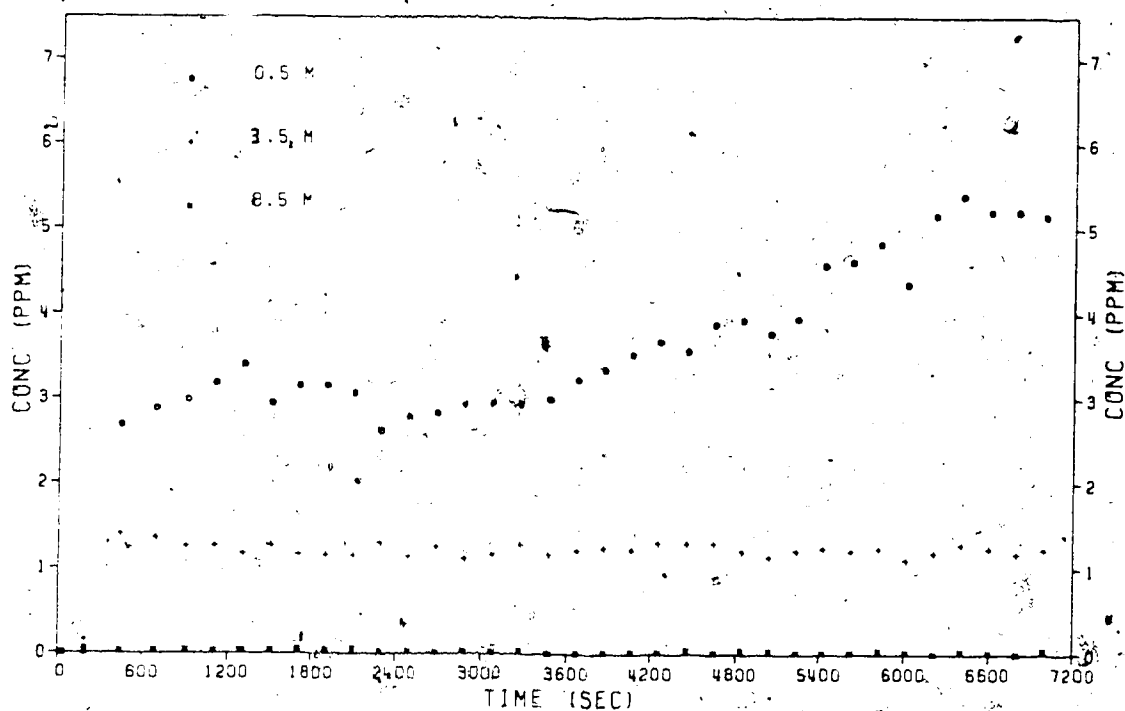


Figure 4.7c: Vertical profile of concentration 100m downslope from source produced by parameters of Table 4.1, except that $INCX=40m$, $INCZ=5m$, $DKMX=1.0 \times 10^{-3} m^2 s^{-1}$, and $DKMZ=5.0 \times 10^{-5} m^2 s^{-1}$.

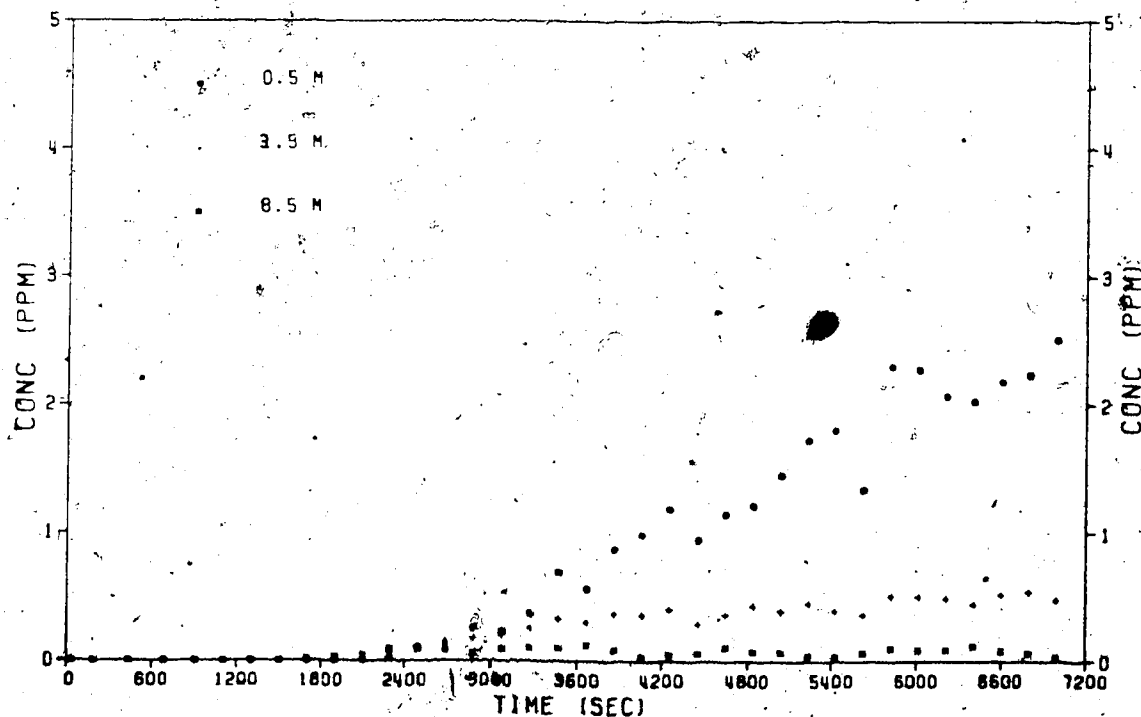


Figure 4.7d: Vertical profile of concentration 50m upslope from source produced by parameters of Table 4.1, except that $INCX=40m$, $INCZ=5m$, $DKMX=1.0 \times 10^{-3} m^2 s^{-1}$, and $DKMZ=5.0 \times 10^{-5} m^2 s^{-1}$.

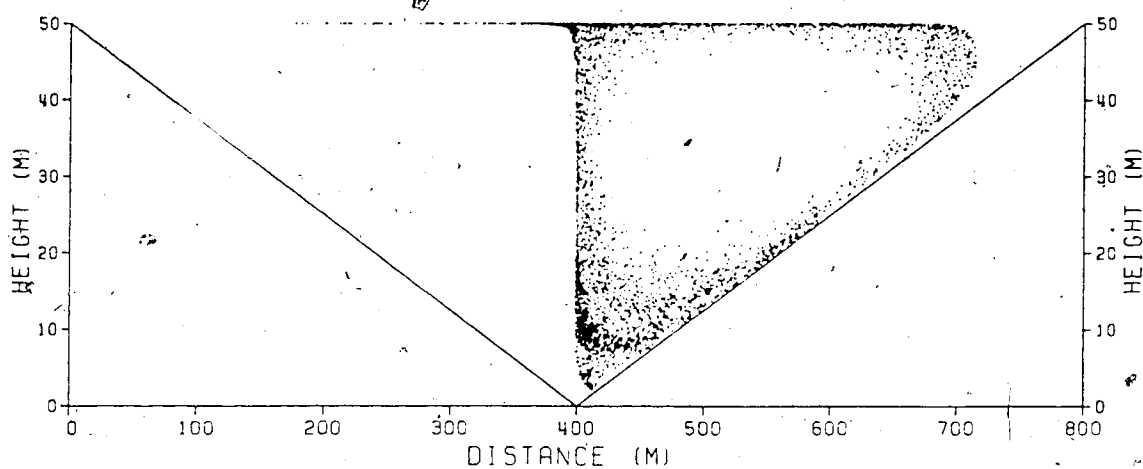


Figure 4.8a: Particle distribution at $t=360$ s produced by parameters of Table 4.1, except that $INCX=40$ m, $INCZ=5$ m, $DKMX=1.0 \times 10^{-1} \text{ m}^2 \text{ s}^{-1}$, and $DKMZ=5.0 \times 10^{-3} \text{ m}^2 \text{ s}^{-1}$.

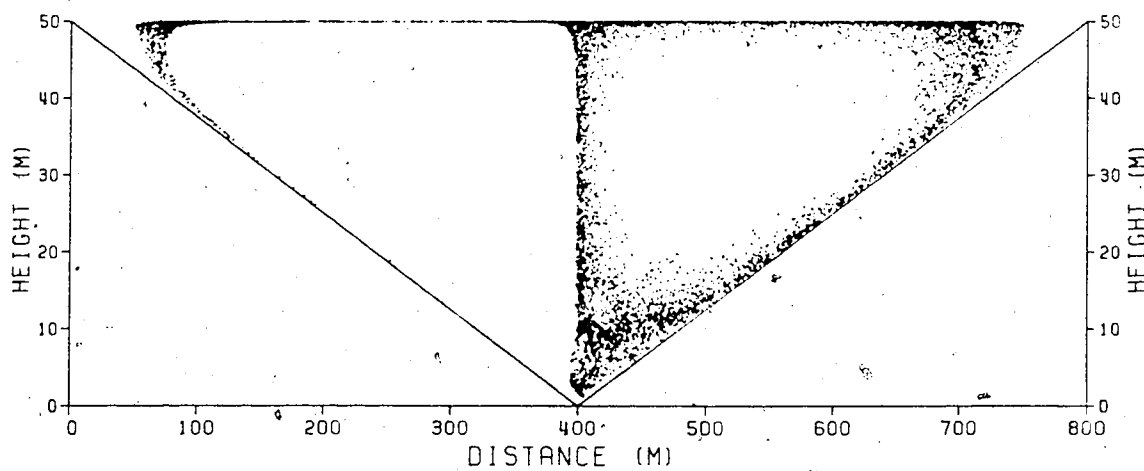


Figure 4.8b: Particle distribution at $t=7218$ s produced by parameters of Table 4.1, except that $INCX=40$ m, $INCZ=5$ m, $DKMX=1.0 \times 10^{-1} \text{ m}^2 \text{ s}^{-1}$, and $DKMZ=5.0 \times 10^{-3} \text{ m}^2 \text{ s}^{-1}$.

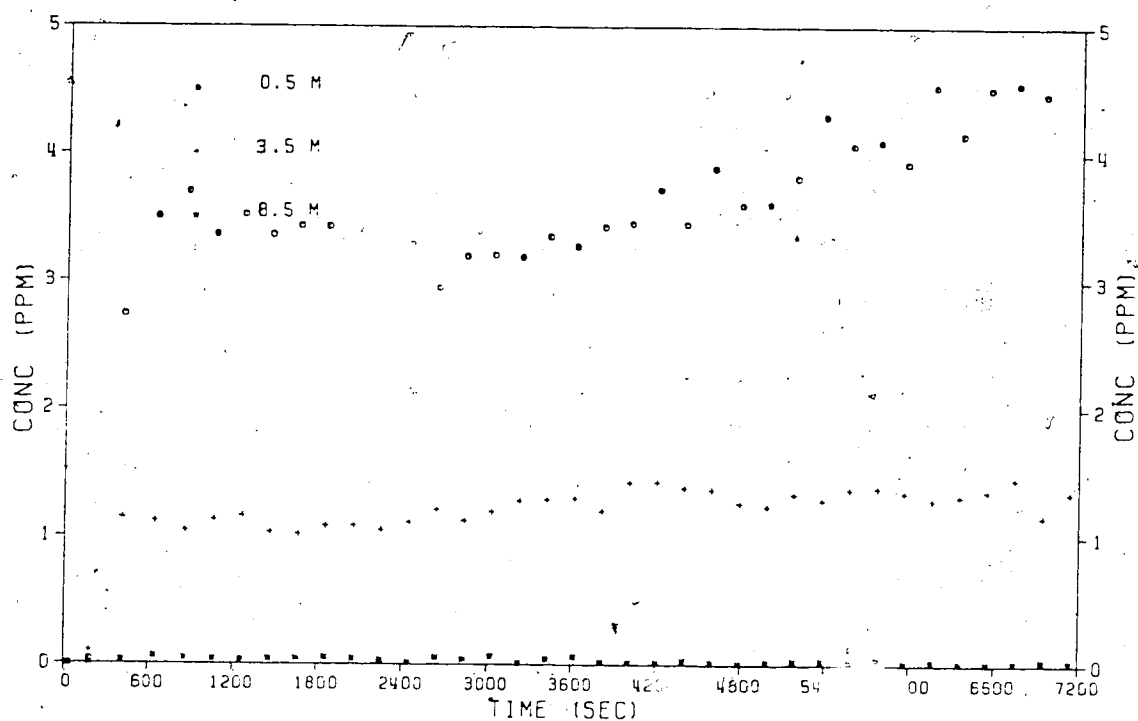


Figure 4.8c: Vertical profile of concentration 100m downslope from source produced by parameters of Table 4.1, except that $INCX=40m$, $INCZ=5m$, $DKMX=1.0 \times 10^{-1} m^2 s^{-1}$, and $DKMZ=5.0 \times 10^{-3} m^2 s^{-1}$.

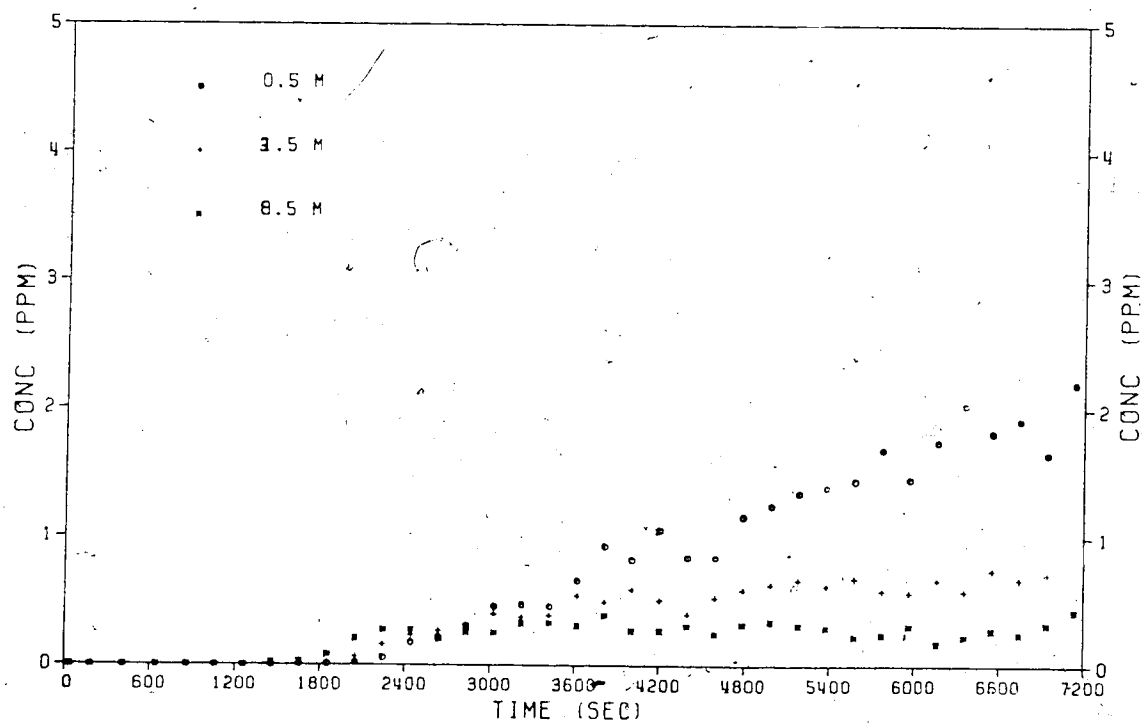


Figure 4.8d: Vertical profile of concentration 50m upslope from source produced by parameters of Table 4.1, except that $INCX=40m$, $INCZ=5m$, $DKMX=1.0 \times 10^{-1} m^2 s^{-1}$, and $DKMZ=5.0 \times 10^{-3} m^2 s^{-1}$.

cells were relatively uninfluenced by changes in diffusivities. Concentrations in the lowest cell decreased with increasing diffusivities. With increased diffusivities, particles were diffused away from the valley slope. This was the expected result. The changes in concentration resulting from a 100-fold change in magnitude of the eddy diffusivities were relatively small, less than 1 ppm (about 20%). Maximum concentrations, found in the lowest cell, ranged from about 4 to 5 ppm.

Concentrations in the lowest cell at the upslope station (Figures 4.3d, 4.7d and 4.8d) show much the same variation with diffusivities as those observed at the downslope station. Concentrations in the lowest cell varied by approximately 20%, ranging about the value 2 ppm. Unlike the downslope case, concentrations in upper cells also varied somewhat with diffusivity. In these cells concentration increased with increasing diffusivities. Concentrations in the 8.5 m cell of Figure 4.8d show a large increase over those in Figure 4.3d. This may indicate that effective velocities produced by diffusion rivalled those of advection at this height.

Results of this section, and those of section 4.6.1, suggest that concentrations are relatively insensitive to large changes in the magnitude of both horizontal and vertical eddy diffusivities. Magnitudes of the diffusivities (if not their spatial and temporal variation) investigated here seem reasonable for the strong inversion and large horizontal temperature gradient observed in the North Saskatchewan River

valley in Edmonton. Because concentrations were relatively insensitive to changes in diffusivities, this suggests that the valley advection wind regime plays an important, if not dominant, role in determining pollutant levels in the valley.

4.7 Sensitivity to Advection Velocity

This section examines the sensitivity of the model to a reduction by a factor of two of the magnitude of the advection velocity. Parameters used are those of Table 4.1, except for cell size and magnitude of advection velocity. For this analysis $INCX = 40$ m, $INCZ = 5$ m, and $AVWF = 0.25 \text{ ms}^{-1}$. Figure 4.3 is the basis of comparison. Figure 4.9 shows the results for a reduced wind speed. Figures 4.9a and 4.9b reveal that, as expected, the distance travelled by the particle plume was much smaller when the wind speed is reduced. In addition, the plume appears more dense. The reduction of wind speed has constrained the same total number of particles to a smaller volume.

Figures 4.3c and 4.9c indicate a substantial increase in concentration in the lower levels at the downslope station in the case of reduced advection velocity. Return flow of pollutants did not dramatically increase the concentration in the 0.5 m cell, at least in the time period modelled, in the case of reduced wind speed. Instead the concentration was

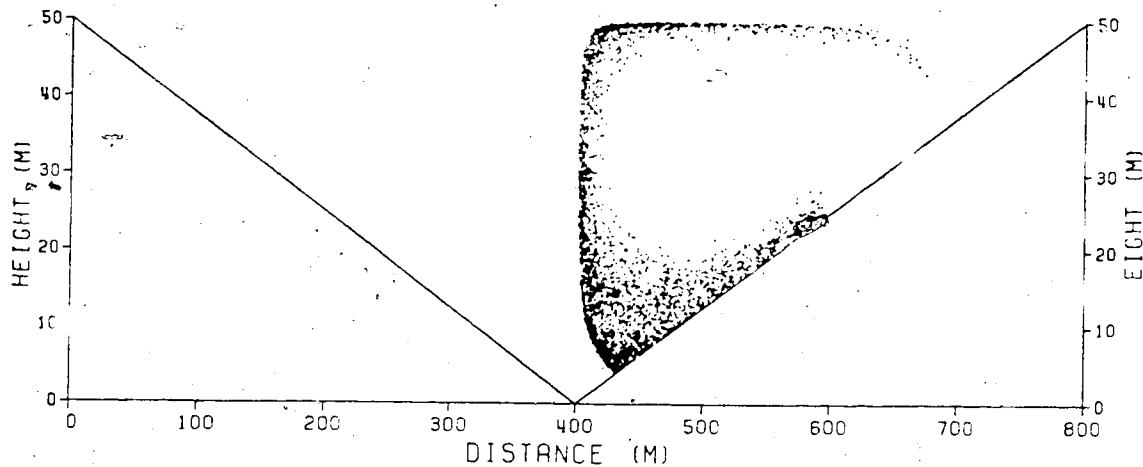


Figure 4.9a: Particle distribution at $t=3633s$ produced by parameters of Table 4.1, except that $INCX=40m$, $INCZ=5m$, and $AVWF=0.25ms^{-1}$.

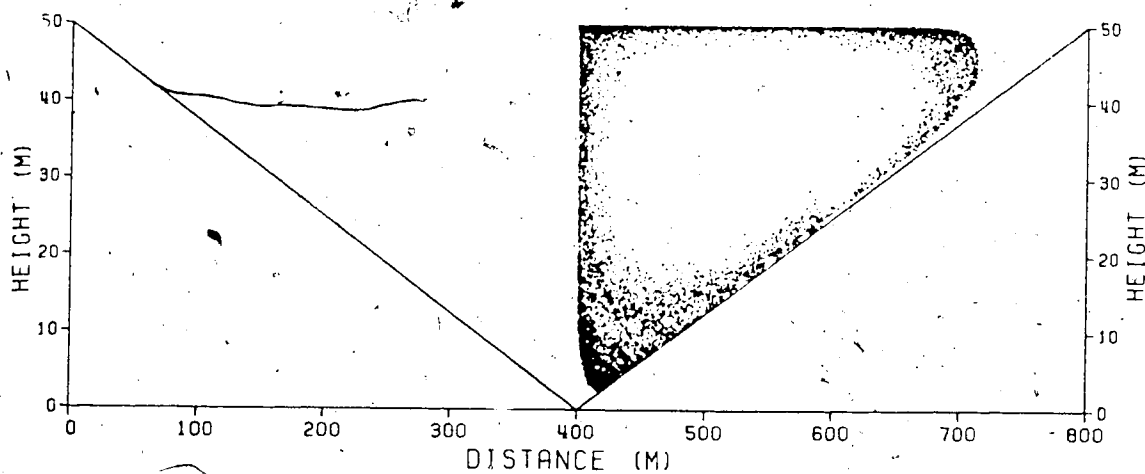


Figure 4.9b: Particle distribution at $t=7225s$ produced by parameters of Table 4.1, except that $INCX=40m$, $INCZ=5m$, and $AVWF=0.25ms^{-1}$.

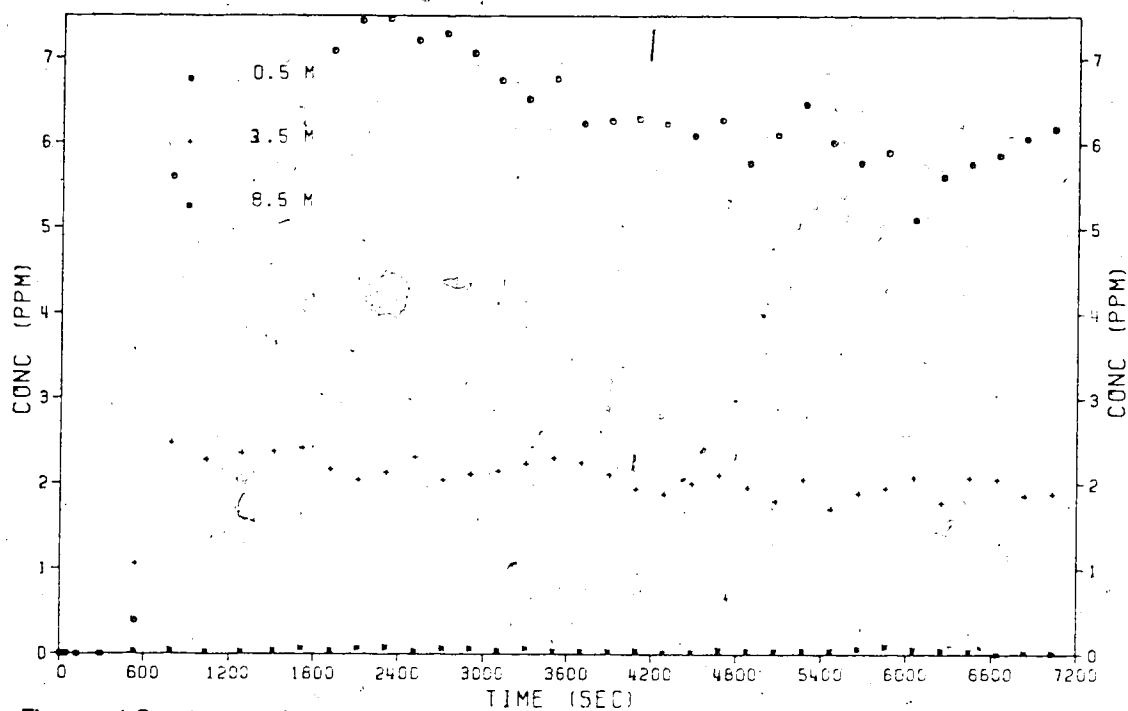


Figure 4.9 c: Vertical profile of concentration 100m downslope from source produced by parameters of Table 4.1, except that $INCX=40m$, $INCZ=5m$, and $AVWF=0.25ms^{-1}$. Concentrations at 0.5m for the period 900s to 1800s are greater than 7.5 ppm.

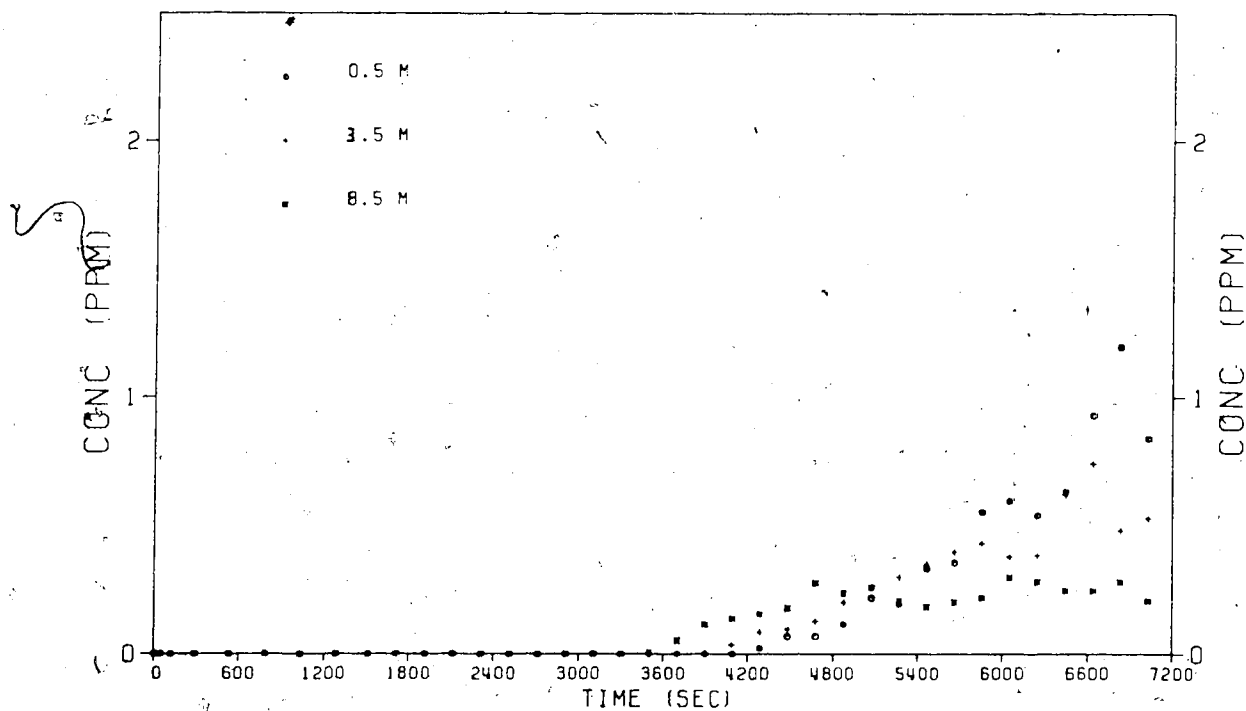


Figure 4.9d: Vertical profile of concentration 50m upslope from source produced by parameters of Table 4.1, except that $INCX=40m$, $INCZ=5m$, and $AVWF=0.25ms^{-1}$.

maintained at a high level. The 0.5 m curve of Figure 4.9c illustrates the decrease in source strength, at least during the first hour of model time. As expected, the increase in concentration with reduced advection velocities was less at greater heights. The 8.5 m cell showed negligible change in concentration.

Figure 4.9d shows that two hours was insufficient for investigation of concentration changes at the upslope position when the slope wind was reduced. The concentration in the uppermost cell was substantially larger in Figure 4.9d than in Figure 4.3d. This may be because the plume had not progressed as far into the upper right corner of the valley (Figure 4.9b). The plume path was somewhat foreshortened; the descending region of the plume was nearer the upslope station in the case of reduced wind speed. Concentrations in the lower cells increased rapidly at the end of the simulation. The fastest particles traversed the vortex in about 3600 s, double that of Figure 4.3d. This was as expected.

The results of this section suggest that concentrations in the valley are sensitive to changes in the magnitude of the advection velocity. This was an expected result. However, observations in the North Saskatchewan River valley (Hage, 1979) indicated that, once developed, the slope wind was steady until its demise at sunrise. Thus, the results of this sensitivity to wind speed analysis may be of little use in elucidating aspects of real valley winds but do indicate that the model

predicts the correct trend of increasing concentrations with decreasing wind speed.

4.8 Computer Requirements

The computer code of this model was written for and run on the University of Alberta's Andahl 470V/6 computer. The program was written in FORTRAN IV and compiled using the FORTRAN H compiler. The University's Andahl computer at present has an 8 M byte core storage capacity. The Michigan Terminal System (MTS) operating system used at the University of Alberta provides large amounts of virtual memory.

Central processing unit (CPU) time and storage space required by the code were dependent on the application. The standard run, using the parameters of Table 4.1, required approximately 100 s CPU time. Reducing by a factor of two the number of particles produced at each timestep (section 4.5) reduced CPU time by about 40% to about 60 s. Reducing the area of each cell by a factor of five (section 4.3) reduced CPU time by 60% to approximately 40 s. Reducing the maximum velocity on the grid by a factor of two also halved CPU time. Changing other parameters had little effect on CPU time. Time required was found, at least in the cases examined, to be primarily dependent on three parameters: vertical grid spacing; vertical velocity and; vertical eddy diffusivity. Combinations

of decreased vertical grid spacing, increased vertical velocity, or increased vertical eddy diffusivity tended to decrease the length of the timestep and so increase CPU time.

Storage space required by the compiled version of the computer program ranged from 0.4 M to 0.5 M bytes, dependent mostly on cell size and number of particles created each timestep. In all cases, the charge for CPU time was approximately equal to the charge for storage space. Total cost for each run (not including plotting) was approximately double the cost of the CPU time alone.

CHAPTER V

SUMMARY AND CONCLUSIONS

5.1 Summary

A series of micrometeorological experiments were conducted in the North Saskatchewan River valley in Edmonton during 1977 and 1978. These experiments provided data from which the microclimatology of small valleys may be deduced. Resultant information about the occurrence of pollution episodes and the levels of pollutant during these episodes may be of interest to those who plan the use of city valleys. This thesis is one part of the effort to understand the micrometeorology of small urban valleys. It is a first step in modelling the transport of pollutants within these valleys.

A two-dimensional model was formulated using a particle-in-cell approach. Particles, representing specified amounts of CO, were created within a V-shaped model valley. These particles were advected by a wind field that was specified for the model, and dispersed by a simulated turbulent diffusion

process. The model used a concentration-gradient diffusion technique for distributions of particles large compared to the grid size. For smaller distributions, diffusion was assumed to be Gaussian in character. The two were found to produce approximately equal rates of diffusion. The source of the particles was a point on the valley slope, representing an infinite line source which in turn represented a roadway running along the valley axis. The advection field was a (somewhat artificial) double vortex representing potential flow. Particles were allowed to diffuse, but were not allowed to be advected, to the adjacent vortex and out of the top of the valley. No interaction of the valley pollutant distribution or wind field with those of the overlying flow was allowed. The valley was essentially a closed system.

The model depicted a situation in which an inversion, and thus the double vortex valley wind system, filled the entire depth of the valley. The slope wind speeds of the advection field were similar to those that have been observed in the North Saskatchewan River valley in Edmonton. Eddy diffusivities used by the model were Fickian, i.e., constant in space and time. Arguments for approximating the magnitudes of the diffusivities were based on the observed intensity of inversions and horizontal temperature gradients deduced to exist near the slope.

The model correctly predicted an increase in concentration with decreasing wind speed and a decrease in concentration with

decreasing source strength, although these results were masked to some degree by the effects of the closed valley system.

These effects were responsible for the model concentrations not reaching steady state. Concentrations downslope from the source reached over 6 ppm. The return flow of the double vortex advection field was capable of producing concentrations of up to 5 ppm. This concentration was found somewhat upslope of the source, out of the range of direct diffusion.

At the upslope position, the effects of the return flow were first observed in cells somewhat above the slope. Some minutes later, concentrations at the slope also increased. The fastest particles traversed the vortex in approximately 25 minutes in a flow with downslope wind speed of 0.5 ms^{-1} . For a wind speed of approximately 0.25 ms^{-1} , travel time increased to about 1 hour. In most sensitivity analyses, concentrations at the downslope station appeared to reach their maximum values within the two hour simulation. Concentrations at the upslope station appeared to be increasing at the end of the simulation. Concentrations near the slope were found to be relatively insensitive to the magnitude of eddy diffusivities and to changes in particle density. Increasing the initial size of the source generally decreased concentrations downslope from the source. Concentrations at the upslope station were unchanged by changes in initial source size. At both stations increasing the initial source size decreased concentrations at the slope and increased concentrations above the slope, but

with no changes in maximum observed concentration. Decreasing by a factor of two the magnitude of the advection velocity doubled the concentration downslope from the source during the first hour and increased it by about 20% at later times.

Decreasing the advection velocity by a factor of two doubled the transit time of particles. Two hours was an insufficient time to investigate concentrations at the upslope station in this case. Increasing by a factor of five the area of each cell resulted in generally lower concentrations at similar heights above the slope. Somewhat surprisingly, the particle scatter graph for this case suggested an increase in concentration in some parts of the valley, at odds with the usual result found when using Eulerian methods. The reason for this was not determined but it is suggested that cell sizes were too large.

It was found that magnitudes of vertical components of model parameters (i.e. cell size, wind speed, and eddy diffusivities) were the limiting factors in determining the cost of computation. This was due principally to the scale of the model valley.

5.2 Conclusions

Within the limits of the present study (small valley, closed valley system, and single, along-valley line source)

the ground-level concentrations downslope from the source were controlled by the interaction between advection and initial source diffusion. Concentrations upslope from the source apparently were influenced less by initial source diffusion. Atmospheric diffusion following the initial plume growth appeared to be of secondary importance for diffusivities that were believed to be realistic in moderate to intense valley inversions.

The time required for a particle to traverse one circuit of the valley vortex appeared to be determined predominantly by advection when diffusion was represented by realistic diffusivities. Although cycle times were found solely from the time of first arrival at the upslope cell, they were similar to the cycle times suggested by Paterson and Hage (1979) when the speed of the downslope wind was about 0.25 ms^{-1} . Cycle times of one hour and typical downvalley wind speeds of 0.5 ms^{-1} suggested the along-valley length of one coil of the helix to be about 2 km. Therefore, in down-valley winds of this magnitude or greater, recirculation of the air past an along-valley line source will be important only if that source extends several kilometers upvalley.

Results of investigations of the effects of changes in cell size on predicted concentrations suggested that the cell sizes used in this application were too large. This throws some doubt on the validity of the results. Since the vertical dimension of the plume was about 5 m, vertical grid size

should be substantially smaller, say 0.5 m. Because vertical components were the limiting factor, computer costs would rise accordingly.

Results showed that predicted concentrations were sensitive to initial source diffusion. This lends support to the conclusion that diffusion following the initial plume growth is of secondary importance. It also suggests that more accurate parameterization of the source is needed. In particular this entails a better representation of the effects of buoyancy and mechanical mixing and perhaps a more detailed analysis of the vehicle emission factor.

The magnitude of the concentration in the return flow is important to discussions of the possible existence and structure of such a flow in small valleys. A typical concentration near the slope surface upslope from the source was 4 ppm after two hours. During this time source strength decreased by nearly 40%. Concentrations of 4 ppm support the existence of return flow. The value is substantial; model refinements such as interaction with the overlying flow and possibly larger initial plume growth would serve to decrease the value but presumably not to an undetectable size. The concentration profiles give little to indicate the depth of the slope wind. The design of the plume resulting from diffusivities which are believed to be realistic indicates, however, that flow in the lowest few meters is important for determining concentrations near the source.

In conclusion, the PIC technique appears to be of value in modelling pollutant transport in small valleys with return flow.

5.3 Suggestions for Future Study

The basis of the model - representing vehicular emissions by Lagrangian particles in an Eulerian grid - appears to have potential for modelling transport in small valleys. However, it is important to develop more realistic boundary layer and source parameters. Although the model wind field appears to simulate adequately the slope wind, it is thought to be less realistic at the top of the valley. The addition of an overlying potential flow with appropriate interaction at the interface is a possible solution. This should allow for some pollutant dilution.

Parameterization of the eddy diffusivities needs further refinement. In the moderate to intense inversions found in small valleys, the effects of mechanical mixing become important. The region beneath the level of the maximum slope wind could be characterized as of neutral stability, as suggested by di Cenzo (1979), thus increasing dispersion in the lowest levels.

Initial source diffusion requires more realistic parameterization. In this application buoyancy was ignored.

Because of the subordinant role of diffusion at locations away from the source, a change in the effective height of the plume by only a few metres may be important for predicting concentrations. If, as suggested, mechanical mixing is important, then perhaps the initial size of the plume also needs to be increased.

The source inventory could be suitably enhanced. Drainage of pollutants from the city might be simulated by positioning sources of appropriate strength at the upper slopes. Valley sources could be accounted for by assuming a background concentration.

Finally, the sensitivity of the model to cell size should be investigated further. In particular, cells that are smaller than those employed here should be used. In addition, the trajectory of several representative particles should be determined. This may clarify typical traverse times for particles in the valley vortex.

REFERENCES

- Amsden, A.A., 1966. The particle-in-cell method for the calculation of the dynamics of compressible fluids. Los Alamos Scientific Laboratory. Report LA-3466. 170 pp.
- Batchelor, G.K., 1974. An introduction to fluid dynamics. Cambridge University Press, Cambridge, England. 615 pp.
- Businger, J.A., 1973. Turbulent transfer in the atmospheric surface layer: Workshop on Micrometeorology. D.A. Haugen, editor. American Meteorological Society, Boston. 392 pp.
- City of Edmonton, 1978. Average annual weekday traffic 1977. Transportation and Planning Branch, Planning Department.
- Courant, R., and D. Hilbert, 1953. Methods of mathematical physics. Volume I. Interscience Publishers, New York. 561 pp.
- Danard, M.B., 1972. Numerical modelling of carbon monoxide concentrations near highways. Journal of Applied Meteorology. 11: 947 - 957.
- Davies, D.R., 1950. Three dimensional turbulence and evaporation in the lower atmosphere, II. Quarterly Journal of Mechanics and Applied Mathematics. 3: 51 - 72.
- Defant, F., 1951. Local winds. Compendium of Meteorology. T.M. Malone, editor. American Meteorological Society, Boston. pp 665 - 672.
- di Cenzo, C.S., 1979. A numerical study of temperature in an urban valley using a radiative-convective model. Department of Geography, University of Alberta, Edmonton. Unpublished M.Sc. thesis. 159 pp.
- Fanaki, F.H. and J. Kovalick, 1974. Diffusion of vehicle exhaust plumes. Atmosphere. 2: 50 - 61.
- Gifford, F.A., 1975. Atmospheric dispersion models for environmental pollution applications. Lectures on Air Pollution and Environmental Impact Analysis. American Meteorological Society, Boston. pp. 35 - 58.
- Hage, K.D., 1972. Nocturnal temperatures in Edmonton, Alberta. Journal of Applied Meteorology. 11: 123 - 129.

- Hage, K.D., 1979. Air pollution study of the North Saskatchewan River valley in Edmonton, Alberta. Research Secretariat, Alberta Environment. Report 1979/3. 90 pp.
- Haltiner, G.J., 1971. Numerical weather prediction. John Wiley and Sons, New York. 317 pp.
- Hanna, S.R., 1975. Urban diffusion problems. Lectures on Air Pollution and Environmental Impact Analysis. American Meteorological Society, Boston. pp 209 - 227.
- Holten, J.R., 1972. An introduction to dynamic meteorology. Academic Press, New York. 319 pp.
- Hwang, C.-C., 1978. Air pollution study within an urban valley. Department of Geography, University of Alberta, Edmonton. Unpublished M.Sc. thesis. 106 pp.
- Klassen, W., 1962. Micrometeorological observations in the North Saskatchewan River valley at Edmonton. Meteorological Branch, Canada Department of Transport. CIR-3652, TPC-408. 24 pp.
- Lamb, R.G., W.H. Cheu, and J.H. Seinfeld, 1974. Numerico-empirical analyses of atmospheric diffusion theories. Symposium on Atmospheric Diffusion and Air Pollution, Preprint, Santa Barbara, Sept. 9 - 13. American Meteorological Society, Boston. pp. 317 - 324.
- Lange, R., 1973. ADPIC: a three dimensional computer code for the study of pollutant dispersal and deposition under complex conditions. Lawrence Livermore Laboratory. Report UCRL-51462.
- Lange, R. and C.A. Sherman, 1977. Particle-in-cell vs. straight line Gaussian calculations for an area of complex topography. Joint Conference on Applications of Air Pollution Meteorology, Preprint, Salt Lake City, Nov. 29 - Dec. 2. American Meteorological Society, Boston. pp 225 - 231.
- Lange, R., 1978. ADPIC - a three dimensional particle-in-cell model for the dispersal of atmospheric pollutants and its comparison to regional tracer studies. Journal of Applied Meteorology. 17: 320 - 329.
- Lin, J.-T., 1972. Relative dispersion in the enstrophy cascading inertial subrange of homogeneous two-dimensional turbulence. Journal of Applied Meteorology. 29: 394 - 396.

- Padro, J., 1979. Review of dispersion models and possible application in the AOSERP study area. Alberta Oil Sands Environmental Research Program, Edmonton. AOSERP Project ME 4.2.1. 64 pp.
- Pasquill, F., 1974. Atmospheric diffusion. 2nd edition. Ellis Horwood, Chichester. 429 pp.
- Paterson, R.D., 1978. A micrometeorological study of an urban valley. Department of Geography, University of Alberta. Unpublished M.Sc. thesis. 91 pp.
- Paterson, R.D. and K.D. Hage, 1979. Micrometeorological study of an urban river valley. Boundary Layer Meteorology. 17: 175 - 186.
- Reid, J.D., J.L. Walmsley, I.B. Findleton, and A.D. Christie, 1979. An assessment of the models LIRAQ and ADPIC for application to the Alberta oil sands area. Alberta Oil Sands Environmental Research Program, Edmonton. AOSERP Report 66. 95 pp.
- Sandhu, H.S., 1975. A study of photochemical air pollutants in the urban airsheds of Edmonton and Calgary. Research Secretariat, Alberta Environment, Edmonton. Staff Report 1. 155 pp.
- Slade, D.H. (ed.), 1968. Meteorology and atomic energy 1968. U.S. Atomic Energy Commission. 445 pp.
- Stovel, L.D., 1979. Private communication based on uncompleted M.Sc. thesis. Department of Geography, University of Alberta, Edmonton.
- Tang, W. and L. Peng, 1974. Mountain valley circulation and dispersion of vehicle exhaust gases from a valley highway. Symposium on Atmospheric Diffusion and Air Pollution, Preprint, Santa Barbara, Sept. 9 - 13. American Meteorological Society, Boston. pp 233 - 237.
- Tang, W., 1976. Theoretical study of cross-valley wind circulation. Arch. Met. Geoph. Biokl., Ser. A. 25: 1 - 18.
- Taylor, G.W., 1973. Automobile emission trends in Canada 1960 - 1985. Air Pollution Control Directorate, Environmental Protection Service, Ottawa. Report EPS 8-73-1. 46 pp.
- Tennekes, H. and J.L. Lumley, 1972. A first course in turbulence. MIT Press, Cambridge, Mass. 300 pp.

Walton, J.J., 1973. Scale-dependent diffusion. Journal of Applied Meteorology. 12: 547 - 549.

Welch, J.E., F.H. Harlow, J.P. Shannon and B.J. Daly, 1965. The MAC method - a computing technique for solving viscous, incompressible, transient fluid-flow problems involving free surfaces. Los Alamos Scientific Laboratory. Report LA-3425. 146 pp.

Zimmerman, J.R. and R.S. Thompson, 1975. User's guide for Hiway, a highway air pollution model. U.S. Environmental Protection Agency. Report EPA - 650/4 - 74 - 008.

APPENDIX A

AN ILLUSTRATION OF A PARTICLE SCATTER
DIAGRAM DISPLAY

This appendix contains a series of particle scatter graphs at intervals of 900 s. The parameters used in these simulations are those of Table 4.1, except that $DKMX = 1.0 \times 10^{-3} m^2 s^{-1}$ and $DKMZ = 5.0 \times 10^{-5} m^2 s^{-1}$.

The dashed line in Figures A1 to A5 is an advection velocity streamline. It is meant to pass through the center of mass of the source puff. For a continuous half-plane Gaussian distribution, the center of mass is near 0.68σ . For a puff with $\sigma = 2$ m, the center of mass should be near 1.4 m. Thus, the streamline in the Figures is near the center of the initial source configuration. At early times (Figures A1 and A2), it is obvious that those particles created in the upper levels of the plume traverse the valley vortex faster than those created in the lower levels, due to shorter path length. Particles require a long period of time to reach the bottom of the valley because of the rapidly decreasing velocities near the valley bottom.

It might be expected that, at later times, the illustrated streamline remains near the center of the plume. Figures A3

to A5 show that this is not the case. Deviations of the streamline from the center of the plume may be caused by the presence of diffusion or by errors produced by inadequate resolution in the finite-difference representations.

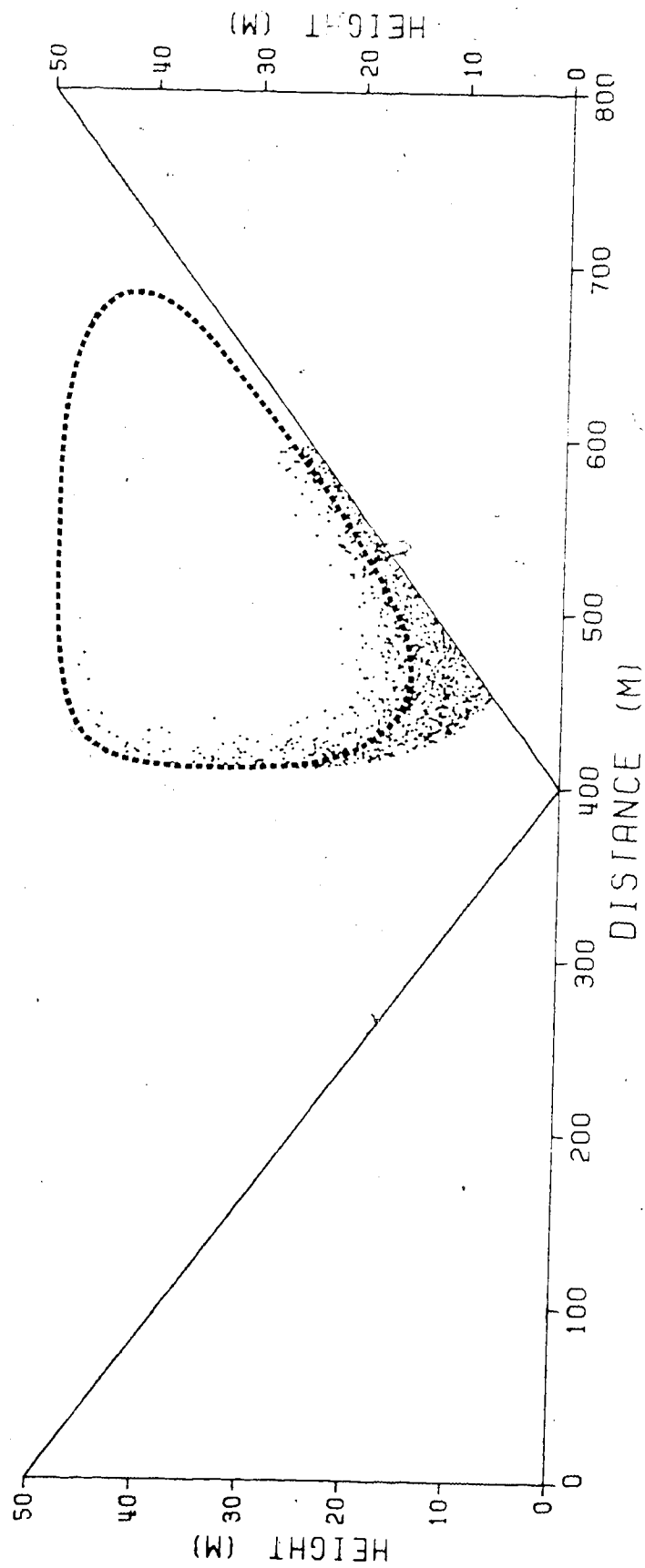


Figure A1: Particle distribution at $t = 900$ s.

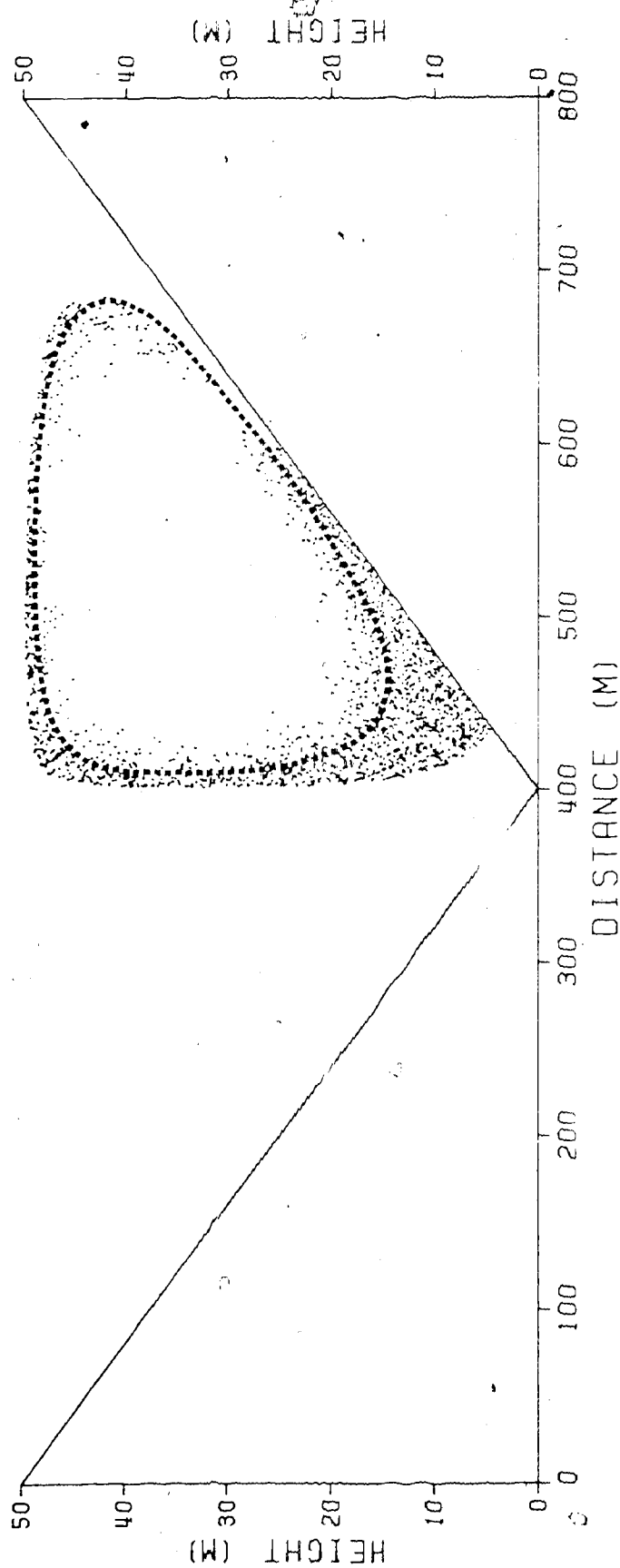


Figure A2: Particle distribution at $t = 1800$ s.

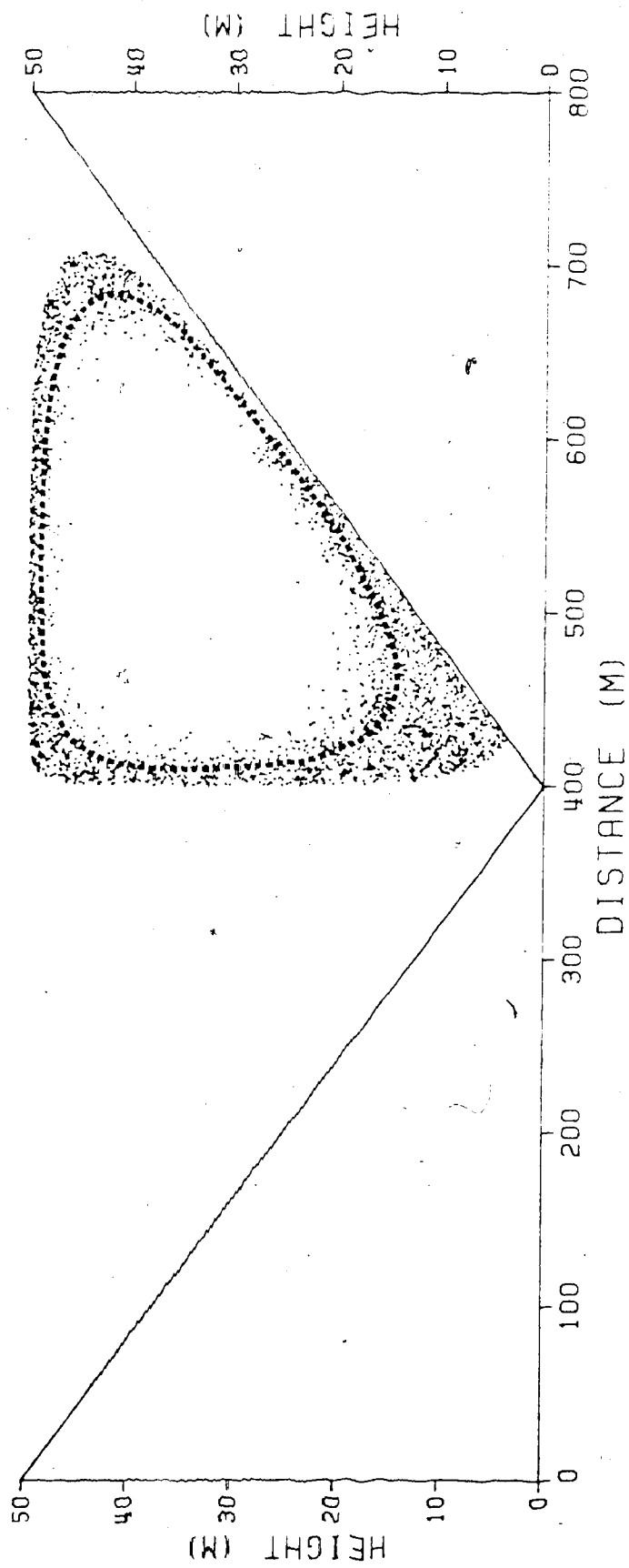


Figure A3: Particle distribution at $t = 2700$ s.

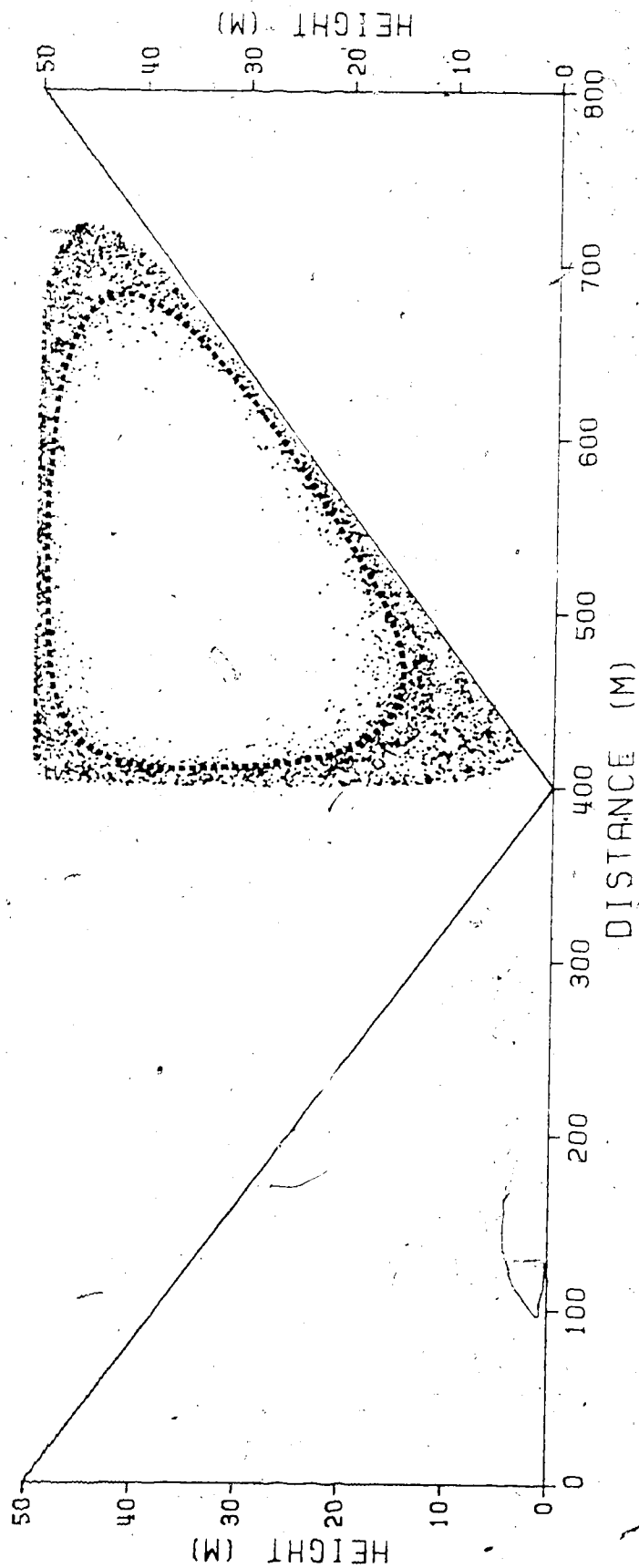


Figure A4: Particle distribution at $t = 3600$ s.

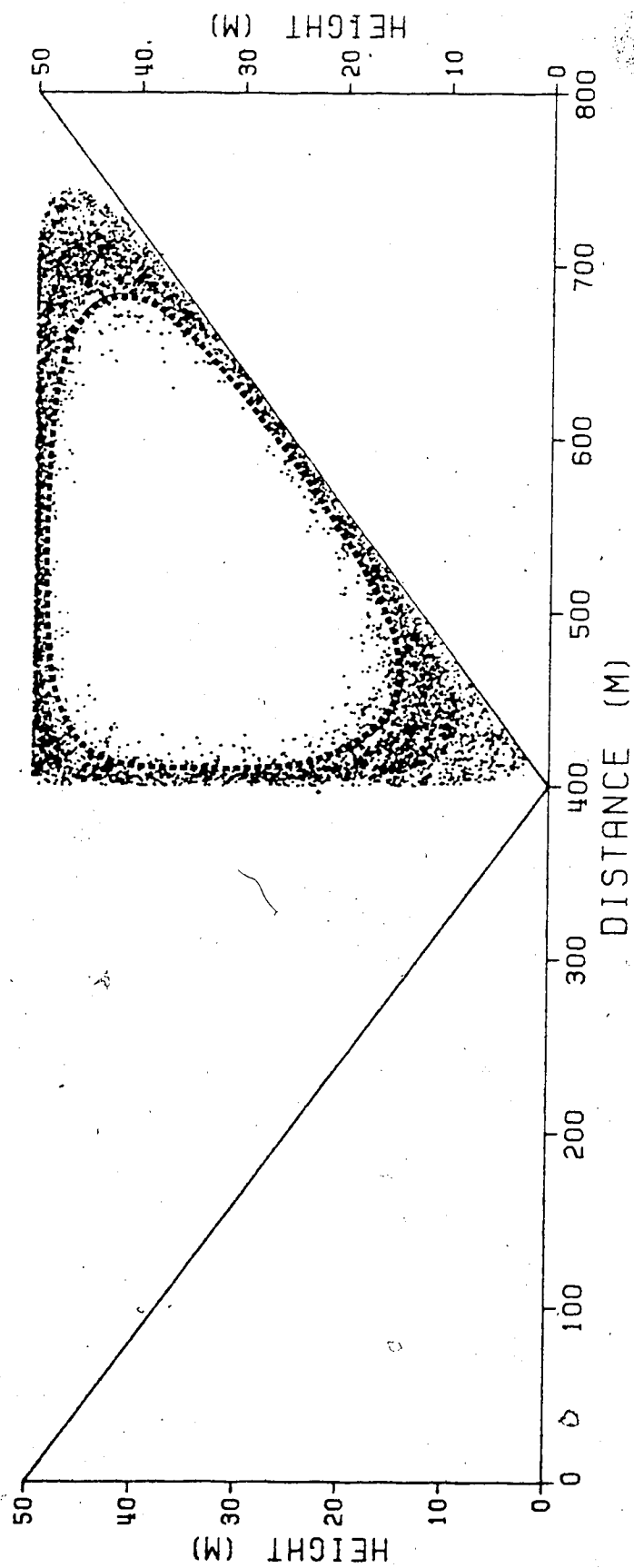


Figure A5: Particle distribution at $t = 7200$ s.

APPENDIX B

COMPUTER PROGRAM

This appendix contains the computer code on which this study is based.

C WRITTEN BY: R. RUDOLPH

C PURPOSE: TO MODEL THE TRANSPORT OF POLLUTANTS IN A VALLEY

C THIS PROGRAM MODELS THE ADVECTION AND DIFFUSION OF GASES AND IS
C BASED ON THE WORK OF ROLF LANGE (REF: JAM(1978), 3, PP 20-329). THE
C REFERENCE CONTAINS A MORE COMPLETE BIBLIOGRAPHY.

C THE CODE SOLVES THE TWO DIMENSIONAL ADVECTION - DIFFUSION EQUATION BY
C THE PSEUDO - VELOCITY TECHNIQUE FOR A GIVEN NON-DIVERGENT ADVECTION
C FIELD. THE METHOD IS BASED ON THE PARTICLE - IN - CELL TECHNIQUE WITH
C THE POLLUTANT CONCENTRATION REPRESENTED BY LAGRANGIAN PARTICLES IN AN
C EULERIAN GRID MESH.

C THE FOLLOWING FORTRAN UNITS ARE USED:

C UNIT 3 : CONCENTRATION OF ONE CELL AS A FUNCTION OF TIME
C UNIT 4 : STREAM FUNCTION ARRAY
C UNIT 5 : INPUT DATA (SEE BELOW)
C UNIT 6 : DIAGNOSTICS
C UNIT 7 : DOCUMENTATION OF ERRORS
C UNIT 8 : SOURCE UNIT (*SOURCE*)
C UNIT 12 : PARTICLE POSITIONS
C UNIT 13 : CONCENTRATION ARRAY

C THE FOLLOWING SUBROUTINES ARE CALLED FROM THE MAIN PROGRAM:

C SRAREA : CALCULATES THE AREA OF EACH CELL. FOR A CELL TOTALLY
C BELOW GROUNDLINE, THE AREA IS SET TO -1. THE BOUNDARY
C IS ASSUMED TO BE A V - SHAPED VALLEY.
C ALTHOUGH MORE COMPLICATED VALLEY SHAPES MAY BE USED,
C IT IS ASSUMED THAT THE SLOPE IS CONSTANT ACROSS ANY
C CELL.
C ADVECT : COMPUTES A STATIONARY ADVECTION FIELD DEFINED AT
C CELL CORNERS.
C SOURCE : DETERMINES THE NUMBER OF PARTICLES AND THEIR INITIAL
C POSITIONS PRODUCED AT EACH SOURCE LOCATION AT EACH
C TIMESTEP. THE DISTRIBUTION IS ASSUMED TO BE APPROX-
C IMATELY GAUSSIAN.
C SUM : DETERMINES THE PARTICLE CONCENTRATION IN EACH CELL
C DIF1 : CALCULATES A DIFFUSION VELOCITY AT EACH CELL CORNER
C FROM THE CONCENTRATION GRADIENT. VELOCITIES ARE SET
C TO ZERO FOR EACH CORNER BELOW GROUNDLINE.
C INTER : INTERPOLATES ADVECTION AND DIFFUSION VELOCITIES
C FROM CELL CORNERS TO PARTICLE POSITIONS. FOR SUB
C GRID SCALE SIZED PUFFS, DIFFUSION VELOCITIES AT
C PARTICLE POSITIONS ARE COMPUTED DIRECTLY FROM
C GAUSSIAN DISPERSION. THE TRANSPORT DISTANCE IS
C FOUND AND THE LENGTH OF THE NEXT TIMESTEP IS CALCU-

LATED.

TSTEP : ADVANCES PARTICLES ALONG PSEUDO VELOCITY STREAMLINES.
IF NECESSARY, PARTICLES ARE REFLECTED AT THE GROUND-
LINE. THE VARIANCE OF EACH PUFF IS CALCULATED.

RENUM : PARTICLES TRANSPORTED OUTSIDE THE GRID ARE DESTROYED;
THOSE REMAINING ARE RENUMBERED.

OUTPUT : WRITES PARTICLE POSITION AND CONCENTRATION DATA
INTO FILES APPROPRIATE FOR USE IN PLOTTING ROUTINES

THE FOLLOWING SYSTEM/IMSL SUBROUTINES ARE CALLED:

TIME : STORES THE NUMBER OF SECONDS SINCE 1900 A.D. IN 'ITM'

GGENOF : DETERMINES ONE NORMALLY DISTRIBUTED RANDOM NUMBER

DEFINITION OF PRIMARY ARRAYS AND VARIABLES:

AREA : THE AREA OF EACH CELL
CONC : THE NUMBER OF PARTICLES/UNIT AREA OF EACH CELL
UD : CROSS VALLEY DIFFUSION VELOCITY
VD : VERTICAL DIFFUSION VELOCITY
UA : CROSS VALLEY ADVECTION VELOCITY
VA : VERTICAL ADVECTION VELOCITY
XP : CROSS VALLEY (HORIZONTAL) PARTICLE COORDINATE
ZP : VERTICAL PARTICLE COORDINATE
JFLAG : POSITION ARRAY. IF JFLAG=1, PARTICLE TO BE DESTROYED
DELX : CROSS VALLEY TRANSPORT DISTANCE
DELZ : VERTICAL TRANSPORT DISTANCE
VAR : VARIANCE OF EACH PUFF
NIT : NUMBER OF PARTICLES IN EACH PUFF
NPIT : NUMBER OF PARTICLES PRODUCED PRIOR TO EACH PUFF
CT : CREATION TIME OF EACH PUFF
CMX : HORIZONTAL CENTER OF MASS COORDINATE OF EACH PUFF
CMZ : VERTICAL CENTER OF MASS COORDINATE
XS : CROSS VALLEY COORDINATE OF EACH POINT SOURCE
INCX : SIZE OF GRID IN HORIZONTAL
INCZ : VERTICAL GRID SIZE
HPRIME : DEPTH OF VALLEY
H : UPPERMOST EXTENT OF THE GRID
L : WIDTH OF THE VALLEY
NP : RUNNING TOTAL OF PARTICLES PRODUCED
USTAR : FRICTION VELOCITY (INPUT)
STAB : DIMENSIONLESS HEIGHT (Z/L); AN INDICATOR OF STABILITY
NT : THE NUMBER OF PUFFS PRODUCED
DELT : THE TIMESTEP INCREMENT
T : TOTAL TIME ELAPSED; THE SUM OF ALL DELT'S
NS : THE NUMBER OF POINT SOURCES IN THE GRID

LOGICAL*1 LFMT(1)/'/
LOGICAL*4 INT,MASK/ZOOOFFFF/
REAL*8 SEED
EQUIVALENCE (INT,ITM)
DIMENSION AREA(41,26),CONC(41,26),UD(41,26),VD(41,26),
1UA(41,26),VA(41,26)
COMMON XP(10000),ZP(10000),JFLAG(10000),
1DELX(10000),DELZ(10000),VAR(5000),NIT(5000),NPIT(5000),CT(5000),
1CMX(5000),CMZ(5000),XS(10),INCX,INCZ,HPRIME,H,L,NP,USTAR,STAB,NT,
1DELT,T,NS


```

C INPUT VALLEY AND GRID INFORMATION:
C
C L : VALLEY WIDTH (IN METERS)
C H : UPPER BOUND (IN METERS)
C HPRIME : HEIGHT OF VALLEY RIDGE (BOTTOM AT (L/2.0))
C INCX, INCZ : HORIZONTAL AND VERTICAL GRID SIZE (IN METERS)
C
  READ(5,LFMT) L,H,HPRIME,INCX,INCZ
C
C INPUT TIME INFORMATION
C
C DELT : LENGTH OF INITIAL TIMESTEP (LATER STEPS CALCULATED)
C TMAX : MAXIMUM TIME MODEL IS TO RUN (IN SECONDS)
C NTMAX : MAXIMUM NUMBER OF TIMESTEPS ALLOWED
C NS : NUMBER OF POINT SOURCES
C
  READ(5,LFMT) DELT,TMAX,NTMAX,NS
C
C INPUT SOURCE AND WIND INFORMATION:
C
C SDEVX,SDEVZ : INITIAL STANDARD DEVIATION OF EXHAUST PLUME
C ICD : ARE EDDY DIFFUSIVITIES CONSTANT? IF YES, ICD=0
C DKMX,DKMZ : VALUES OF CONSTANT DIFFUSIVITIES
C IAV : ARE ADVECTION VELOCITIES ZERO (DIFFUSION ONLY) ? IF YES, IAV=0
C AVWF : ADVECTION VELOCITY WEIGHTING FACTOR IF AVWF=5, U=0( 5M/S)
C USTAR,STAB : FRICTION VELOCITY (M/S) AND STABILITY (Z/L) FROM DATA
C XS(NS) : X-POSITION OF SOURCES (IN METERS)
C
  READ(5,LFMT) SDEVX,SDEVZ,ICD,DKMX,DKMZ,IAV,AVWF,USTAR,STAB,(XS(I)
  1,I=1,NS)
C
C INPUT OUTPUT INFORMATION
C
C IPSO : IF IPSO=0, VALUES OF STREAM FUNCTIONS ARE WRITTEN ON UNIT 4
C NO : WRITE CONC. AND PART. POSITIONS ONTO UNITS 12 AND 13 EVERY NO SEC.
C ICO : WRITE CONC. OF ONE SPECIFIED CELL EVERY ICO TIMESTEPS ONTO UNIT 3
C X,Z : X AND Z COORDINATES (IN METERS) OF ONE SPECIFIED CELL
C
  READ(5,LFMT) IPSO,NO,ICO,X,Z
C
C
C
  DATA NOI/O/,NOTIN/O/,IX/41/,IZ/26/
  CALL TIME(13,O,ITM)
  INT=INT AND MASK
  SEED=ITM
  CALL SRAREA(IX,IZ,AREA)
  CALL ADVECT(IAV,AVWF,IPSO,IX,IZ,UA,VA)
  T=0
  NT=0
  NP=0
100 T=T+DELT
  CALL SOURCE(SDEVX,SDEVZ,SEED,IX,IZ)
  CALL SUM(ICO,X,Z,IX,IZ,CONC,AREA)
  CALL DIF1(ICO,DKMX,DKMZ,IX,IZ,UD,VD,CONC)
  CALL INTER(SDEVX,SDEVZ,ICD,DKMX,DKMZ,IOUT,IX,IZ,UD,VD,UA,VA)
  CALL TSTEP(IOUT,NOTIN)
  CALL RENUM
  IF(T.LT.NOI) GO TO 200
  CALL OUTPT(IX,IZ,CONC)
  NOI=NOI+NO
200 IF(T.LT.TMAX AND NT.LT.NTMAX) GO TO 100
  CALL OUTPT(IX,IZ,CONC)
  STOP
  END

```

```

SUBROUTINE SRAREA(IXX,IZZ,AREA)
C
C WRITTEN BY R.RUDOLPH
C
C COMPUTES CELL AREAS FOR A GIVEN VALLEY SHAPE
C
  DIMENSION AREA(IXX,IZZ)
  COMMON XP(10000),ZP(10000),JFLAG(10000),
1DELX(10000),DELZ(10000),VAR(5000),NIT(5000),NPIT(5000),QT(5000),
1CMX(5000),CMZ(5000),XS(10),INCX,INCZ,HPRIME,H,L,NP,USTAR,STAB,NT,
1DELT,T,NS
  PI=3.1415926
  S=2*HPRIME/L
C
C IGRIDX,IGRIDZ ARE NUMBER OF CELLS IN HORIZONTAL,VERTICAL
C
  IGRIDX=L/INCX
  IGRIDZ=H/INCZ
C
C DETERMINE CELL CORNERS
C
  IFLAG=0
  DO 200 IZ=1,IGRIDZ
    Z1=(IZ-1)*INCZ
    Z2=Z1+INCZ
    DO 190 IX=1,IGRIDX
      X1=(IX-1)*INCX
      X2=X1+INCX
      N=0
      IF(Z1.GE.HPRIME) GO TO 50
C
C CHECK WHICH CELL CORNERS ARE ABOVE THE GROUNDLINE
C
      A1=L/2-Z1/S
      IF(X1.GE.L/2) A1=L-A1
      A2=L/2-Z2/S
      IF(X1.GE.L/2) A2=L-A2
      A3=(L/2-X1)*S
      IF(X1.GE.L/2) A3=-A3
      A4=(L/2-X2)*S
      IF(X1.GE.L/2) A4=-A4
      IF(((L/2.GE.X1) AND (X1.GT.A1)) OR ((L/2.LE.X1)
1 AND (X1.LT.A1))) N=N+1
      IF(((L/2.GE.X2) AND (X2.GT.A1)) OR ((L/2.LE.X2)
1 AND (X2.LT.A1))) N=N+10
      IF(((L/2.GE.X2) AND (X2.GT.A2)) OR ((L/2.LE.X2)
1 AND (X2.LT.A2))) N=N+100
      IF(((L/2.GE.X1) AND (X1.GT.A2)) OR ((L/2.LE.X1)
1 AND (X1.LT.A2))) N=N+1000
C
C CHECK N AND CALCULATE APPROPRIATE AREA
C
      IF(N.EQ.0) GO TO 40
      IF(N.EQ.1111) GO TO 50
      IF(N.EQ.1110) GO TO 60
      IF(N.EQ.1101) GO TO 70
      IF(N.EQ.1100) GO TO 80
      IF(N.EQ.0110) GO TO 110
      IF(N.EQ.1001) GO TO 120
      IF(N.EQ.1000) GO TO 130
      IF(N.EQ.0100) GO TO 140
20      WRITE(7,30)IX,IZ,N
30      FORMAT(5X,'SHAPE NOT ALLOWED FOR CELL',2X,IZ,1X,IX,5X,'N=

```

```

14)
AREA(IX,IZ)=-2
GO TO 150
40 AREA(IX,IZ)=-1
GO TO 150
50 AREA(IX,IZ)=INCZ*INCX
GO TO 150
60 AREA(IX,IZ)=INCZ*INCX-((A1-X1)*(A3-Z1)/2)
GO TO 150
70 AREA(IX,IZ)=INCX*INCZ-((X2-A1)*(A4-Z1)/2)
GO TO 150
80 IF(A3 LT A4) GO TO 90
A5=A3
DIF=A3-A4
GO TO 100
90 A5=A4
DIF=A4-A3
100 AREA(IX,IZ)=INCX*(Z2-A5)+INCZ/2*(DIF)
GO TO 150
110 Z1INT=A1
Z2INT=A2
IF(Z1INT LT Z2INT) GO TO 20
AREA(IX,IZ)=(X2-Z1INT)*INCZ+INCX*(Z1INT-Z2INT)/2
GO TO 150
120 Z1INT=A1
Z2INT=A2
IF(Z1INT GT Z2INT) GO TO 20
AREA(IX,IZ)=INCZ*(Z1INT-X1)+INCX*(Z2INT-Z1INT)/2
GO TO 150
130 AREA(IX,IZ)=(A2-X1)*(Z2-A3)/2
GO TO 150
140 AREA(IX,IZ)=(X2-A2)*(Z2-A4)/2
C
C IS AREA REASONABLE?
C
150 RECT=INCX*INCZ
IF(RECT LT AREA(IX,IZ) OR AREA(IX,IZ) EQ 0) GO TO 160
IF(AREA(IX,IZ) EQ -1 OR AREA(IX,IZ) GT 0) GO TO 190
IF(AREA(IX,IZ) EQ -2) GO TO 180
160 WRITE(7,170)IX,IZ,AREA(IX,IZ),N
170 FORMAT(3X,'AREA OF CELL',I3,' ',I3,2X,'NOT IN PROPER RANGE
180 3X,'AREA=',F8.2,5X,'N=',I4)
180 IFLAG=1
190 CONTINUE
200 CONTINUE
IF(IFLAG NE 1) GO TO 220
WRITE(8,210)
210 FORMAT(//3X,'PREMATURE TERMINATION IN SRAREA. CHECK ERROR FILE.
//)
STOP
220 RETURN
END

```

```

      SUBROUTINE ADVECT(K,C,KKK,IXX,IZZ,UA,VA)
C
C WRITTEN BY : R. RUDOLPH
C
C DETERMINES STREAMFUNCTIONS AND GRID POINT VELOCITIES FROM
C POTENTIAL FLOW.
C
      DIMENSION UA(IXX,IZZ),VA(IXX,IZZ),PS(81,52)
      COMMON XP(10000),ZP(10000),JFLAG(10000),
      1DELX(10000),DELZ(10000),VAR(5000),NIT(5000),NPIT(5000),CT(5000),
      1CMX(5000),CMZ(5000),XS(10),INCX,INCZ,HPRIME,H,L,NP,USTAR,STAB,NT,
      1DELT,T,NS
      DATA PI/3.1415926/
      IGRIDX=L/INCX+1
      JGRIDZ=L/(2*INCZ)+1
      IGRIDZ=HPRIME/INCZ+1
      LD2=L/2
      S=2*HPRIME/L
C
C IF K=0, DIFFUSION ONLY
C
      IF(K.EQ.C) GO TO 600
      DO 200 J=1,IGRIDZ
      Z=INCZ*(J-1)
      A=SIN(2*PI*Z/HPRIME)
      B=SIN(PI*Z/HPRIME)
      DO 100 I=1,UGRIDX
      X=INCX*(I-1)
      PS(I,J)=C*(-SIN(PI*X/LD2)+B*SIN(2*PI*X/LD2))
      K=IGRIDX+1-I
      PS(K,J)=-PS(I,J)
100 CONTINUE
200 CONTINUE
      IGRIDX=IGRIDX-1
      JGRIDZ=JGRIDZ-1
      DO 500 J=1,JGRIDZ
      Z=INCZ*(J-1)
      XCPT=LD2-Z/S
      DO 400 I=2,IGRIDX
      X=INCX*(I-1)
      A=PS(I,J-1)
      IF(J.EQ.1) A=0
      B=PS(I,J+1)
      IF(J.EQ.JGRIDZ) B=PS(I,J)+(PS(I,J)-PS(I,J-1))
280 UA(I,J)=(A-B)/(2*INCZ)
      VA(I,J)=(PS(I+1,J)-PS(I-1,J))/(2*INCX)
400 CONTINUE
500 CONTINUE
      GO TO 800
600 DO 700 I=1,IGRIDX
      DO 700 J=1,IGRIDZ
      UA(I,J)=0
      VA(I,J)=0
700 CONTINUE
800 IF(KKK.NE.0) GO TO 900
      IGRIDX=IGRIDX+1
      IGRIDZ=IGRIDZ+1
      DO 890 J=1,IGRIDZ
      WRITE(4,888)(PS(I,J),I=1,IGRIDX)
888 FORMAT(100(1X,F8.5))
890 CONTINUE
900 RETURN
      END

```

```

SUBROUTINE SOURCE(SDEVX,SDEVZ,ITM,IXX,IZZ)
C
C WRITTEN BY: R. RUDOLPH
C
C DETERMINES AN INITIAL PARTICLE CONFIGURATION, ASSUMED TO BE APPRO-
C XIMATELY GAUSSIAN, FOR EACH POINT SOURCE AT EACH TIMESTEP.
C
  REAL*8 ITM
  COMMON XP(10000),ZP(10000),JFLAG(10000),
  1DELX(10000),DELZ(10000),VAR(5000),NIT(5000),NPIT(5000),CT(5000),
  1CMX(5000),CMZ(5000),XS(10),INCX,INCZ,HPRIME,H,L,NP,USTAR,STAB,NT,
  1DELT,T,NS
  DATA IFLAG/O/,PWT/O 2/
C
C CONSTANTS:
C NP= NUMBER OF PARTICLES PRODUCED PER PUFF
C XO= X-AXIS SOURCE COORDINATE
C USTAR,STAB ARE FRICTION VELOCITY AND STABILITY (Z/L)
C VK= VON KARMEN COEFFICIENT
C DKZZ= VERTICAL EDDY DIFFUSIVITY
C DKXX=HORIZONTAL EDDY DIFFUSIVITY
C
C ARRAYS:
C XP,ZP ARE PARTICLE POSITIONS
C VAR IS VARIANCE OF EACH PUFF
C NIT IS NUMBER OF PARTICLES IN EACH PUFF
C NPIT IS NUMBER OF PARTICLES PRODUCED PRIOR TO EACH PUFF
C CT IS THE CREATION TIME OF EACH PUFF
C
C
C GGNQF IS A SYSTEM SUBROUTINE THAT COMPUTES NORMALLY DISTRIBUTED RANDOM
C NUMBERS, WITH MEAN ZERO AND STANDARD DEVIATION ONE. I.E. N(0,1)
C
C
  LD2=L/2
  S=2*HPRIME/L
  DO 300 K=1,NS
    NT=NT+1
    XO=XS(K)
    ZO=(XO-LD2)*S
    IF(XO.LT.LD2) ZO=-ZO
    SZ=0
    SX=0
    SVAR=0
C
C DETERMINE NUMBER OF PARTICLES PRODUCED AND THEIR POSITIONS, ASSUMING
C THAT THEY ARE PART OF A NORMAL DISTRIBUTION
C
  N=5.24/PWT*DELT*(0.04-0.0075*T/3600)
  IF(N.LT.2) N=2
  LL=NP+1
100 Z=GGNQF(ITM)
  Z=SDEVZ*Z+ZO
  A=LD2-Z/S
  X=GGNQF(ITM)
  X=SDEVX*X+XO
  IF(.NOT.(X.GE.A.AND.X.LE.L-A)) GO TO 100
  XP(LL)=X
  ZP(LL)=Z
  SX=SX+X
  SZ=SZ+Z
  IF(LL-NP.GE.N) GO TO 200
  LL=LL+1

```

```

      GO TO 100
C
C CHECK: IS VARIANCE OF SOURCE DISTN. LARGE ENOUGH FOR THE PARTICLES
C TO BE INCLUDED IN DIFFUSION ROUTINE? IF YES,VAR=-1
C
200 CMX(NT)=SX/N
    CMZ(NT)=SZ/N
    NNP=NP+N
    NPP1=NP+1
    DO 250 I=NPP1,NNP
      SVAR=SVAR+(ZP(I)-CMZ(NT))*(ZP(I)-CMZ(NT))+(XP(I)-CMX(NT))*
1(XP(I)-CMX(NT))
250 CONTINUE
    VAR(NT)=SVAR/N
    IF(VAR(NT).NE.0) GO TO 260
    IFLAG=1
    WRITE(7,111) NT,N
111 FORMAT(1X,'VARIANCE OF PUFF',1X,I4,1X,'IS ZERO. NUMBER OF PART',
1'ICLES IN PUFF IS',1X,I2)
260 SIG=SQRT(VAR(NT))
    AA=AMAXO(INCX,INCZ)
    IF(SIG.GT.AA) VAR(NT)=-1
    NIT(NT)=N
    NPIT(NT)=NP
    NP=NP+N
    CT(NT)=T
    WRITE(6,333) NT,T,VAR(NT),NPIT(NT),NIT(NT),NP
333 FORMAT(3X,I4,2(3X,F8.1),3(3X,I5))
    IF(IFLAG.NE.1) GO TO 300
    WRITE(8,222)T,NT,K
222 FORMAT(/3X,'PREMATURE TERMINATION IN SUBROUTINE SOURCE. CHECK
1 ERROR FILE',1X,'TIME=',1X,F8.1,1X,'FOR PUFF',1X,I5,1X,'FOR SOU',
2'RCE LOCATION',1X,I2//)
    STOP
300 CONTINUE
    RETURN
    END

```

```

      SUBROUTINE DIF1(III,DKMX,DKMZ,IXX,IZZ,UD,VD,CONC)
C
C   WRITTEN BY:  R. RUDOLPH
C
C   COMPUTES DIFFUSION VELOCITIES AT GRIDPOINTS
C
      DIMENSION UD(IXX,IZZ),VD(IXX,IZZ),CONC(IXX,IZZ)
      COMMON XP(10000),ZP(10000),JFLAG(10000),
      2DELX(10000),DELZ(10000),VAR(5000),NIT(5000),NPIT(5000),CT(5000),
      3CMX(5000),CMZ(5000),XS(10),INCX,INCZ,HPRIME,H,L,NP,USTAR,STAB,NT,
      4DELT,T,NS
      DATA VK/.35/,AA/.0/
      LD2=L/2
      IGRIDX=L/INCX
      IGRIDZ=HPRIME/INCZ+1
      S=HPRIME*2/L
C
C   IS DIFFUSION TO BE NEGLECTED (EXCEPT INITIALLY) ?
C
      IF(AA GE. 1.0) GO TO 30
      DO 20 J=1,IGRIDZ
      DO 20 I=1,IGRIDX
      UD(I,J)=0
      VD(I,J)=0
20    CONTINUE
      GO TO 800
30    B=1+.7*STAB
      IF(STAB LT. 0) B=(1-.15*STAB)**(-.025)
      IFLAG=0
      DO 500 J=1,IGRIDZ
      Z=INCZ*(J-1)
      DO 460 I=2,IGRIDX
      X=INCX*(I-1)
      IF(III.EQ.0) GO TO 40
      SZ=(LD2-X)*S
      IF(X GT. LD2) SZ=-SZ
      SZ=ABS(Z-SZ)
      DKZZ=VK*USTAR*SZ/B
      DKXX=DKZZ*SZ**(0.07)
      GO TO 50
40    DKXX=DKMX
      DKZZ=DKMZ
50    VM=ABS(2*DKZZ/INCZ)
      UM=ABS(2*DKXX/INCX)
      A1=CONC(I,J)
      A2=CONC(I-1,J)
      IF(J.NE.IGRIDZ) GO TO 60
      A1=CONC(I,J-1)
      A2=CONC(I-1,J-1)
60    A3=CONC(I-1,J-1)
      A4=CONC(I,J-1)
      IF(J.NE.1) GO TO 70
      A3=CONC(I-1,J)
      A4=CONC(I,J)
70    IF((Z-INCZ).GE.HPRIME) GO TO 100
C
C   FOR INTERSECTION BELOW VALLEY BOUNDARY
C
      Z1=(X-LD2)*S
      IF(X LT. LD2) Z1=-Z1
      IF((Z1-Z).LT.0) GO TO 100
      UD(I,J)=0
      VD(I,J)=0

```

```

      GO TO 460
C
C CHECK - ALL CONCENTRATIONS SHOULD BE POSITIVE
C
100  IF(.NOT.(A1.LT.0.OR.A2.LT.0.OR.A3.LT.0.OR.A4.LT.0)) GO TO 200
      WRITE(7,111) I,J,A1,A2,A3,A4
111  FORMAT(3X,'ERROR IN DETERMINING GRIDPOINT DIFFUSION VELOCITY
1    FOR GRID',2X,I3,'',I3,2X,'- NEGATIVE CONCENTRATION ENCOUNTERED'//
2    'A1=',F8.3,'A2=',F8.3,'A3=',F8.3,'A4=',F8.3//)
      UD(I,J)=-999999
      VD(I,J)=-999999
      IFLAG=1
      GO TO 460
C
C CALCULATE DIFFUSION VELOCITIES (REF LANGE,1973, P9)
C
200  D=A1+A2+A3+A4
      IF(D.EQ.0) GO TO 400
      UD(I,J)=2*DKX*(A2+A3-A1-A4)/(INCX*D)
      VD(I,J)=2*DKZZ*(A3+A4-A1-A2)/(INCZ*D)
      GO TO 460
400  UD(I,J)=0
      VD(I,J)=0
460  CONTINUE
500  CONTINUE
      IF(IFLAG.NE.1) GO TO 800
      WRITE(8,777) T,NT
777  FORMAT(//1X,'PREMATURE TERMINATION IN DIF1'/10X/'AT TIME',
11X,F9.1,'FOR PUFF',1X,I7,'CHECK ERROR FILE'//)
      STOP
800  RETURN
      END

```



```

      SUBROUTINE SUM(JJJ,X,Z,IXX,IZZ,CONC,AREA)
C  WRITTEN BY R. BUDDOLPH
C
C  DETERMINES CELL PARTICLE CONCENTRATION
C
      DIMENSION CONC(IXX,IZZ),AREA(IXX,IZZ),ISUM(81,52)
      COMMON XP(10000),ZP(10000),JFLAG(10000),
      1DELX(10000),DELZ(10000),VAR(5000),NIP(5000),NPIT(5000),CT(5000),
      1CMX(5000),CMZ(5000),XS(10),INCX,INCZ,HPRIME,H,L,NP,USTAR,STAB,NT,
      1DELT,T,NS
      II=X/INCX+1
      JU=Z/INCZ+1
      IU=(X+150)/INCX+1
      JI=(Z-250)/(8*INCZ)+1
      IF(NT.EQ.1) WRITE(3,300) AREA(II,JU),AREA(IU,JI)
      IGRIDX=L/INCX
      IGRIDZ=H/INCZ
C
C  INITIALIZE PARTICLE/CELL ARRAY
C
      DO 240 I=1,IGRIDX
        DO 240 J=1,IGRIDZ
          ISUM(I,J)=0
240  CONTINUE
      DO 250 I=1,NP
        INT=XP(I)/INCX+1
        UNT=ZP(I)/INCZ+1
        ISUM(INT,UNT)=ISUM(INT,UNT)+1
250  CONTINUE
C
C  CALCULATE CELL PARTICLE CONCENTRATION
C
      DO 290 I=1,IGRIDX
        DO 290 J=1,IGRIDZ
          IF(AREA(I,J).LT.1.E-4) GO TO 260
          CONC(I,J)=ISUM(I,J)/AREA(I,J)
          GO TO 290
260  CONC(I,J)=0
290  CONTINUE
      IF(JJJ.EQ.0) GO TO 350
      III=MOD(NT,JJJ)
      IF(III.NE.0) GO TO 350
      WRITE(3,300)CONC(11,JJ),CONC(11,JJ+1),CONC(11,JJ+2),
      1CONC(IJ,JI),CONC(IJ,JI+1),CONC(IJ,JI+2),T
300  FORMAT(1X,6F9.5,1X,F8.1)
350  RETURN
      END

```

```
SUBROUTINE INTER(SDEVX,SDEVZ,III,DKMX,DKMZ,INV,IXX,IZZ,UD,
  (VD,UA,VA)
```

```
C WRITTEN BY: R. RUDDOLPH
```

```
C INTERPOLATES VELOCITIES FROM GRID PTS TO PARTICLE POSITIONS;
C DIFFERENTIATING BETWEEN "NORMAL" AND SUBGRID SCALE DIFFUSION
C CALCULATES MAX GRID VELOCITY AND LENGTH OF SUBSEQUENT TIMESTEP
```

```
C SYMBOLS:
```

```
C UA,UD : ADVECTION AND DIFFUSION VELOCITIES INTERPOLATED FROM GRID
C INTERSECTIONS
C PHIM : DIMENSIONLESS WIND SHEAR
C EPS : RATE OF DISSIPATION OF EDDY ENERGY
C VK : VON KARMAN COEFFICIENT
```

```
  DIMENSION UD(IXX,IZZ),VD(IXX,IZZ),UA(IXX,IZZ),VA(IXX,IZZ)
  COMMON XP(10000),ZP(10000),JFLAG(10000),
  IDLX(10000),DELZ(10000),VAR(5000),NIT(5000),NPIT(5000),CT(5000),
  ICMX(5000),CMZ(5000),XS(10),INCX,INCZ,HPRIME,H,L,NP,USTAR,STAB,NT,
  IDLT,T,NS
  REAL UDX,UDZ,UAX,UAZ
  DATA VK/ .35/.88/.1 OE-4/ .CC/1 OE-7/.EE/O. 10/
  UMAX=0
  VMAX=0
  AMUAX=0
  IFLAG=0
  LD2=L/2
  S=HPRIME/LD2
  PHIM=1+.7*STAB
  IF(STAB.LT.0) PHIM=(1-15*STAB)**(-.25)
  DO 500 L1=1,NT
  LL=NIT(L1)
  DO 400 I=1,LL
  II=I+NPIT(L1)
  INT=XP(II)/INCX+1
  UNT=ZP(II)/INCZ+1
  X1=XP(II)-(INT-1)*INCX
  X2=INCX-X1
  Z1=ZP(II)-(UNT-1)*INCZ
  Z2=INCZ-Z1
```

```
C INTERPOLATE ADVECTION VELOCITIES TO PARTICLE POSITION
```

```
  UAX=Z2*(UA(INT,UNT)*X2+UA(INT+1,UNT)*X1)
  UAY=UAX+Z1*(UA(INT,UNT+1)*X2+UA(INT+1,UNT+1)*X1)
  UAX=UAX/(INCX*INCZ)
  UAZ=X2*(VA(INT,UNT)*Z2+VA(INT,UNT+1)*Z1)
  UAZ=UAZ+X1*(VA(INT,UNT+1)*Z2+VA(INT+1,UNT+1)*Z1)
  UAZ=UAZ/(INCX*INCZ)
  A=ABS(UAZ)
  MUAX=AMAX1(AMUAX,A)
```

```
C TEST VARIANCE : IF POSITIVE USE SUBGRID DIFFUSION
```

```
  IF(VAR(L1).GE.0) GO TO 200
```

```
C INTERPOLATE DIFFUSION VELOCITIES TO PARTICLE POSITION
```

```
  UDX=Z2*(UD(INT,UNT)*X2+UD(INT+1,UNT)*X1)
  UDX=UDX+Z1*(UD(INT,UNT+1)*X2+UD(INT+1,UNT+1)*X1)
  UDX=UDX/(INCX*INCZ)
  UDX=X2*(VD(INT,UNT)*Z2+VD(INT,UNT+1)*Z1)
```

```

      UDZ=UDZ+X1*(VD(INT+1,JNT+1)*Z1+VD(INT+1,JNT)*Z2)
      UDZ=UDZ/(INCX*INCZ)
      DELX(II)=(UDX+UAX)*DELT
      DELZ(II)=(UDZ+UAZ)*DELT
      GO TO 300
C
C ASSUME PUFF TO BE IN CONSTANT (SURFACE) STRESS LAYER AND TURBULENCE
C TO BE IN THE INERTIAL SUBRANGE
C
C
C CALCULATE THE DISTANCE DIFFUSED BY THE PARTICLE
C REF. LANGE, 1973 P.30
C
200 IF(III.EQ.0) GO TO 291
      Z=(LD2-XP(II))*S
      IF(XP(II).GT.LD2) Z=-Z
      Z=ZP(II)-Z
      IF(Z.GE.0) GO TO 240
      WRITE(7,222) XP(II),ZP(II),Z,UAX,UAZ
222  FORMAT(1X,'XP,ZP',1X,2F12.8,1X,'Z',1X,1F12.8,1X,'U,W',1X,2F12.8)
      STOP
240 IF(ABS(Z).LT.BB) GO TO 250
      EPS=USTAR*USTAR/(VK*Z)*(PHI-STAR)
      D=T-CT(L1)+1.5*(SDEVZ*SDEVZ/EPS)**(.333)
      DD=T-CT(L1)+1.5*(SDEVX*SDEVX/EPS)**(.333)
      GO TO 270
250 D=T-CT(L1)
      DD=D
270 IF(.NOT.(D.LT.CC.OR.DD.LT.CC)) GO TO 290
      DELZ(II)=UAZ*DELT
      DELX(II)=UAX*DELT
      GO TO 300
290 DELZ(II)=UAZ*DELT+(((1+DELT/D)**(1.5))-1)*(ZP(II)-CMZ(L1))
      DELX(II)=UAX*DELT+(((1+DELT/DD)**(1.5))-1)*(XP(II)-CMX(L1))
      GO TO 300
291 DX=SDEVX*SDEVX/(2*DKMX)+T-CT(L1)
      IF(DX.EQ.0) GO TO 292
      DELX(II)=UAX*DELT+(XP(II)-CMX(L1))*(SORT(1+DELT/DX)-1)
      GO TO 294
292 A=1
      B=XP(II)-CMX(L1)
      IF(B.EQ.0) GO TO 293
      DELX(II)=INCX/2*SIGN(A,B)
      GO TO 294
293 DELX(II)=UAX*DELT
294 DZ=SDEVZ*SDEVZ/(2*DKMZ)+T-CT(L1)
      IF(DZ.EQ.0) GO TO 295
      DELZ(II)=UAZ*DELT+(ZP(II)-CMZ(L1))*(SORT(1+DELT/DZ)-1)
      GO TO 300
295 A=1
      B=ZP(II)-CMZ(L1)
      IF(B.EQ.0) GO TO 296
      DELZ(II)=INCZ/2*SIGN(A,B)
      GO TO 300
296 DELZ(II)=UAZ*DELT
C
C FIND MAXIMUM VELOCITY ON THE GRID
C
300 U=ABS(DELX(II)/DELT)
      V=ABS(DELZ(II)/DELT)
      UMAX=AMAX1(UMAX,U)
      VMAX=AMAX1(VMAX,V)
400 CONTINUE
500 CONTINUE
C
C DETERMINE THE LENGTH OF THE NEXT TIMESTEP

```

C AND THE RATIO OF DIFFUSION TO TOTAL VELOCITIES

```

C
  IF(VMAX.EQ.0) VMAX=1.0E-5
  V=(VMAX-AMUAZ)/VMAX
  IF(V.EQ.0) V=1.0E-5
  INV=1.0/V

C
  A1=INCX/(2*UMAX)
  A2=INCZ/(2*VMAX)
  DT=AMIN1(A1,A2)
  A3=DELT*1.3
  DELT=AMIN1(DT,A3)
  IF(DELT.LT.EE) IFLAG=1
  WRITE(6,666)A3,DT,UMAX,VMAX,DELT
666  FORMAT(5(3X,F10.3))
  IF(IFLAG.NE.1) GO TO 700
  WRITE(8,777) T,EE
777  FORMAT(//1X,'PROGRAM ABORT IN SR INTER AT TIME',1X,F8.1,5X,
1' Timestep less than ',1X,F8.5//)
  STOP
700  RETURN
  END

```

```

SUBROUTINE TSTEP(IOUT,NOTIN)
C
C WRITTEN BY: R. RUDDOLPH
C
C ADVANCES PARTICLES ALONG STREAMLINES, REFLECTS PARTICLES
C AT APPROPRIATE BOUNDARIES, AND RECALCULATES THE VARIANCE OF EACH PUFF.
C
COMMON XP(10000), ZP(10000), JFLAG(10000),
1DELX(10000), DELZ(10000), VAR(5000), NIT(5000), NPIT(5000), CT(5000),
1CMX(5000), CMZ(5000), XS(10), INCX, INCZ, HPRIME, H, L, NP, USTAR, STAB, NT,
1DELT, T, NS
DATA IFLAG/0/, PI/3.1415926/, BB/1.00E-4/, CC/1.00E-3/
LD2=L/2
S=2*HPRIME/L
BD=ARSIN(S)
DO 1000 L1=1, NT
SX=0
SZ=0
IF(NIT(L1).EQ.0) GO TO 950
LL=NIT(L1)
DO 800 I=1, LL
II=I+NPIT(L1)
JFLAG(II)=0
XP1=XP(II)
ZP1=ZP(II)
C
C DETERMINE NEW PARTICLE POSITIONS
C
XP2=XP(II)+DELX(II)
ZP2=ZP(II)+DELZ(II)
C
C CHECK IS PARTICLE OUT OF BOUNDS? IF YES, JFLAG=1
C
IF((XP2.LT.INCX).OR.(XP2.GT.(L-INCX))) JFLAG(II)=1
IF(ZP2.GE.0.0) GO TO 10
JFLAG(II)=1
GO TO 90
10 IF(ZP2.LE.HPRIME) GO TO 90
C
C PARTICLE TRANSPORTED ABOVE RIDGELINE
C
NOTIN=NOTIN+1
IF(NOTIN.LT.IOUT) GO TO 20
JFLAG(II)=1
NOTIN=0
GO TO 90
20 ZP2=2*HPRIME-ZP2
IF(ZP2.GT.HPRIME) JFLAG(II)=1
IF(ZP2.EQ.ZP1) JFLAG(II)=1
90 IF(JFLAG(II).EQ.1) GO TO 95
X1=LD2-ZP2/S
IF(XP2.LT.X1.OR.XP2.GT.L-X1) GO TO 100
95 XP2H=XP2
ZP2H=ZP2
GO TO 700
C
C PARTICLE ADVECTED INTO GROUND. FIND GROUND-TRAJECTORY INTERCEPT
C
100 IF(XP1.EQ.XP2) GO TO 110
S1=(ZP1-ZP2)/(XP1-XP2)
S2=S.
IF(XP2.LT.LD2) S2=-S
C

```

C IF S1=S2, PARTICLE IS AT GROUND LINE, AND THEREFORE IN THE ATMOSPHERE

```

C
  IF(S1.EQ.S2) GO TO 700
  B2=HPRIME
  IF(S2.GT.0) B2=-B2
  X=(S1*XP1+B2-ZP1)/(S1-S2)
  Z=(S2*ZP1-S1*B2-S1*S2*XP1)/(S2-S1)
  GO TO 140
110 X=XP2
  Z=(X-LD2)*S
  IF(X.LT.LD2) Z=-Z
140 IF((X.GT.XP1.AND.X.GT.XP2).OR.(X.LT.XP1.AND.X.LT.XP2).OR.
  1(Z.GT.ZP1.AND.Z.GT.ZP2).OR.(Z.LT.ZP1.AND.Z.LT.ZP2)) GO TO 145
  GO TO 160
145 WRITE(7,150)XP1,ZP1,XP2,ZP2,X,Z
150 FORMAT(3X,'UNREASONABLE INTERSECTION',3X,'BEGIN=',E23.16,'',
  1E23.16,'/3X','END=',E23.16,'',E23.16,3X,'INTERSECT=',E23.16,'',
  2E23.16)
  IF(ABS(XP1-X).GE.CC.AND.ABS(XP2-X).GE.CC.AND.ABS(ZP1-Z).GE.CC
  1.AND.ABS(ZP2-Z).GE.CC) GO TO 155
  JFLAG(11)=1
  XP2H=XP2
  ZP2H=ZP2
  GO TO 700
155 IFLAG=1
  GO TO 700

```

C
C REFLECT THE PARTICLE

```

C
160 A1=COS(B0)
  A2=S
  D1=SQRT((XP1-XP2)*(XP1-XP2)+(ZP1-ZP2)*(ZP1-ZP2))

```

C
C IF D1=0, PARTICLE IS ON THE GROUND

```

C
  IF(D1.EQ.0) GO TO 700
  D3=SQRT((X-XP2)*(X-XP2)+(Z-ZP2)*(Z-ZP2))
  IF(XP2.GT.LD2) GO TO 200
  X=LD2-X
  XP1=LD2-XP1
  XP2=LD2-XP2
  JJ=2
  GO TO 300
200 X=X-LD2
  XP1=XP1-LD2
  XP2=XP2-LD2
  JJ=0

```

C
C ROTATE AXIS BY B0 RADIAN

```

C
300 XP1R=XP1*A1+ZP1*A2
  XP2R=XP2*A1+ZP2*A2
  X1=X*A1+Z*A2
  Z1=-X*A2+Z*A1
  IF(Z1.LT.0) Z1=0
  ARG=(XP1R-XP2R)/D1
  IF(ABS(ARG).GT.1.0) ARG=SIGN(1.0,ARG)
  B=ARCOS(ARG)
  IF(XP1R.LT.XP2R) GO TO 400
  I1=-1
  GO TO 500
400 I1=1
  B=PI-B
500 XP2R=X1+I1*D3*COS(B)
  ZP2R=Z1+D3*SIN(B)

```

C

C ROTATE AXIS TO ORIGINAL POSITION

C

```

      XPN=XP2R*A1-ZP2R*A2
      ZPN=XP2R*A2+ZP2R*A1
      IF(JJ.GE.1) GO TO 600
      XPN=XPN+LD2
      GO TO 650
600  XPN=LD2-XPN
650  XP2H=XPN
      ZP2H=ZPN
      A2=LD2-ZP2H/S
      IF(XP2H.GE.A2.AND.XP2H.LE.L-A2) GO TO 700
      IF(XP2H.GT.LD2) GO TO 660
      R=(XP2H-A2)/(XP2H+1)
      GO TO 670
660  R=(XP2H-L+A2)/XP2H
670  IF(ABS(R).GT.BB) GO TO 680
      JFLAG(II)=1
      GO TO 700
680  IFLAG=1
      WRITE(7,777)XP1,ZP1,X,Z,XP2,ZP2,XP1R,XP2R,X1,Z1,XP2H,ZP2H
777  FORMAT(1X,'REFL. BELOW GND',1X,'XP1,ZP1',1X,2F12.8,1X,
     1'X,Z',1X,2F12.8/1X,'XP2,ZP2',1X,2F12.8,1X,'XP1R,ZP1R',
     21X,2F12.8,1X,'X1,Z1',1X,2F12.8,/1X,'XP2H,ZP2H',
     32F12.8)
700  XP(II)=XP2H
      ZP(II)=ZP2H
      SX=SX+XP2
      SZ=SZ+ZP2
800  CONTINUE

```

C

C IF DISTRIBUTION IS SUB-GRID SCALE, CALCULATE CMX,CMZ
 C CMX,CMZ ARE COORDINATES OF THE CENTER OF MASS OF THE PUFF

C

```

      IF(VAR(L1).LT.0) GO TO 950
      CMX(L1)=SX/LL
      CMZ(L1)=SZ/LL
C CALCULATE NEW PUFF VARIANCE
      SVAR=0
850  DO 900 I=1,LI
      II=I+NPIT(L1)
      SVAR=SVAR+(XP(II)-CMX(L1))*(XP(II)-CMX(L1))+(ZP(II)-CMZ(L1))
     1*(ZP(II)-CMZ(L1))
900  CONTINUE
      SVAR=SVAR/LL
      AA=AMAX0(INCX,INCZ)
      IF(SQRT(SVAR).GT.AA.OR.SQRT(SVAR).LT.BB) SVAR=-1
      VAR(L1)=SVAR
      GO TO 960
950  VAR(L1)=-1
960  IF(IFLAG.NE.1) GO TO 1000
      WRITE(8,999) NT,T
999  FORMAT(/3X,'PREMATURE TERMINATION IN SUBROUTINE TSTEP AT TIMESTEP
     1',1X,15/10X,'AND TIME',1X,F8.1,3X,'CHECK ERROR FILE'//)
      STOP
1000 CONTINUE
      RETURN
      END

```

```

      SUBROUTINE RENUM
C
C WRITTEN BY: R. RUDDOLPH
C
C RENUMBERS EXISTING PARTICLES, DESTROYING THOSE FOUND TO BE OUTSIDE
C THE GRID SYSTEM ( VIA JFLAG ARRAY )
      COMMON XP(10000),ZP(10000),JFLAG(10000),
      1DELX(10000),DELZ(10000),VAR(5000),NIT(5000),NPIT(5000),CT(5000),
      1CMX(5000),CMZ(5000),XS(10),INCX,INCZ,HPRIME,H,L,NP,USTAR,STAB,NT,
      1CT,T,T,NS
      DIMENSION TX(10000),TZ(10000),DF1(5000)
      N=1
      J=1
      DF1(J)=0
      DO 200 L1=1,NT
      IF(NIT(L1).EQ.0) GO TO 150
      LL=NIT(L1)
      DO 100 I=1,LL
      II=I+NPIT(L1)
      IF(JFLAG(II).EQ.1) GO TO 50
      TX(I)=XP(II)
      TZ(I)=ZP(II)
      J=J+1
      GO TO 100
50 NIT(L1)=NIT(L1)-1
      N=N+1
      WRITE(6,111) XP(II),ZP(II)
111 FORMAT(1X,'DETECTED OUT-OF-BOUNDS X=',1X,F8.4,2X,'Z=',1X,F8.4)
100 CONTINUE
      DF1(L1+1)=NPIT(L1+1)-N
      GO TO 200
150 DF1(L1+1)=DF1(L1)
200 CONTINUE
      NP=J-1
      DO 500 L1=1,NT
      NPIT(L1)=DF1(L1)
C      WRITE(6,444) L1,T,CT(L1),VAR(L1),CMX(L1),CMZ(L1),NPIT(L1),
C      1NIT(L1),NP
C 444 FORMAT(3X,I3,5(3X,F8.4),3(3X,I4))
500 CONTINUE
      IF(NP.LT.1) GO TO 700
      DO 600 I=1,NP
      XP(I)=TX(I)
      ZP(I)=TZ(I)
600 CONTINUE
700 RETURN
      END

```



```

      SUBROUTINE OUTPT(IXX,IZZ,CONC)
C
C
C WRITTEN BY: R. RUDDOLPH
C
C WRITES CONCENTRATION AND PARTICLE POSITION DATA INTO FILES (12,13)
C FOR USE IN PLOTTING PROGRAMS.
C
      DIMENSION CONC(IXX,IZZ)
      COMMON XP(10000),ZP(10000),CFLAG(10000),
      1DELX(10000),DELZ(10000),VAR(5000),NIT(5000),NPIT(5000),CT(5000),
      1CMX(5000),CMZ(5000),XS(10),INCX,INCZ,HPRIME,H,L,NP,USTAR,STAB,NT,
      1DELT,T,NS
      DATA ZAP/'****'/
      IGRIDX=L/INCX
      IGRIDZ=H/INCZ
C
C
      WRITE(12,900)NP
900  FORMAT(1X,100)
C
      WRITE(13,1400) (I,ZP(I),IF=1,NP)
C
      WRITE(13,1400) (I,NT,I)
C
      DO 1300 I=1,NP
      WRITE(13,1400) (I,ZP(I),IF=1,IGRIDX)
1300  CONTINUE
1400  CONTINUE
C
      WRITE(13,1444) ZAP,NT,T
1444  FORMAT(1X,A4,1X,'Timesteps=',1X,I5,3X,'Time=',1X,F8.1)
      RETURN
      END

```